

**MAPPING THE EXPRESSION OF KEY FUNCTIONAL GENES  
ASSOCIATED WITH MURINE CORNEAL ENDOTHELIAL  
DEVELOPMENT**

BY

**MICHEL BENGTON**

Submitted in fulfillment of the academic requirements for the degree of Master of Science  
in the School of Life Sciences, University of KwaZulu-Natal Durban

July 2015

As the candidate's supervisor I have approved this dissertation for submission.

Signed: \_\_\_\_\_ Name: Dr Paula Sommer Date: \_\_\_\_\_

## ABSTRACT

The cornea is a complex, layered, transparent structure that is responsible for transmitting and refracting light to ensure vision. Of all the layers, the corneal endothelium is physiologically the most important layer. Its principle function is to regulate deturgescence, a requirement for corneal transparency. Corneal deturgescence is regulated by key functional genes that include a network of tight junctions, water channels and ion pumps.

In this study, we created an *in vitro* model of murine corneal endothelial development by immortalising endothelial cells at significant stages in corneal endothelial morphogenesis. Primary cultures of presumptive corneal endothelial cells were immortalised from wild-type mouse embryos at embryonic day (E) 14.5 and E15.5, and mature corneal endothelial cells were immortalised from wild-type pups at post-natal day (P) 13. These cell lines, together with already established cell lines at earlier stages in corneal endothelial development (E12.5 and E13.5), were used to map the expression patterns of three functional genes associated with corneal endothelial function, *Zo1*, *Aqp1* and *Slc4a4*.

*Zo1* is a tight junction protein that facilitates the formation of the resilient monolayer that is characteristic of the corneal endothelium. *Aqp1* is a water channel protein that mediates transcellular fluid transport while *Slc4a4* is an ion pump that transports cellular bicarbonate ions across plasma membranes. *Aqp1* and *Slc4a4* are disease target genes which is indicative of their functional significance in corneal endothelial physiology.

Quantitative real-time PCR (qPCR) and western blot analysis showed that *Zo1* expression at both mRNA and protein level was progressively down-regulated from E12.5 to E15.5, after which it was up-regulated at P13 ( $p < 0.05$  relative to E15.5 at mRNA level). *Aqp1*

gene expression was up-regulated at E13.5, with subsequent down-regulation at E14.5. Thereafter, *Aqp1* gene expression was up-regulated at E15.5. Interestingly, *Aqp1* gene expression was significantly down-regulated at P13 when the endothelium is completely matured ( $p < 0.05$  relative to all other cell lines). Western blot analysis demonstrated Aqp1 expression throughout development in this model. Densitometric analysis showed that glycosylated Aqp1 protein expression levels decreased gradually from E12.5 to P13. Unglycosylated Aqp1 protein expression was only present at E12.5 and E13.5, and was up-regulated at E13.5. *Slc4a4* was expressed at low levels during corneal endothelial development. However, it was highly expressed at P13 ( $p < 0.05$  relative to all other cell lines). Protein expression for Slc4a4 could not be determined due to the lack of a commercially available antibody specific for murine Slc4a4. Confocal microscopy analysis demonstrated the protein localisation patterns for Zo1 and Aqp1 in monolayer and hanging drop culture, mimicking the 3D environment in which corneal endothelial development occurs.

The results of this study provide valuable insight into the expression patterns of key functional genes associated with corneal endothelial development.

## **PREFACE**

The experimental work described in this dissertation was carried out in the School of Life Sciences, University of KwaZulu-Natal, Durban, from January 2013 to June 2015, under the supervision of Doctor Paula Sommer.

These studies represent original work by the author and have not otherwise been submitted in any form for any degree or diploma to any tertiary institution. Where use has been made of the work of others it is duly acknowledged in the text.

Michel Bengtson (Candidate)

Dr Paula Sommer (Supervisor)

## DECLARATION OF PLAGIARISM

I, Michel Bengtson, declare that

1. The research reported in this theses, except where otherwise indicated, is my original research.
2. This thesis has not been submitted for any degree or examination at any other university.
3. This thesis does not contain other persons' data, pictures, graphs or other information, unless specifically acknowledged as being sourced from other persons.
4. This thesis does not contain other persons' writing, unless specifically acknowledged as being sourced from other researchers. Where other written sources have been quoted, then:
  - a. Their words have been re-written but the general information attributed to them has been referenced
  - b. Where exact words have been used, then their writing has been placed in italics and inside quotation marks, and referenced.
5. This thesis does not contain text, graphics or tables copied and pasted from the internet, unless specifically acknowledged, and the source being detailed in the thesis and in the References sections.

Signed:.....

## TABLE OF CONTENTS

ABSTRACT.....	ii
PREFACE.....	iv
DECLARATION OF PLAGIARISM.....	v
TABLE OF CONTENTS.....	vi
LIST OF TABLES.....	xi
LIST OF FIGURES.....	xii
ABBREVIATIONS.....	xviii
ACKNOWLEDGEMENTS.....	xxi
1 INTRODUCTION AND LITERATURE REVIEW.....	1
1.1 The eye.....	1
1.2 The anterior segment of the eye.....	2
1.3 The cornea.....	3
1.4 The corneal endothelium.....	5
1.5 Embryonic development of the anterior segment of the eye.....	7
1.6 Postnatal development – morphological and proliferative changes associated with eyelid opening.....	11
1.7 Key regulatory genes and signaling molecules in corneal endothelial development.....	13
1.7.1 The role of <i>Foxc1</i> and <i>Pitx2</i> in development.....	13
1.7.2 The role of the lens in corneal endothelial development.....	15
1.7.3 Key signaling molecules secreted by the lens during corneal endothelial development – transforming growth factors.....	16
1.8 Intercellular junctions in the corneal endothelium.....	16
1.8.1 The role of <i>Zo1</i> in corneal endothelial development and physiology.....	18
1.9 Water transport proteins – Aquaporin 1.....	20

1.10	The role of solute carriers in the pump function of the corneal endothelium.....	26
1.11	Research aims and objectives.....	29
2	MATERIALS AND METHODS.....	33
2.1	Animal Handling.....	33
2.1.1	Timed matings.....	33
2.2	Derivation of primary cultures.....	33
2.3	Immortalisation of primary cultures.....	35
2.4	Cell culture.....	36
2.5	RNA extraction.....	37
2.5.1	RNA quantification.....	39
2.5.2	Validation of RNA integrity.....	39
2.6	cDNA synthesis.....	40
2.6.1	Poly(A) Tailing.....	40
2.6.2	First strand cDNA synthesis.....	40
2.7	Conventional PCR.....	41
2.7.1	Agarose gel electrophoresis.....	42
2.8	Real-time quantitative PCR (qPCR).....	43
2.8.1	Statistics.....	44
2.9	Polyacrylamide gel electrophoresis (PAGE) and immunoblot analysis.....	45
2.9.1	Protein extraction and sample preparation.....	45
2.9.2	Protein quantification.....	46
2.9.2.1	Preparation of BCA standards.....	46
2.9.2.2	Preparation of BCA working reagent (WR).....	46
2.9.2.3	The microplate procedure.....	47
2.9.3	Polyacrylamide gel assembly.....	47
2.9.3.1	Sample preparation and loading into the gel.....	49
2.9.3.2	PAGE gel electrophoresis and protein transfer.....	49
2.9.3.3	Membrane blocking and antibody incubations.....	50
2.9.4	Imaging the western blot.....	52

2.9.5	Densitometry.....	54
2.10	Immunocytochemistry – confocal microscopy.....	54
2.10.1	Monolayer culture.....	55
2.10.2	Hanging drop culture.....	55
2.10.3	Immunostaining.....	56
2.10.3.1	Sample preparation of the monolayer and hanging drop cultures... 56	
2.10.3.2	Antibody incubations.....	56
2.10.4	Visualisation.....	58
2.11	<i>Foxc1</i> knockdown using <i>pSilencer</i> <sup>TM</sup> hygro kit.....	58
2.11.1	Overview.....	58
2.11.2	<i>Foxc1</i> -shRNA sequence.....	60
2.11.3	Cloning hairpin siRNA inserts into the <i>pSilencer</i> vector.....	60
2.11.3.1	Oligonucleotide annealing and ligation.....	60
2.11.3.2	Plasmid transformation.....	61
2.11.3.3	Plasmid mini-prep.....	61
2.11.3.4	PCR amplification to verify that the clones contained the siRNA insert.....	62
2.11.3.5	Digestion of purified plasmid DNA.....	63
2.11.4	Troubleshooting.....	64
2.11.4.1	Native polyacrylamide gel electrophoresis (PAGE).....	64
2.11.4.2	Plasmid midi-prep.....	64
2.11.5	Sequencing.....	66
3	RESULTS.....	67
3.1	Establishment of immortalised murine corneal endothelial cultures at various stages of development.....	67
3.2	Gene expression analysis.....	69
3.2.1	Validation of RNA integrity.....	69
3.2.2	Efficacy of primer sets confirmed by conventional PCR.....	69

3.2.3	mRNA expression patterns of key functional genes expressed in immortalised murine corneal endothelial cultures at various stages of development.....	70
3.2.3.1	Characterisation of <i>Zo1</i> mRNA expression levels.....	71
3.2.3.2	Characterisation of <i>Aqp1</i> mRNA expression levels.....	72
3.2.3.3	Characterisation of <i>Slc4a4</i> mRNA expression levels.....	73
3.2.3.4	Verification of the qPCR results obtained for the immortalised cell lines used in this study.....	74
3.3	Protein expression analysis.....	75
3.3.1	Protein expression patterns of <i>Zo1</i> and <i>Aqp1</i> determined by western blot analysis.....	75
3.3.2	Protein localisation patterns of <i>Zo1</i> and <i>Aqp1</i> determined by immunocytochemistry.....	78
3.4	Establishment of a stable <i>Foxc1</i> knockdown cell line.....	85
4	DISCUSSION.....	86
4.1	Establishing an <i>in vitro</i> model of corneal endothelial development.....	88
4.2	Characterising intercellular junctions present in the corneal endothelium by assessing <i>Zo1</i> gene and protein expression at various stages of development.....	89
4.3	Characterising the pump function of the corneal endothelium.....	97
4.3.1	Characterising the water channels present in corneal endothelial cells by assessing <i>Aqp1</i> gene and protein expression at various stages of development.....	97
4.3.2	Characterising the ion pumps present in corneal endothelial cells by assessing <i>Slc4a4</i> gene expression at various stages of development.....	102
4.4	Conclusion and future considerations.....	104
5	APPENDIX.....	106
5.1	The Minimum Information for Publication of Quantitative Real-time Experiments (MIQE).....	106
5.1.1	Experimental design.....	106
5.1.2	Sample information.....	107

5.1.3	RNA extraction.....	107
5.1.4	RNA quantification.....	108
5.1.5	RNA gel electrophoresis.....	109
5.1.6	Reverse transcription.....	109
5.1.7	Primer information.....	109
5.1.7.1	The Basic Alignment Search tool (BLAST).....	110
5.1.8	qPCR protocol.....	113
5.1.8.1	SYBR <sup>®</sup> Green JumpStart <sup>™</sup> Taq ReadyMix <sup>™</sup> mastermix.....	113
5.1.8.2	SYBR <sup>®</sup> select Master Mix.....	115
5.1.9	qPCR Melt analysis.....	117
5.1.10	Evaluation of qPCR reaction efficiency.....	122
5.1.11	Data analysis.....	125
5.1.12	Reference genes.....	128
5.1.13	<sup>-ΔΔCt</sup> Method.....	128
5.1.14	Statistics.....	129
5.2	Ponceau S staining used to detect total protein for western blot analysis.....	130
5.3	Immunocytochemistry controls.....	131
5.4	Recipes.....	135
5.4.1	General recipes.....	135
5.4.2	Immunoblot recipes.....	139
5.4.3	Immunocytochemistry recipes.....	143
5.4.4	Cloning recipes.....	145
5.5	Cloning results.....	149
6	REFERENCES.....	153

## LIST OF TABLES

Table 1.1: Tissue specific roles of aquaporin homologues and their associated experimental phenotype.....	24
Table 2.1: Primer sequences of the genes of interest and reference genes used in this study.....	41
Table 2.2: Antibodies (AB) used in this study for western blot analysis.....	51
Table 2.3: Antibodies (AB) used in this study for immunocytochemistry analysis.....	57

## LIST OF FIGURES

Figure 1.1: Structure of the adult human eye showing the anterior segment (A) and posterior segment (B).....	1
Figure 1.2: The flow of aqueous humor in the anterior segment of the eye.....	3
Figure 1.3: Structure of the eye and layers of the mature cornea.....	4
Figure 1.4: Histochemical staining of a mouse cornea (haematoxylin and eosin to stain the nuclei and membranes respectively, and periodic acid Schiff to stain mucopolysaccharides). EP - epithelium. S - stroma. EN - endothelium.....	4
Figure 1.5: Schematic diagram of murine eye development.....	8
Figure 1.6: Cell migration patterns in the developing eye. Neural crest cells are shown in green and mesodermal cells are shown in red.....	9
Figure 1.7: Eyelid development between E13.5 and E15.5. Presumptive corneal endothelium and stroma of neural crest derivation are shown in green. Developing eyelids are shown in blue.....	11
Figure 1.8: The functions of tight junctions termed ‘fence’; ‘barrier’ and ‘signaling’.....	17
Figure 1.9: The formation of tight junctions (A). Zo1 binding domains (B).....	19
Figure 1.10: Sites of aquaporin expression in the eye.....	23
Figure 1.11: Molecular mechanisms underlying the corneal endothelial pump function - Bicarbonate transport model for the corneal endothelium.....	27
Figure 1.12: Proposed method of band keratopathy caused by NBCe1 mutations (encoded by <i>Slc4a4</i> ) (A). Image adapted from Suzuki <i>et al.</i> , 2010. Calcific band keratopathy (B).....	29
Figure 1.13: Schematic representation of the research aims.....	31
Figure 2.1: The stepwise procedure for the derivation of peri-ocular mesenchyme cells from the eyes of mouse embryos. Black denotes the tissue of the eye, dark blue the position of the iris and lens within the eye and light blue the remainder of the embryo.....	34
Figure 2.2: BCA standard curve used to extrapolate unknown protein concentrations.....	47
Figure 2.3: Polyacrylamide gel assembly apparatus.....	48
Figure 2.4: The chemiluminescent detection system. After the primary antibody binds to the target protein, a complex with a HPR-linked secondary antibody is formed. The	

chemiluminescent substrate is added and emits light during enzyme catalysed decomposition.....	53
Figure 2.5: <i>pSilencer</i> hygro vector map.....	59
Figure 2.6: siRNA expression vector design.....	59
Figure 2.7: shRNA-2- <i>Foxc1</i> .....	60
Figure 2.8: A temperature gradient PCR of the T7 primers showing the optimal melting temperature at 57.3°C.....	63
Figure 3.1: Cell morphology at each stage of development in this model (400x). Scale bar is 16 $\mu$ m.....	68
Figure 3.2: RNA integrity of samples extracted from the cells at each stage of development. 1) MW; 2) E12.5; 3) E13.5; 4) MW; 5) E14.5; 6) E15.5; 7) P13. RNA extracted for the first biological repeat is shown as a representative image for all the biological replicates.....	69
Figure 3.3: PCR amplicons showing the efficacy of the primer set used in this study. 1) MW, 2) <i>Zol</i> (100bp), 3) <i>Zol</i> No template control (NTC), 4) <i>Aqp1</i> (143bp), 5) <i>Aqp1</i> NTC, 6) <i>Slc4a4</i> (151bp), 7) <i>Slc4a4</i> NTC. cDNA synthesised from E15.5 cells is shown as a representative image for all cell lines.....	70
Figure 3.4: The relative fold change in <i>Zol</i> mRNA expression in corneal endothelial cells at various stages of development. <i>Zol</i> was normalised to the geometric mean of two reference genes, <i>Hprt</i> and $\beta$ <i>actin</i> . Expression values are normalised to E125 which is set to 1. Values are presented as the mean $\pm$ SEM. A dissimilar character (a/b) denotes statistical significance ( $p < 0.05$ , $n = 3$ ).....	71
Figure 3.5: The relative fold change in <i>Aqp1</i> mRNA expression in corneal endothelial cells at various stages of development. <i>Aqp1</i> was normalised to the geometric mean of two reference genes, <i>Hprt</i> and $\beta$ <i>actin</i> . Expression values are normalised to E125 which is set to 1. Values are presented as the mean $\pm$ SEM. A dissimilar character (a/b) denotes statistical significance ( $p < 0.05$ , $n = 3$ ).....	72
Figure 3.6: The relative fold change in <i>Slc4a4</i> mRNA expression in corneal endothelial cells at various stages of development. <i>Slc4a4</i> was normalised to the geometric mean of two reference genes, <i>Hprt</i> and $\beta$ <i>actin</i> . Expression values are normalised to E125 which is set to 1. Values are presented as the mean $\pm$ SEM. A dissimilar character (a/b) denotes statistical significance ( $p < 0.05$ , $n = 3$ ).....	73
Figure 3.7: The relative fold change in <i>Aqp1</i> mRNA expression in non-immortalised corneal endothelial cells at various stages of development. <i>Aqp1</i> was normalised to the geometric mean of two reference genes, <i>Hprt</i> and $\beta$ <i>actin</i> . Expression values are normalised to E12.5 which is set at 1. The results depicted represent one experiment.....	74

Figure 3.8: Western blot image of Zo1 protein expression at different stages of corneal endothelial development. This is a representative image (n=3).....	75
Figure 3.9: Western blot image of glycosylated and unglycosylated Aqp1 protein expression at different stages of corneal endothelial development. This is a representative image (n=3).....	76
Figure 3.10: Densitometric analysis of Zo1 protein expression relative to the total protein extracted. Expression values are normalised to E12.5 which is set at 1. Values are presented as the mean $\pm$ SEM (n=3).....	77
Figure 3.11: Densitometric analysis of glycosylated and unglycosylated Aqp1 protein expression relative to the total protein extracted. Expression values are normalised to E12.5 which is set at 1. Values are presented as the mean $\pm$ SEM (n=3).....	78
Figure 3.12: 63x confocal microscopy image of monolayer cultures for Zo1. A) DAPI stained cells B) Zo1 stained cells C) Merged DAPI and Zo1 image. PN=perinuclear staining of Zo1. Scale bar is 20 $\mu$ m.....	79
Figure 3.13: 63x confocal microscopy image of hanging drop cultures for Zo1. A) DAPI stained cells B) Zo1 stained cells C) Merged DAPI and Zo1 image. CM=membrane localisation of Zo1. Scale bar is 20 $\mu$ m.....	81
Figure 3.14: 63x confocal microscopy image of monolayer cultures for Aqp1. A) DAPI stained cells B) Aqp1 stained cells C) Merged DAPI and Aqp1 image. The antibody recognises both glycosylated and unglycosylated protein. PN= perinuclear localisation of Aqp1. CM=membrane localisation of Aqp1. Scale bar is 20 $\mu$ m.....	82
Figure 3.15: 63x confocal microscopy image of hanging drop cultures for Aqp1. A) DAPI stained cells B) Aqp1 stained cells C) Merged DAPI and Aqp1 image. CM=membrane localisation of Aqp1. Scale bar is 20 $\mu$ m.....	84
Figure 4.1: A patient presenting with a severe form of ARS with iris hypoplasia, peripheral anterior synechiae and a prominent Schwalbe's line.....	86
Figure 4.2: Endothelial junction maturation in WT mice at P14 and P30. Red staining represents Zo1 expression in the corneal endothelium of WT mouse corneas. (A) Zo1 is expressed in the apical and lateral corneal endothelial membrane at P14. (B, C) Zo1 expression becomes localised to the lateral membrane at P30. The yellow box in (B) outlines the area in (C). Scale bar is 40 $\mu$ m.....	94
Figure 5.1: <i>In silico</i> screen of RNA quantification using a Spectrophotometer ND1000 (V3.5.2 software).....	108

Figure 5.2: <i>In silico</i> screen of the <i>Zo1</i> primer BLAST against the <i>Mus musculus</i> genome. <i>Zo1</i> is also referred to as tight junction protein ( <i>Tjp1</i> ).....	110
Figure 5.3: <i>In silico</i> screen of the <i>Aqp1</i> primer BLAST against the <i>Mus musculus</i> genome.....	111
Figure 5.4: <i>In silico</i> screen of the <i>Slc4a4</i> primer BLAST against the <i>Mus musculus</i> genome.....	111
Figure 5.5: <i>In silico</i> screen of the <i>Hprt</i> primer BLAST against the <i>Mus musculus</i> genome.....	112
Figure 5.6: <i>In silico</i> screen of the $\beta$ -actin primer BLAST against the <i>Mus musculus</i> genome.....	112
Figure 5.7: The qPCR cycling protocol using SYBR <sup>®</sup> Green JumpStart <sup>™</sup> Taq ReadyMix <sup>™</sup> mastermix (Sigma-Aldrich <sup>®</sup> , USA).....	114
Figure 5.8: Amplification curves of $\beta$ actin (A); <i>Hprt</i> (B) and <i>SLC4a4</i> (C) amplified with SYBR <sup>®</sup> Green JumpStart <sup>™</sup> Taq ReadyMix <sup>™</sup> mastermix.....	115
Figure 5.9: The qPCR cycling protocol using SYBR <sup>®</sup> Select Master Mix (Applied Biosystems), which requires an additional activation temperature at 50°C for 2 minutes before the initial denaturation.....	116
Figure 5.10: Amplification curves of $\beta$ -actin (A); <i>Hprt</i> (B) and <i>SLC4a4</i> (C) amplified with SYBR select mastermix.....	117
Figure 5.11: Melt curve analysis and agarose gel verification of the <i>Zo1</i> primer set. <i>Zo1</i> qPCR melting temperature at 80.14°C and a product size of 100bp.....	118
Figure 5.12: Melt curve analysis and agarose gel verification of the <i>Aqp1</i> primer set. <i>Aqp1</i> qPCR melting temperature at 85.94°C and a product size of 143bp.....	119
Figure 5.13: Melt curve analysis and agarose gel verification of the <i>Slc4a4</i> primer set. <i>Slc4a4</i> qPCR melting temperature at 84.02°C and a product size of 151bp.....	120
Figure 5.14: Melt curve analysis and agarose gel verification of the <i>Hprt</i> primer set. <i>Hprt</i> qPCR melting temperature at 80.03°C and a product size of 180bp.....	121
Figure 5.15: Melt curve analysis and agarose gel verification of the $\beta$ -actin primer set. <i>B-actin</i> qPCR melting temperature at 82.23°C and a product size of 104bp.....	122
Figure 5.16: Linear analysis of a) <i>Zo1</i> ( $r^2 = 0.9897$ ; reaction efficiency = 140.41%, n=3), b) <i>Aqp1</i> ( $r^2 = 0.9766$ ; reaction efficiency = 73.94%, n=3), c) <i>Slc4a4</i> ( $r^2 = 0.9353$ ; reaction efficiency = 168.31%, n=3), d) <i>Hprt</i> ( $r^2 = 0.9994$ ; reaction efficiency = 106%, n=3), e) $\beta$ -actin ( $r^2 = 0.9812$ ; reaction efficiency = 64.68%, n=3).....	123

Figure 5.17: A QC summary of the parameters used to exclude reactions from the analyses, as shown in the HID Real-Time PCR Analysis Software program.....	126
Figure 5.18: Melt curve analysis for an <i>Aqp1</i> NTC control with a melting temperature at 66.69°C.....	127
Figure 5.19: Melt curve analysis for an <i>Aqp1</i> ‘no-RT’ control with a melting temperature at 64.84°C.....	127
Figure 5.20: Ponceau S image of Aqp1 protein expression at different stages of corneal endothelial development. This is a single representative image.....	130
Figure 5.21: 63x confocal microscopy image showing no-primary antibody control for Zo1 monolayer cultures. A) DAPI stained cells B) no-primary control C) Merged image. Scale bar is 20 $\mu\text{m}$ .....	131
Figure 5.22: 63x confocal microscopy image showing no-secondary antibody control for Zo1 monolayer cultures. A) DAPI stained cells B) no-secondary control C) Merged image. Scale bar is 20 $\mu\text{m}$ .....	132
Figure 5.23: 63x confocal microscopy image showing no-primary antibody control for Aqp1 monolayer cultures. A) DAPI stained cells B) no-primary control C) Merged image. Scale bar is 20 $\mu\text{m}$ .....	132
Figure 5.24: 63x confocal microscopy image showing no-secondary antibody control for Aqp1 monolayer cultures. A) DAPI stained cells B) no-secondary control C) Merged image. Scale bar is 20 $\mu\text{m}$ .....	133
Figure 5.25: 25x confocal microscopy image showing no-primary antibody control for Zo1 hanging drop cultures. A) DAPI stained cells B) no-primary control C) Merged image. Scale bar is 50 $\mu\text{m}$ .....	133
Figure 5.26: 25x confocal microscopy image showing no-secondary antibody control for Zo1 hanging drop cultures. A) DAPI stained cells B) no-secondary control C) Merged image. Scale bar is 50 $\mu\text{m}$ .....	134
Figure 5.27: 25x confocal microscopy image showing no-primary antibody control for Aqp1 hanging drop cultures. A) DAPI stained cells B) no-primary control C) Merged image. Scale bar is 50 $\mu\text{m}$ .....	134
Figure 5.28: 25x confocal microscopy image showing no-secondary antibody control for Aqp1 hanging drop cultures. A) DAPI stained cells B) no-secondary control C) Merged image. Scale bar is 50 $\mu\text{m}$ .....	135
Figure 5.29: T7 sequencing primers used for conventional PCR to verify that the clones contained the siRNA insert.....	147

Figure 5.30: siRNA insert. The annealed oligonucleotides were separated on a 1.5% agarose gel to confirm the insert size of 65bp.....	150
Figure 5.31: PCR products using T7 primers. The expected product size was 590bp....	150
Figure 5.32: PCR and restriction digest products separated on an 8% native PAGE gel. 1) MW (1Kb); 2) MW (50bp); 3-6) PCR products (590bp); 7-14) restriction digest products. Vector size is 4900bp. The siRNA insert (65bp) was not detected.....	151
Figure 5.33: <i>In silico</i> screen of the sequencing results obtained from BiQ Analyzer Software version 2.00. The insert was not 100% similar to the designed oligonucleotides.....	152

## ABBREVIATIONS

ANOVA	Analysis of Variance
AQP	Aquaporin
ARS	Axen-Reiger Syndrome
ASD	Anterior segment dysgenesis
ATPase	Adenotriphosphatase
BCA	Bicinchoninic Acid
BK	Bullous Keratopathy
BLAST	Basic Alignment Search Tool
BSA	Bovine serum albumin
cDNA	Complimentary DNA
CHED	Congenital hereditary endothelial dystrophy
DABCO	1,4-diazabicyclo [2.2.2]octane
DAPI	4'6,-diamidino-2-phenylindole
DMEM	Dulbecco's modified essential eagle's medium
DNA	Deoxyribonucleic acid
E	Embryonic day
<i>E.coli</i>	<i>Eschericia coli</i>
ECM	Extracellular matrix
EOB	Eye-open-at-birth
FBS	Foetal bovine serum
Gapdh	Glyceraldehyde-3- phosphate dehydrogenase
GTPase	Guanosinetriphosphate hydrolase
HCO <sub>3</sub> <sup>-</sup>	Bicarbonate ions
HIV	Human immunodeficiency virus
HPR	Horseradish peroxidase

IOP	Intraocular pressure
iPS	cells Induced pluripotent stem cells
JAM	Junction adhesion molecule
KO	Knockout
LB	Luria-Bertani
MDCK-1	Canine kidney cells type I
MET	Mesenchyme to epithelial transition
MIQE	Minimum information for publication of quantitative real-time PCR experiments
MW	Molecular weight marker
No-RT	No-reverse transcriptase
NTC	No template control
P	Postnatal day
PAGE	Polyacrylamide gel electrophoresis
PAMR	Perijunctional actomyosin ring
PBS	Phosphate buffered saline
PCR	Polymerase chain reaction
POM	Periocular mesenchyme
PPMD	Posterior polymorphous dystrophy
qPCR	Quantitative real-time PCR
RIPA	Radio-immunoprecipitation assay
RNA	Ribonucleic acid
RT	Reverse transcriptase
SEM	Standard error mean
siRNA	small interfering RNA
SOB	Super optimal broth

SOC	SOB with catabolite repression
TBS-T	Tris-buffered saline-tween
TF	Transcription factor
TGF	Transforming growth factor
WR	Working Reagent
WT	Wild type

## ACKNOWLEDGMENTS

First and foremost, I would like to thank my supervisor Dr Paula Sommer for your guidance and support throughout this research project.

Thank you to Dr Dalene Vosloo, Dr Andre Vosloo, and Prof. Jenny Lamb for the use of your laboratory and equipment.

To my family, friends and the postgraduate students of the Sommer lab and School of Life Sciences, UKZN; thank you for your continuous assistance and support.

Thank you to the staff at the Microscopy unit, UKZN Pietermaritzburg campus, for your assistance with confocal microscopy.

To the staff at Mega Petroleum (Pty) Ltd., your assistance is greatly appreciated.

Lastly, thank you to the National Research Foundation (NRF) for the financial support towards this research.

## 1. INTRODUCTION AND LITERATURE REVIEW

### 1.1 The eye

The mammalian eye is a complex sensory organ composed of an array of interdependent tissues that function together to ensure vision (Figure 1.1) (Kidson *et al.*, 1999). Optimal functioning of the eye depends on co-ordinated interactions between the structures of the functionally distinct anterior and posterior segments (Reneker *et al.*, 2000). The anterior segment consists of the anterior chamber filled with aqueous humor, the lens, iris, ciliary body, trabecular meshwork and the cornea (Figure 1.1 A). Together, the lens and the cornea play a role in refracting and regulating light as it enters the eye (Thut *et al.*, 2001). The posterior segment consists of the eye muscle, hyaloid membrane, optic nerve, choroid, sclera, retina and vitreous humor (Figure 1.1 B). These components act to convert refracted light transmitted by structures of the anterior segment into electrical impulses which are then transduced to the brain to produce an image (Cvekl and Tamm, 2004).

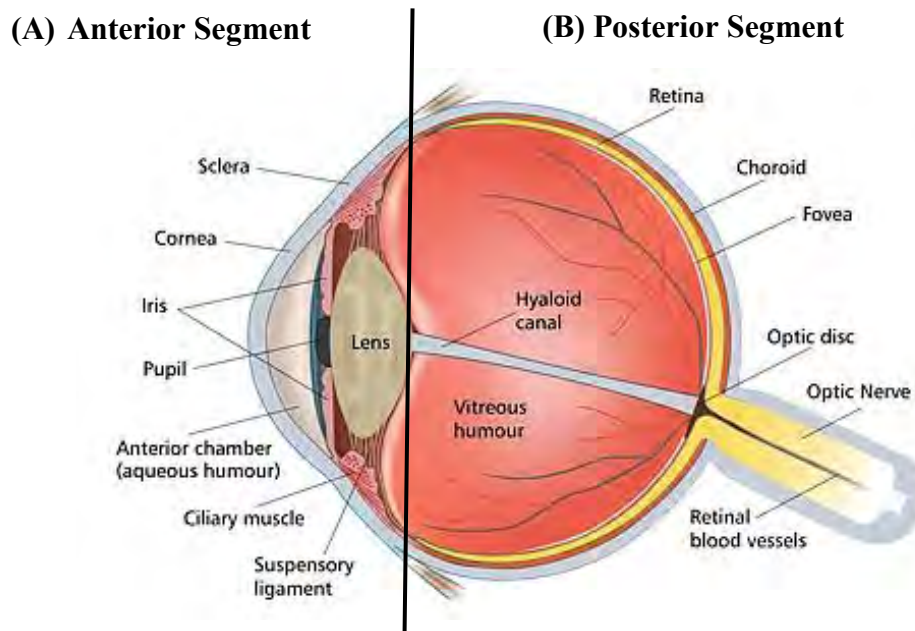


Figure 1.1: Structure of the adult human eye showing the anterior segment (A) and posterior segment (B). Image adapted from <http://focuseye.com/facts-info/the-anatomy-of-the-eye/>.

Light passes through the transparent cornea which serves as the first point of refraction. Refracted light then passes through the anterior chamber and through the opening in the iris (pigmented structure of the eye) known as the pupil. The iris controls the diameter of the pupil and thus the amount of refracted light that enters the eye. After passing through the cornea and the iris, light is further refracted by the lens and focused onto the retina. The retina is a layer of photosensitive rods and cones that convert light waves into electrical impulses that are transmitted to the brain by the optic nerve to produce an image. Preservation of the integrity and arrangement of the ocular structures in both segments is essential as any abnormalities can lead to impaired vision and possibly vision loss (Reneker *et al.*, 2000, Araujo Silva *et al.*, 2011).

## **1.2 The anterior segment of the eye**

The structures of the posterior segment are functionally dependent on the structures of the anterior segment to ensure vision. The cornea and the lens, which provide the refractive power of the eye, are both avascular structures allowing for optimal transparency (Cvekl and Tamm, 2004). Their nutrition is derived from the aqueous humor produced by the ciliary bodies (Kidson *et al.*, 1999, Cvekl and Tamm, 2004). The avascular stroma, which makes up 90% of the murine cornea, consists of regularly spaced collagen fibrils that reduce light scatter to ensure corneal transparency (Bonanno, 2012). The trabecular meshwork and Schlemm's canal are involved in the outflow of aqueous humor (Cvekl and Tamm, 2004, Ito and Walter, 2014). The trabecular meshwork is a porous network of cells located between the iris and the cornea. Aqueous humor exits the eye through the trabecular meshwork into Schlemm's canal, subsequently entering the venous system (Figure 1.2) (Kidson *et al.*, 1999, Cvekl and Tamm, 2004).

The trabecular network provides resistance to the flow of aqueous humor as it exits the eye. This resistance creates intraocular pressure (IOP) that is slightly greater than that of the

veins outside the eye. Regulated IOP is required to maintain the correct shape and curvature of the eye. IOP depends on the ability of the anterior segment structures to balance the production of aqueous humor with its exit from the eye (Thut *et al.*, 2001). Elevated IOP affects the distance between the refractive surfaces of the cornea and lens, and the retina. Consequently, image formation is distorted and vision becomes impaired (Kidson *et al.*, 1999, Cvekl and Tamm, 2004). Elevated IOP is a key risk factor for glaucoma which is a progressive blinding condition characterized by optic nerve damage and vision loss (Thut *et al.*, 2001, Ito and Walter, 2014).

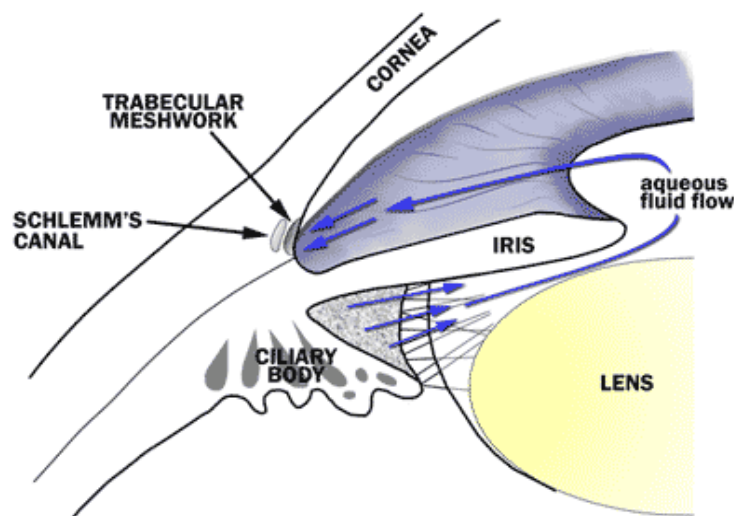


Figure 1.2: The flow of aqueous humor in the anterior segment of the eye. Image obtained from: <https://www.google.co.za/search?q=aqueous+humor+outflow+pathway>

### 1.3 The cornea

The highly specialised transparent and avascular cornea consists of six distinct layers: the outer epithelium, Bowman's layer, the stroma, Dua's layer, Descemet's membrane and the corneal endothelium (Figures 1.3 and 1.4) (Kidson *et al.*, 1999, Reneker *et al.*, 2000).

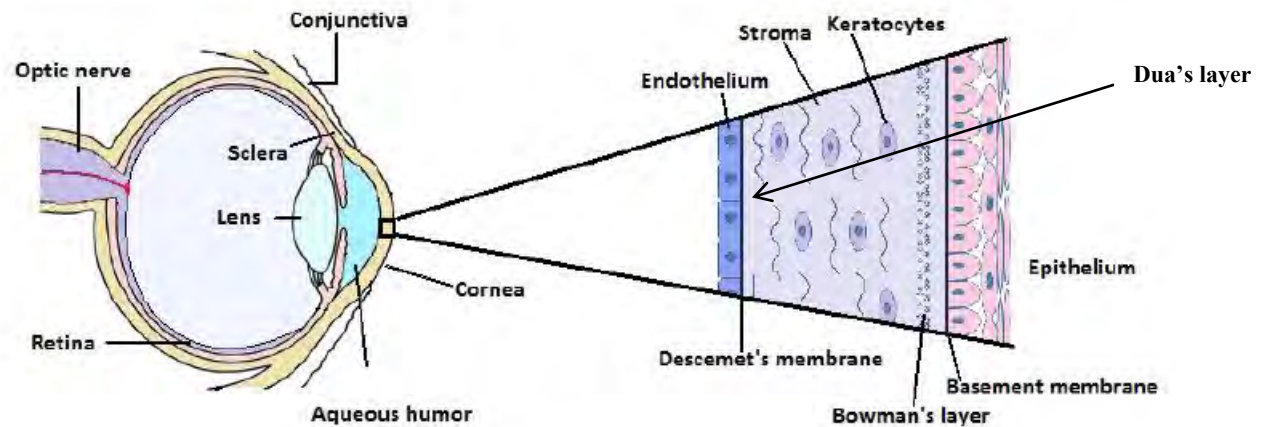


Figure 1.3: Structure of the eye and layers of the mature cornea. Image adapted from Parekh *et al.* (2013).

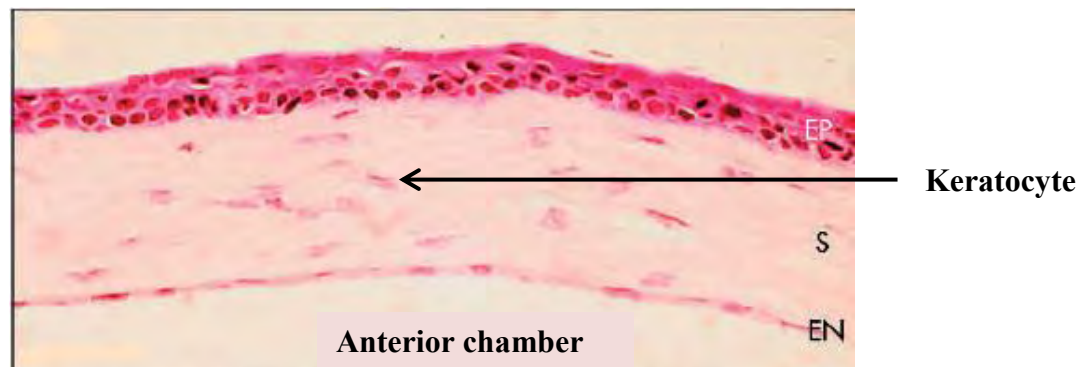


Figure 1.4: Histochemical staining of a mouse cornea (haematoxylin and eosin to stain the nuclei and membranes respectively, and periodic acid Schiff to stain mucopolysaccharides). EP - epithelium. S - stroma. EN - endothelium. Image adapted from Ramaldo *et al.* (2004).

The anterior surface of the mature cornea is covered with stratified squamous nonkeratinised epithelium that rests firmly on Bowman's layer, an acellular layer composed of collagen fibrils embedded in a matrix of glycosaminoglycans. The corneal stroma consists of type I collagen fibrils and keratocytes (specialised fibroblast cells) that produce collagen and other essential substances such as glycosaminoglycans (Flügel-Koch *et al.*, 2002, Macnamara *et al.*, 2004). Glycosaminoglycans are hydrophilic proteins that control the regular spaces between the stromal fibrils, thus playing a role in the maintenance of

corneal hydration and transparency, both of which are essential for optical function (Bonanno, 2012). The recently discovered Dua's layer is located between the corneal stroma and Descemet's membrane. Although relatively thin, Dua's layer is a resilient collagenous layer that forms a barrier between stromal keratocytes and Descemet's membrane (Dua *et al.*, 2013). Descemet's membrane is a thick elastic layer located beneath the stroma that serves as a basement membrane for the corneal endothelium (Bonanno, 2012).

#### **1.4 The corneal endothelium**

The mature corneal endothelium is physiologically the most important layer of the cornea. It consists of a monolayer of mitotically inactive hexagonal cells (Bi *et al.*, 2013, Kim *et al.*, 2014), joined by tight junctions (Pajoohesh-Ganji and Stepp, 2005), that form a barrier between the stroma and the aqueous humor in the anterior chamber (Araujo Silva *et al.*, 2011). Corneal deturgescence is the active physiological process of maintaining a relatively dehydrated state required for transparency. The corneal endothelium is responsible for transporting nutrients between the stroma and the aqueous humor. Nutrients that are pumped out of the aqueous humor into the stroma passively diffuse throughout the entire cornea and nourish the epithelial cells and stromal fibroblasts. Furthermore, the corneal endothelium is responsible for pumping out excess fluid and metabolic waste from the stromal and epithelial cells into the aqueous humor to prevent swelling and maintain deturgescence (Reneker *et al.*, 2000, Pajoohesh-Ganji and Stepp, 2005, Peh *et al.*, 2011).

The physical separation of the stroma and aqueous humor is important as excess fluid in the stroma can disrupt the organisation of the keratocytes and collagen fibrils, which would reduce corneal transparency (Kidson *et al.*, 1999, Reneker *et al.*, 2000, Pajoohesh-Ganji and Stepp, 2005). These corneal layers are collectively responsible for transmitting and refracting light as part of the optical system. They also form a protective barrier against

infections and chemical or physical injury to the eye, thus protecting the delicate intraocular structures (Flügel-Koch *et al.*, 2002, Kao *et al.*, 2008).

Corneal endothelial cells have a mitochondria-rich cytoplasm that is essential for the cells to act as a fluid pump. They have a well-developed Golgi apparatus that is required for the production and transport of extracellular proteins that carry out the pump function (Besharse *et al.*, 2010, Bonanno, 2012). Bowman's layer is embedded in a matrix of negatively charged glycosaminoglycans that are bound to proteoglycans, causing a constant influx of cations into the stroma. These cations are accompanied by water due to osmosis, thus causing corneal stromal swelling. The regular aqueous-filled spaces between the collagen fibers in the stroma are necessary for entry of light and therefore transparency (Besharse *et al.*, 2010). Excess water can alter the spacing between the collagen fibrils, thus increasing light scatter and causing opacity (Thiagarajah and Verkman, 2002, Bonanno, 2012). Therefore, the principle function of the corneal endothelium is to regulate the pump function in order to maintain optimal stromal hydration and preserve transparency.

The cornea is responsible for 70-75% of the refractive power of the eye (Zieske, 2004). This refractive power greatly depends on corneal deturgescence. Structural and/functional disruption of the endothelium can compromise its pump function, leading to corneal edema and subsequent vision loss (Macnamara *et al.*, 2004). A minimum cell density of 500cells/mm<sup>2</sup> is required to actively pump fluid and nutrients from the stroma into the anterior chamber (Fujita *et al.*, 2013, Parekh *et al.*, 2013). Unlike epithelial cells that undergo continuous self-renewal, corneal endothelial cells do not proliferate *in vivo* as they are arrested in the G<sub>1</sub> phase. As they are unable to proliferate, a decrease in cell density through aging, trauma or disease causes them to spread out to maintain a continuous monolayer. When the endothelial layer becomes too thin, the pump function is compromised and it can no longer maintain corneal deturgescence (Peh *et al.*, 2011, Parekh *et al.*, 2013).

## 1.5 Embryonic development of the anterior segment of the eye

Embryonic development of the anterior segment depends on co-ordinated cellular events and precise molecular cues that direct cellular migration, proliferation and differentiation (Kao *et al.*, 2008). Much of our knowledge is derived from research based on animal models that are genetically and physiologically similar to humans such as chick and mouse (Kidson *et al.*, 1999, Reneker *et al.*, 2000, Ittner *et al.*, 2005).

The earliest known molecular event in vertebrate eye development is the formation of the eye field within the anterior neural plate during gastrulation. Activation of a network of transcription factors within the eye field initiates anterior segment morphogenesis. Structures of the anterior segment are constructed from four embryonic tissues: neural ectoderm, surface ectoderm, neural crest and mesoderm mesenchyme (Chow and Lang, 2001, Gage and Zacharias, 2009, Ju *et al.*, 2012). Mesenchyme cells, derived from predominantly neural crest with contributions from lateral plate mesoderm, are collectively known as periocular mesenchyme (POM) (Beebe and Coats, 2000, Langenberg *et al.*, 2008).

Eye development is initiated by a thickening of the neural ectoderm to form the optic pits, which marks the first morphologically distinct phase in anterior segment morphogenesis (Gage and Zacharias, 2009).

In the mouse, by embryonic day (E) 9 the optic pits mature to form the optic vesicles which extend towards the outer surface neural ectoderm on either side of the diencephalon of the developing head (Figure 1.5 A) (Chow and Lang, 2001). The optic vesicle extends laterally until it makes contact with the outer surface ectoderm (Cvekl and Tamm, 2004, Gage and Zacharias, 2009). The outer surface ectoderm is a region of head ectoderm that is destined

to contribute to the lens, epithelia of the cornea, conjunctiva and limbus, and the eyelid epidermis (Chow and Lang, 2001). Direct contact between the optic vesicle and outer surface ectoderm induces the formation of the lens placode from a region of competent surface ectoderm (Cvekl and Tamm, 2004).

At E10, the lens placode invaginates towards the head midline to form the lens pit and eventually detaches from the surrounding surface ectoderm to form the lens vesicle (fated to become the mature lens) by E11 (Reneker *et al.*, 2000, Gage and Zacharias, 2009). Lens development has been well characterized by Chow and Lang (2001). As the lens vesicle forms, the optic vesicle is transformed into the optic cup (Figure 1.5 B) (Cvekl and Tamm, 2004, Gage and Zacharias, 2009). The inner layer of the optic cup will form the retina and the outer layer will form the pigmented retinal epithelium. Furthermore, cells lining the anterior surface of the optic cup will ultimately become the epithelial cells of the ciliary body and the iris (Figure 1.5 C and D) (Thut *et al.*, 2001, Cvekl and Tamm, 2004, Gage and Zacharias, 2009).

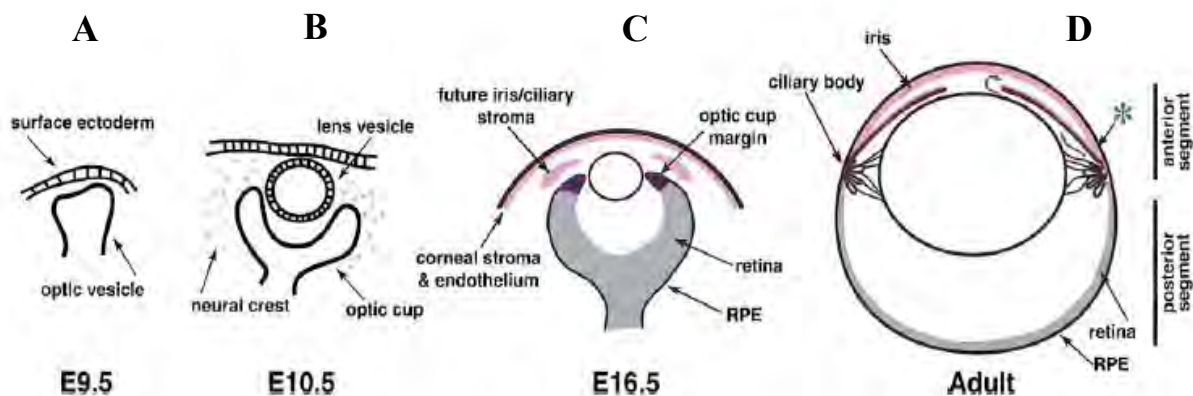


Figure 1.5: Schematic diagram of murine eye development. Image adapted from Thut *et al.*, 2001.

From E12, POM cells of predominantly neural crest derivation migrate between the anterior portion of the developing lens and the surface ectoderm (Figure 1.6). This region of the surface ectoderm will mature into the corneal epithelium. Between E12.5 and E13.5, POM cells that cover the anterior lens and optic cup respond to signals from the developing lens and surrounding cells, thereby initiating corneal endothelial development by a process of mesenchyme-to-epithelial transition (Thut *et al.*, 2001, Gage *et al.*, 2005).

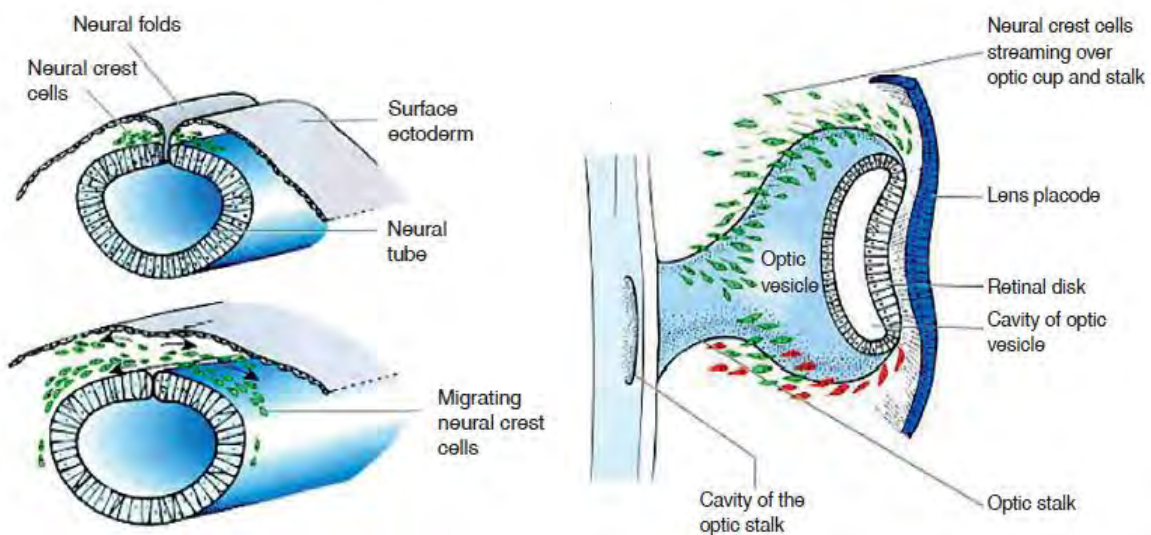


Figure 1.6: Cell migration patterns in the developing eye. Neural crest cells are shown in green and mesodermal cells are shown in red. Image adapted from Besharse *et al.*, 2010.

Between E13.5 and E14.5, the developing corneal endothelium dissociates from the lens. The resultant space between the corneal endothelium and the lens will become the fluid-filled anterior chamber. By E15, corneal endothelial precursor cells mature to form tight junctions and eventually develop into a monolayer of corneal endothelial cells (Gage and Zacharias, 2009). POM cells between the presumptive corneal epithelium and differentiated corneal endothelium differentiate into stromal keratocytes. By late gestation in the mouse, these stromal keratocytes begin to synthesise collagen and produce an extracellular matrix

(ECM) that is required to maintain corneal transparency. Precursor cells of the ciliary body and iris migrate into the angle between the iris and the cornea, known as the iridocorneal angle. Once the cornea is completely separated from the lens, these precursor cells become pigmented and mature into the epithelial cells of the ciliary body and the iris (Cvekl and Tamm, 2004, Gage *et al.*, 2005, Zhang *et al.*, 2007).

The trabecular meshwork and Schlemm's canal are the last structures to differentiate during anterior segment development (Cvekl and Tamm, 2004). Both structures develop in the iridocorneal angle when a dense mass of mesenchyme cells elongates and separates. The resultant spaces between the cells become filled with extracellular fibers that are organised into lamella, thus forming a sieve-like trabecular meshwork (Kidson *et al.*, 1999). This sieve-like arrangement is functionally important as it facilitates the outflow of aqueous humor. Scleral vessels next to the iridocorneal angle fuse to form the Schlemm's canal which is in direct contact with the outer side of the trabecular meshwork (Cvekl and Tamm, 2004).

A set of mesenchyme cells with a stellate phenotype develop cell-cell contacts between the lamella of the trabecular meshwork and the endothelial lining of Schlemm's canal. The trabecular network and Schlemm's canal are directly responsible for aqueous humor outflow, thus these mesenchyme cells are particularly important as they provide the resistance that is required for aqueous humor outflow. By providing resistance to aqueous humor outflow, they play an important role in maintaining optimal IOP (Kidson *et al.*, 1999, Cvekl and Tamm, 2004).

## 1.6 Postnatal development - morphological and proliferative changes associated with eyelid opening

Eyelid development is initiated at E13.5 when the surface ectoderm adjacent to the developing cornea folds to form the lid buds (Figure 1.7). At this stage, the eyelids are simply surface ectoderm overlying undifferentiated mesenchyme.

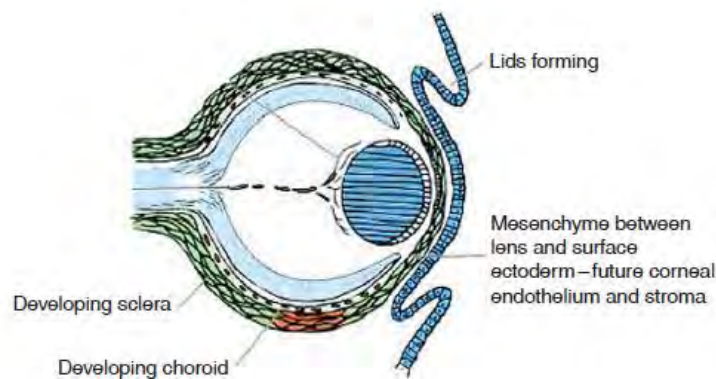


Figure 1.7: Eyelid development between E13.5 and E15.5. Presumptive corneal endothelium and stroma of neural crest derivation are shown in green. Developing eyelids are shown in blue. Image adapted from Besharse *et al.*, 2010.

Between E13.5 and E15.5, the eyelid buds continue to grow and extend over the ocular surface to form an outer epithelial layer that will become the epidermis and an inner epithelial layer that will become the conjunctiva (Kao *et al.*, 2008, Gage and Zacharias, 2009). The conjunctiva lines the inner surface of the eyelid. Mesenchyme cells, derived from migrating neural crest, differentiate into muscle cells, tarsal plate cells and other connective tissue within the eyelid.

By E16, the epithelial cells along the edge of the upper and lower eyelid start to migrate over the developing cornea and subsequently fuse to form desmosomal junctions. Between E17 and early postnatal stages, appendix structures such as hair follicles, eyelid muscles,

cilia and lacrimal glands start to develop. Mouse eyelids are closed at birth and open at postnatal day 13 (P13) when the eyelid epithelial cells undergo apoptosis and necrosis at the fusion junctions causing the lids to open. By this stage, the corneal and conjunctival epithelia are completely matured, suggesting that closed eyelids at birth also serve as a protective barrier for the immature ocular tissues that are vulnerable to harmful environmental factors (Kao *et al.*, 2008).

Eyelid opening and epithelial stratification occur simultaneously. Eyelid opening exposes the eye to various environmental factors including changing oxygen levels, light and pathogens. It is therefore possible that the stratified epithelium serves as a protective barrier against fluctuating environmental factors, as well as fluid loss (Norman *et al.*, 2004). Kao *et al.* (2008) hypothesised that closed eyelids at birth prevent the epithelium from keratinisation, thus maintaining corneal transparency.

In the mouse, the epithelial cells undergo an exceptional level of differentiation that begins prior to eyelid opening. Between E10 and P13, the number of epithelial cell layers increases and the shape of the cells change from a flattened, ovoid phenotype to a more cuboidal phenotype following eyelid opening at P13. The epithelial cells proliferate to form intercellular junctions, which then become desmosomes. The mature cornea contains 3-4 layers of desmosomes that prevent fluid loss and provide protection against pathogens (Zieske, 2004). Defects in eyelid closure cause an eye-open-at-birth (EOB) phenotype that exposes the delicate immature ocular structures to secondary defects (Kao *et al.*, 2008).

## **1.7 Key regulatory genes and signaling molecules in corneal endothelial development**

Cellular migration and differentiation are directed by tissue specific expression of key regulatory genes and signaling molecules such as transcription factors, growth factors, nuclear proteins and enzymes, and other signal transduction molecules (Kao *et al.*, 2008, Acharya *et al.*, 2011). Transcription factors (TFs) are modular proteins that facilitate DNA binding, trans-activation or trans-repression (Carlsson and Mahlapuu, 2002). These regulatory genes and signaling molecules initiate a series of inductive events that direct morphogenesis of neural crest derived structures in the anterior segment of the eye (Ittner *et al.*, 2005, Acharya *et al.*, 2011).

Based on literature to date, there is substantial evidence that POM cells migrate and differentiate into mature corneal endothelium under the influence of inductive signals from the lens and changes in key regulatory gene expression that direct this morphogenesis (Besharse *et al.*, 2010). However, the precise molecular mechanisms of corneal endothelial differentiation are not completely understood (Langenberg *et al.*, 2008).

Transgenic and knockout models have been valuable tools in identifying and understanding the roles of genes and growth factors that are essential for corneal endothelial morphogenesis (Kao *et al.*, 2008).

### **1.7.1 The role of *Foxc1* and *Pitx2* in development**

TFs bind to DNA in a specific manner that plays a role in controlling mRNA synthesis of downstream targets. *Foxc1*, previously known as FKHL7 in humans or *Mfl* (the murine homologue), is a member of the forkhead/winged helix family of TFs that are characterized by a conserved 110 amino acid DNA-binding domain known as the forkhead domain.

*Foxc1* is widely expressed during embryogenesis and plays an important role in cell fate determination (Kume *et al.*, 2000, Kume *et al.*, 2001, Sommer *et al.*, 2006). *Foxc1* expression is detected as early as E7.5 in neural crest cells and E12.5 POM cells in the developing eye (Kidson *et al.*, 1999).

*Pitx2* is a member of the paired-bicoid family of homeodomain transcription factors that are involved in various developmental processes, notably anterior segment morphogenesis (Berry *et al.*, 2006, Acharya *et al.*, 2011). In the developing mouse eye, *Pitx2* is expressed in POM cells, presumptive cornea and presumptive eyelids (Cvekl and Tamm, 2004). Both *Foxc1* and *Pitx2* are key regulatory TFs that direct differentiation of periorbital mesenchyme into corneal endothelium (Besharse *et al.*, 2010).

*Foxc1* and *Pitx2* are involved in numerous developmental processes. Mutations in either result in a wide range of defects with different clinical phenotypes (Cvekl and Tamm, 2004). *Foxc1* null mutants are born with multiple developmental defects including hydrocephalus, abnormal kidney and ureter development, as well as abnormal cardiovascular development (Kume *et al.*, 2000, Kume *et al.*, 2001). The anterior segment of the eye is severely defective in *Foxc1* null mice. The cornea fails to separate from the lens and the corneal endothelium is unable to differentiate (Kidson *et al.*, 1999). The precise role of *Foxc1* in during the development of the eye is extensively reviewed by Nishimura *et al.*, (2001).

*Pitx2* has been identified as a critical developmental gene as homozygous mutants die prenatally (Sowden, 2007). It is involved in the Nodal/Sonic hedgehog pathway that determines left/right axis formation during development (Hjalt *et al.*, 2000). Numerous studies provide compelling evidence that *Pitx2* plays an important role in anterior segment development (Hjalt *et al.*, 2000, Hjalt *et al.*, 2001, Berry *et al.*, 2006, Strungaru *et al.*,

2007). *Pitx2* knockout mice display a range of abnormalities that include a drastic increase in corneal thickness and a disorganised corneal endothelium due to uncontrolled POM cell migration. These results suggest that *Pitx2* controls the migration of presumptive corneal endothelium during murine corneal endothelial development (Gage *et al.*, 1999). *Pitx2* and *Foxc1* mutations are directly associated with Axenfeld-Reiger syndrome (ARS) (Nishimura *et al.*, 2001, Acharya *et al.*, 2011).

### **1.7.2 The role of the lens in corneal endothelial development**

Numerous studies have focused on identifying key organisers during eye development (Beebe and Coats, 2000, Thut *et al.*, 2001, Zhang *et al.*, 2007). Beebe and Coats (2000) investigated the role of the lens during avian eye development and found that complete ablation of the lens or replacement with a cellulose bead inhibited development of the corneal endothelium, corneal stroma, iris stroma and the anterior segment (Beebe and Coats, 2000). A study by Zhang *et al.* (2007) generated *DREAM-Tox176* transgenic mice to show that corneal endothelial precursors are unable to undergo mesenchymal-to-epithelial transition to form mature corneal endothelium in the absence of the lens. Furthermore, lens ablation disrupted differentiation of the iris and interactions between the neuroectoderm and ocular mesenchyme. These results support the hypothesis that the lens is a key organiser during eye development (Zhang *et al.*, 2007).

The lens produces key signaling molecules that are required for the expression of TFs *Foxc1* and *Pitx2* during corneal development (Ittner *et al.*, 2005). A recent study provides additional support for the role of the lens as a regulator of *Foxc1* and *Pitx2* expression during corneal endothelial development (Silla *et al.*, 2014). Apart from transforming growth factor  $\beta$ -2 (*TGF $\beta$ 2*), other signaling molecules that are produced and secreted by the lens have not been identified.

### **1.7.3 Key signaling molecules secreted by the lens during corneal endothelial development- transforming growth factors**

Transforming growth factors (TGFs) are a group of polypeptides that play important roles in cell differentiation and proliferation. TGFs are signaling molecules that are produced as a result of DNA binding to TFs (Besharse *et al.*, 2010). TGF- $\beta$  signaling is essential for normal corneal development as ligand inactivation or overexpression results in defective eye development (Saika *et al.*, 2001, Flügel-Koch *et al.*, 2002, Ittner *et al.*, 2005). Tgf- $\beta$  is expressed in the embryonic lens from E12.5 in wild type (WT) mice. Tgf- $\beta$ 2 null mice fail to develop a corneal endothelium as POM cells do not migrate over the developing lens (Saika *et al.*, 2001, Besharse *et al.*, 2010) and they exhibit a thin stromal layer compared to WT mice (Sanford *et al.*, 1997).

Although the importance of *Foxc1* and Tgf- $\beta$  expression in normal corneal development has been well established, few *Foxc1* downstream targets have been identified. Transforming growth factor  $\beta$ -1 induced transcript 4 (*Tgf $\beta$ 1i4*) has been identified as a downstream target of *Foxc1*, which provides a functional link between *Foxc1* and Tgf- $\beta$  and highlights their importance in eye development (Sommer *et al.*, 2006).

## **1.8 Intercellular junctions in the corneal endothelium**

Intercellular junctions play a pivotal role in cell-cell adhesion and communication. They are especially important in cells such as corneal endothelial cells that require selective permeability between neighboring cells (Besharse *et al.*, 2010). Intercellular junctions, namely gap, adherens and tight junctions, facilitate cell adhesion between adjacent cells, thus allowing the formation of a monolayer that is characteristic of corneal endothelial cells (Zhu *et al.*, 2008). The mature corneal endothelium expresses both adherens and tight junctions that facilitate cell adhesion and form a tight barrier respectively.

Cellular communication is regulated by the transport of molecules through the trans-cellular pathway (via the cytoplasm) and the para-cellular pathway (via spaces between cells). Tight junctions are essentially the cell-cell junctions that divide plasma membranes into apical and basolateral compartments and regulate the permeability of the para-cellular pathway (Ryeom *et al.*, 2000, Ban *et al.*, 2003).

The functions of tight junctions can therefore be described as the ‘fence’ function, ‘barrier’ function and signaling function (Kojima *et al.*, 2009). Tight junctions have a ‘barrier’ function as they are semipermeable and therefore inhibit the movement of solutes and water between paracellular spaces. By separating cells in apical and basolateral compartments, tight junctions create cell polarity and therefore exhibit a ‘fence’ function. The ‘signaling’ function of tight junction proteins was reviewed by Kojima *et al.*, (2009) in hepatocytes (Figure 1.8).

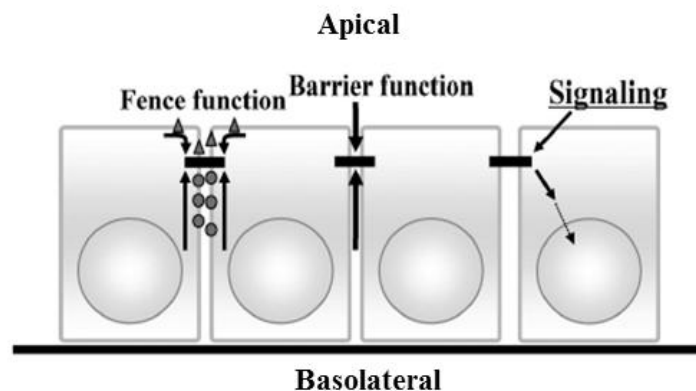


Figure 1.8: The functions of tight junctions termed ‘fence’; ‘barrier’ and ‘signaling’. Image adapted from Kojima *et al.* (2009).

The primary function of tight junctions is to regulate solute, ion and fluid transport between adjacent cells. Tight junctions consist of two main transmembrane proteins: claudins and occludins. Both claudins and occludins have extracellular domains that extend across the

plasma membranes of adjacent cells, thus forming a branching network that seals the spaces between cells. They connect to the actin cytoskeleton in the cell through a network of proteins known as zonula occludins (Zo) (Figure 1.9 A) (Niessen, 2007).

### **1.8.1 The role of *Zo1* in corneal endothelial development and physiology**

Zonula occludin-1 (Zo1) is a selectively semipermeable tight junction protein that belongs to the membrane-associated guanylate kinase (MAGuK) family of proteins (Ryeom *et al.*, 2000). Protein members of the MAGuK family have a cassette of protein binding domains that include one or more PSD95/dlg/Zo-1 (PDZ) domains, a SH3 domain and a region homologous to guanylate kinase (GuK) (Figure 1.9 B). These domains serve as receptor, signaling and transport complexes within the plasma membrane. Zo1 proteins bind to claudins and occludins, as well as other cytoskeletal proteins such as vinculin and cingulin (Figure 1.9 A). These proteins collectively form the structural components of the tight junctions that bridge the paracellular spaces between adjacent cells (Stevenson *et al.*, 1986, Sugrue and Zieske, 1997, Ban *et al.*, 2003, Kojima *et al.*, 2009). Claudin and occludin are integral membrane proteins that limit intercellular spaces, thereby forming channels that regulate the movement of ions between adjacent cells (Ryeom *et al.*, 2000). Zo1 is therefore the scaffold to which other integral membrane proteins bind. Zo1 expression is therefore required for other tight junction proteins such as claudins and occludins to connect to the cytoskeleton of the cell (Figure 1.9 A).

The junction adhesion molecule (JAM) is a transmembrane protein that is associated with the formation of tight junctions. JAM proteins, however, are not directly involved in forming the claudin and occludin branching network. Although their exact function is unknown, JAM proteins are thought to be involved in strengthening the tight junctions between adjacent cells (Figure 1.9 B) (Niessen, 2007).

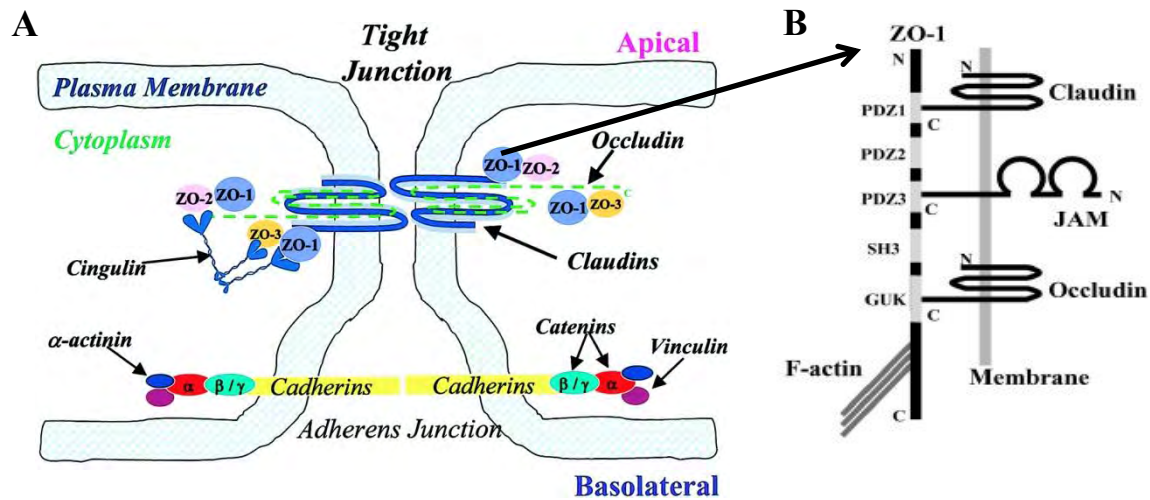


Figure 1.9: The formation of tight junctions (A). Image adapted from <https://www.google.co.za/search?q=tight+junctions+physiology.org>. Zo1 binding domains (B). Image adapted from Kojima *et al.*, 2009.

Given the dual role of Zo1 as a ‘barrier’ and a signal transducer, studies have suggested various functions for the domains of Zo1 proteins. The domains are required for structural organisation and each domain is thought to be responsible for various signal transduction pathways (Ryeom *et al.*, 2000, Bauer *et al.*, 2010). Zo1 has a cassette of protein binding domains that includes a PSD95/dgl/Zo-1 (PDZ) domain, a SH3 domain and a region homologous to guanylate kinase (GuK). Bauer *et al.* (2010) reported that the PDZ domain plays a role in cell signaling and the SH3 domain is involved in signaling pathways that regulate the cytoskeleton. These functions play a role in determining the protein localisation of Zo1. Ryeom *et al.* (2000) analysed exogenous Zo1 expression using stable mutant corneal epithelial cell lines that were generated to exclude each domain. They then assessed Zo1 cellular localisation in each mutant cell line and found that the C-terminal mutant was localised to cell borders, and the N-terminal mutant was localised in the cytoplasm of the corneal epithelial cells.

*Zo1* is expressed very early in embryonic development and has been shown to be required for morula to blastocyst transformation in the mouse (Wang *et al.*, 2008). *Zo1* is a predominant function related protein whose expression has been used as a marker of mature corneal endothelium in rat (Ju *et al.*, 2012), human (Zhu *et al.*, 2008, Fan *et al.*, 2011) and mouse corneal tissue (Cao *et al.*, 2002). Corneal endothelial tight junctions are expressed as a discontinuous band which allows aqueous humor to flow into the stroma through the gaps between the cells.

Adherens junctions are mediated by cadherins and catenins, such as *N-cadherin* (*N-cad*) and  $\beta$ -*catenin* respectively. Notably, *N-cad* is also an important marker of function in corneal endothelial cells (Zhu *et al.*, 2008).

## **1.9 Water transport proteins – Aquaporin 1**

Aquaporins (AQPs) are a family of membrane spanning proteins that have diverse physiological functions as key mediators of transcellular fluid transport. Research spanning decades has led to the identification of 13 mammalian AQP homologues (Agre *et al.*, 1993, Montiel *et al.*, 2014) that are expressed in endothelial and epithelial tissues, as well as other tissues that are involved in fluid transport such as kidney tubules (Thiagarajah and Verkman, 2002). AQPs can be clustered into two subsets: classical aquaporins (as they were initially considered to be exclusive water pores) and aquaglyceroporins (as they are permeable to water and glycerol) (Agre *et al.*, 1993). Functional studies show that *Aqp1*, *Aqp2*, *Aqp4*, *Aqp5* and *Aqp8* are water selective and are therefore classical AQPs, and *Aqp3*, *Aqp7* and *Aqp9* also transport glycerol and other small solutes and are therefore aquaglyceroporins (Verkman, 2009).

*Aqp1* was the first to be discovered by Agre and colleagues in 1991. It is constitutively organised as a homotetramer. Each monomeric subunit contains 269 amino acid residues that form two tandem repeats of three membrane spanning alpha-helices, each forming 6 transmembrane domains connected by 5 loops (A-E). As a result of the repeated Asu-Pro-Ala consensus motif, the cytoplasmic loop B and extracellular loop E domains dip into the membrane, thus contributing to the central constriction site within the pore. The second arginine outer constriction group confers selectivity in solute permeation. Structural studies have demonstrated that each monomer functions as an independent water pore but overall the tetrameric organisation is required for correct functioning of the protein (Hendriks *et al.*, 2004, Montiel *et al.*, 2014).

The plasma membrane is essentially a lipid bilayer that is permeable to water, in addition to a set of proteins that form water channels such as AQPs. There is a distinct difference between diffusional and channel-mediated water transport. Diffusion is a low capacity, bidirectional movement of water that occurs across all cell membranes, whereas channel-mediated permeability has a higher capacity for water transport. AQP channel-mediated permeability is selective as water crosses the channel without resistance while hydrophobic ions, for example, cannot permeate the channel. AQPs therefore function as water selective plasma membrane transporters that facilitate the bidirectional movement of water between the endothelium and the stroma in response to osmotic gradients and hydrostatic pressure (Thiagarajah and Verkman, 2002, Macnamara *et al.*, 2004). Since the movement of water is directed by osmotic gradients, AQPs are not pumps or exchangers, but simply form a channel that allows water to move through the membrane (Agre *et al.*, 1993, Agre, 2004).

As previously discussed, the corneal endothelium maintains deturgescence by transporting water and other solutes between the stroma and the aqueous humor in the anterior chamber. Corneal transparency requires constant regulation of solute content and water. The stroma is hyperosmolar relative to the aqueous fluid due to the high concentration of negatively charged glycosaminoglycans and consequent accumulation of cations, thus causing stromal

swelling (Thiagarajah and Verkman, 2002, Macnamara *et al.*, 2004). Therefore, active solute transport out of the stroma, across the endothelium and into the anterior chamber is critical for transparency to counteract the tendency of the stroma to absorb water. The endothelium utilises transport proteins such as sodium potassium ATPase ( $\text{Na}^+ \text{K}^+$  ATPase) and sodium potassium chloride (Na/KCl) that pump solutes, primarily sodium and bicarbonate, from the stroma into the aqueous chamber (Thiagarajah and Verkman, 2002, Besharse *et al.*, 2010). These salt pumps create an osmotic gradient that allows excess water to passively move from the stroma across the endothelium into the anterior chamber through AQP water channels (Thiagarajah and Verkman, 2002, Macnamara *et al.*, 2004). Corneal transparency requires approximately 78% water by weight (Thiagarajah and Verkman, 2002, Macnamara *et al.*, 2004), thus excess water entering the cornea must be extruded through AQP water channels to maintain a natural hyperosmotic state (Zhang *et al.*, 2002) and overall corneal deturgescence (Besharse *et al.*, 2010).

Hydrostatic pressure, defined as IOP, is an important index of eye physiology (Zhang *et al.*, 2002). Regulated IOP depends on the rate of aqueous fluid production by the ciliary epithelium and the rate of aqueous fluid outflow from Schlemm's canal into the venous system (Zhang *et al.*, 2002). Aqueous fluid production involves passive water transport which is driven by active salt transport across the ciliary epithelium, whereas aqueous fluid outflow involves pressure driven bulk outflow from Schlemm's canal (Zhang *et al.*, 2002). Such water transport is facilitated by AQP water channels (Zhang *et al.*, 2002). Therefore, AQPs are involved in regulating IOP by facilitating aqueous fluid production and outflow (Zhang *et al.*, 2002).

Tissue distribution has provided indirect roles for AQPs in various physiological processes. The eye expresses several AQPs at important sites of fluid transport (Figure 1.10) (Verkman, 2009).

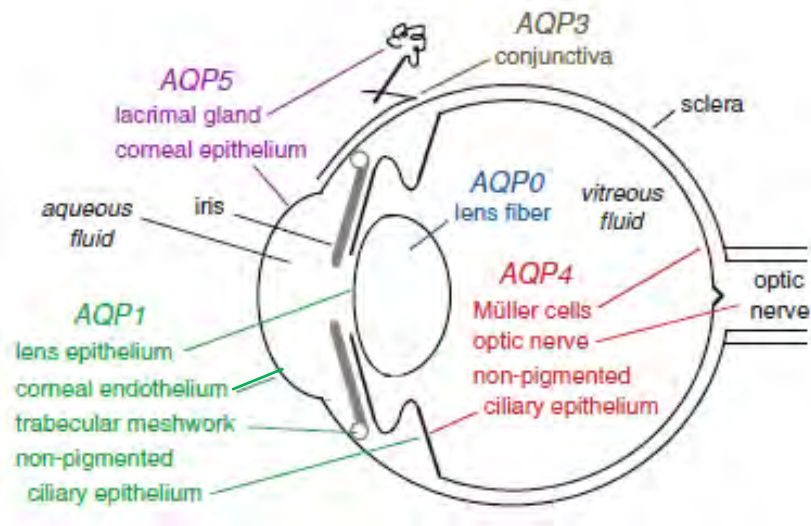


Figure 1.10: Sites of aquaporin expression in the eye. Image adapted from Verkman 2009.

Tissues that express *Aqp1* and *Aqp4* are involved in IOP regulation and *Aqp0*, *Aqp1* and *Aqp5* are responsible for lens and corneal transparency. *Aqp4* is expressed in tissue responsible for visual signal transduction and *Aqp3* is involved in tear film homeostasis and conjunctival barrier function. *Aqp5* is involved in tear formation by the lacrimal glands (Verkman, 2009).

Knockout (KO) models have provided compelling evidence for the roles of AQPs in transcellular fluid transport (Table 1.10) (Verkman, 2009).

Table 1.1: Tissue specific roles of aquaporin homologues and their associated experimental phenotype.

AQP Homologue	Site related function	Experimental phenotype	Additional notes	Reference
<i>Aqp1</i>	Sites of fluid production (ciliary epithelium) and outflow (trabecular meshwork) in the cornea. It is expressed in the lens epithelium and corneal endothelium. Plays a role in corneal and lens transparency	<i>Aqp1</i> null mice have reduced corneal thickness (WT 123 $\mu$ m in WT mice compared to 101 $\mu$ m in <i>Aqp1</i> null mice)  Delayed recovery of corneal transparency and thickness after exposure to hypotonic saline solution (75% recovery at 7 minutes in WT mice compared to 5% recovery in <i>Aqp1</i> null mice)  KO mice show a small yet significant reduction in IOP with reduced aqueous fluid secretion  Lenses from <i>Aqp1</i> null mice have reduced osmotic permeability across the lens epithelium. Also, significantly greater water content of the lens	Baseline transparency did not change by <i>Aqp1</i> deletion. Hypothesized that <i>Aqp1</i> upregulation may reduce corneal swelling after injury  Aqueous fluid outflow was unimpaired  Baseline lens morphology or transparency was not altered by <i>Aqp1</i> KO	(Thiagarajah and Verkman, 2002)  (Verkman, 2009)  (Zhang <i>et al.</i> , 2002)  (Ruiz-Ederra and Verkman, 2006)
		<i>Aqp1</i> Null mice: <i>in vitro</i> , accelerated loss of lens transparency following incubation in high glucose solution. <i>In vivo</i> , accelerated cataract formation	Data suggest that <i>Aqp1</i> facilitates lens transparency and opposes cataract formation	(Ruiz-Ederra and Verkman, 2006)

<b>AQP Homologue</b>	<b>Site related function</b>	<b>Experimental phenotype</b>	<b>Additional notes</b>	<b>Reference</b>
<i>Aqp3</i>	Conjunctival epithelium, plays a role in the epithelial barrier function and water permeability	<i>Aqp3</i> KO mice have a slower water permeability in conjunctiva	A mathematical model of tear film osmolarity was developed, providing insights into the pathophysiology of dry eye disorders	(Levin and Verkman, 2004)
<i>Aqp5</i>	Corneal epithelium and lacrimal gland	<i>Aqp5</i> deletion in mice showed reduced corneal swelling after exposure to hypotonic saline solution  <i>Aqp5</i> null mice have increased corneal thickness (WT 123µm in WT mice compared to 144µm in <i>Aqp5</i> null mice)		(Verkman, 2009)  (Thiagarajah and Verkman, 2002)

The data reviewed in table 1.10 collectively provide functional evidence for the roles of AQPs in eye physiology, particularly the role of *Aqp1* in fluid extrusion from the stroma across the endothelium.

The entire cornea is nourished by proteins and other essential substances found in the aqueous humor. These nutrients are transported across the endothelium and into the rest of the cornea by the endothelial pump function. Knockout models and techniques such as siRNA knockdown have facilitated new ways of testing and understanding the molecular mechanisms underlying the corneal endothelial pump function. *Aqp1* knockout models have encouraged researchers to re-evaluate the mechanisms underlying solute-fluid coupling and the corneal endothelial pump (Bonanno, 2012).

### **1.10 The role of solute carriers in the pump function of the corneal endothelium.**

Bicarbonate ions ( $\text{HCO}_3^-$ ) play an important role in the pump function of the corneal endothelium that is required to maintain deturgescence (Suzuki *et al.*, 2012). Proteins belonging to the solute carrier 4 (Slc4) family transport cellular  $\text{HCO}_3^-$  across plasma membranes (Bonanno, 2012, Shei *et al.*, 2013). The Slc4 family consists of 3 functionally distinct groups: electroneutral sodium-independent chloride bicarbonate exchangers ( $\text{Cl}^-/\text{HCO}_3^-$ ), electroneutral sodium-bicarbonate ( $\text{Na}^+:\text{HCO}_3^-$ ) cotransporters and sodium driven exchangers. *Slc4a4*, which encodes the sodium bicarbonate cotransporter NBCe1 gene, is a  $\text{Na}^+:\text{HCO}_3^-$  cotransporter that is localized to the basolateral membrane of corneal endothelial cells (Shei *et al.*, 2013).

Aqueous humor secretion that is coupled to ion changes depends on active transport mechanisms to create osmotic gradients that direct the movement of water across the endothelium (Bonanno, 2012). Ion pumps create an osmotic gradient that allows water to passively move from the stroma across the endothelium into the anterior chamber. As discussed previously, the hyperosmolar stroma absorbs water by osmosis (Thiagarajah and Verkman, 2002, Macnamara *et al.*, 2004). Therefore, active solute transport across the endothelium is critical for deturgescence to counteract the tendency of the stroma to absorb water.

The pump function is energy driven and requires  $\text{Na}^+\text{K}^+\text{ATPase}$  and carbonic anhydrase, which is an enzyme that converts carbon dioxide and water to bicarbonate ions. These bicarbonate ions are translocated across plasma membranes and allow water to passively flow through. Studies show that carbonic anhydrase inhibitors prevent the process of fluid reabsorption and result in a loss of deturgescence (Besharse *et al.*, 2010, Suzuki *et al.*, 2012).

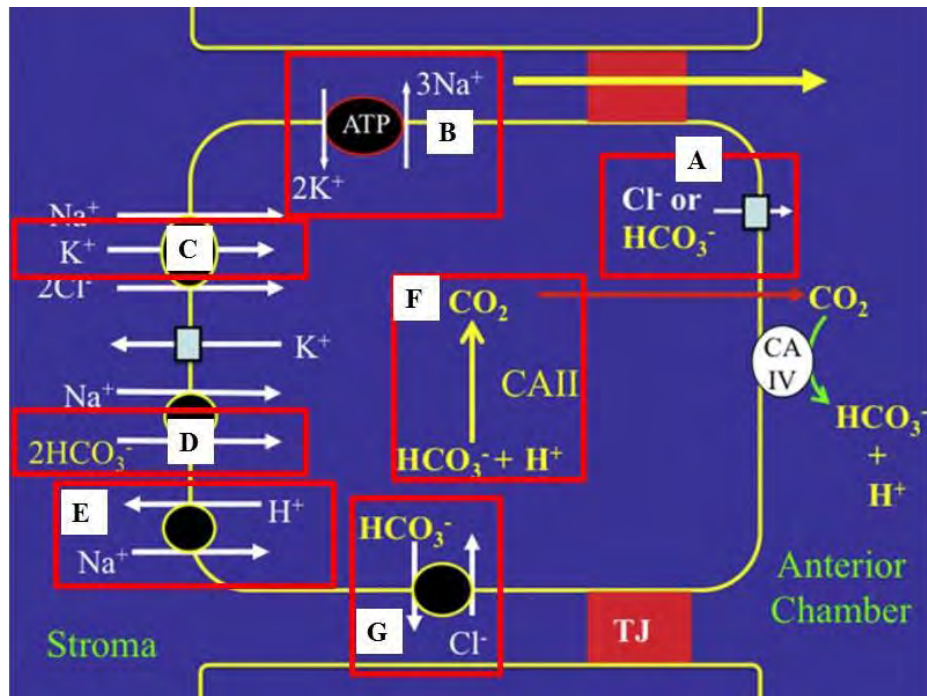


Figure 1.11: Molecular mechanisms underlying the corneal endothelial pump function - Bicarbonate transport model for the corneal endothelium. Image adapted from Bonanno 2012.

Bonanno (2012) proposed a possible bicarbonate transport model for the corneal endothelium (Figure 1.11). Fluid coupled anion secretion requires transendothelial transport of  $\text{Cl}^-$  and  $\text{HCO}_3^-$  (Figure 1.11 A).  $\text{Na}^+\text{K}^+\text{ATPase}$ , present in the basolateral membrane, creates a low intracellular concentration of  $\text{Na}^+$  ions (Figure 1.11 B) and a high intracellular concentration of  $\text{K}^+$  ions (Figure 1.11 C). The net negative charge creates a small potential difference that attracts  $\text{Na}^+$  through the paracellular pathway across tight junctions. The net movement of  $\text{Na}^+$  and  $\text{HCO}_3^-$  creates an osmotic driving force that facilitates the movement of water along the osmotic gradient. The basolateral membrane also contains the electrogenic sodium bicarbonate cotransporter ( $1\text{Na}^+/2\text{HCO}_3^-$ ), the chloride bicarbonate exchanger ( $\text{Cl}^-/\text{HCO}_3^-$ ) and the sodium hydrogen exchanger ( $\text{Na}^+/\text{H}^+$ ). The sodium bicarbonate cotransporter *Slc4a4* directly deposits  $\text{HCO}_3^-$  into the cell (Figure 1.11 D). The  $\text{Na}^+/\text{H}^+$  exchanger (Figure 1.11 E) can deposit  $\text{HCO}_3^-$  into the cell indirectly because the

removal of protons favors formation of  $\text{HCO}_3^-$  from carbon dioxide, which is catalyzed by carbonic anhydrase II (Figure 1.11 F). The  $\text{Cl}^-/\text{HCO}_3^-$  exchanger removes  $\text{HCO}_3^-$  from the cell and adds intracellular  $\text{Cl}^-$  (Figure 1.11 G). This model suggests that  $\text{HCO}_3^-$  is taken up on the basolateral side and  $\text{HCO}_3^-$  outflow occurs across the apical side through anion channels (Bonanno, 2012).

Immunohistochemistry studies indicate that *Slc4a4* is exclusively expressed in the basolateral membrane of rat, bovine and human corneal endothelium. NBCe1 siRNA knockdown experiments in cultured bovine corneal endothelium show significantly reduced basolateral  $\text{HCO}_3^-$  permeability and reduced basolateral to apical  $\text{HCO}_3^-$  transport. Notably, apical  $\text{HCO}_3^-$  to basolateral transport was not affected by siRNA knockdown, indicating that functional *Slc4a4* is only present in the basolateral membrane and that it is required for majority of basolateral  $\text{HCO}_3^-$  inflow (Bonanno, 2012).

Several members of the Slc4 family have been implicated in the development of ocular and corneal diseases such as cataracts, band keratopathy and glaucoma. Band keratopathy is a form of corneal degeneration that is characterized by the appearance of bands around the cornea formed by elevated levels calcium deposition. NBCe1 mutations increase the concentration of intracellular  $\text{HCO}_3^-$  which causes an increase in calcium deposition that may result in band keratopathy (Figure 1.12) (Suzuki *et al.*, 2012, Shei *et al.*, 2013).

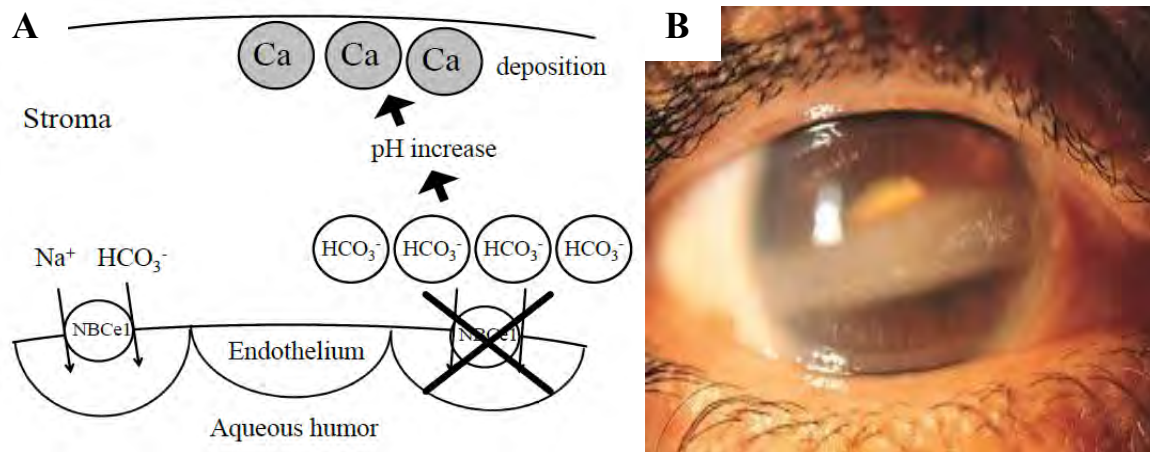


Figure 1.12: Proposed method of band keratopathy caused by NBCe1 mutations (encoded by *Slc4a4*) (A). Image adapted from Suzuki *et al.*, 2010. Calcific band keratopathy (B). Image adapted from <https://www.google.co.za/search?q=calcific+band+keratopathy>.

Developmental eye disorders affect millions worldwide. Axen-Reiger Syndrome (ARS) and Peters Anomaly are two of the most cited developmental eye disorders that occur as a result of disrupted morphogenesis in the anterior segment of the eye. Corneal endothelial dystrophies such as Bullous Keratoplasty and Fuch's endothelial dystrophy are the two leading causes of corneal transplant surgery in the United States. Despite the high success rates of corneal transplant surgery, donor graft tissue is a limited resource (Alward, 2000, Reneker *et al.*, 2000, Nishimura *et al.*, 2001). There is therefore an urgent need for innovative regenerative techniques to further our understanding of corneal endothelial dysfunction and to produce viable bio-engineered corneal tissue.

### 1.11 Research aims and objectives

The principle function of the corneal endothelium is to regulate and maintain optimal stromal hydration, consequently preserving corneal transparency. Simple diffusion cannot sustain the metabolic needs of the cornea. Co-ordinated and tightly regulated ion pumps,

transporters, channels and tight junctions facilitate fluid production, absorption and secretion of nutrients and metabolites throughout the cornea (Ruiz-Ederra and Verkman, 2006).

This study aims to establish an *in vitro* model of murine corneal endothelial development in order to elucidate the molecular events that result in proper differentiation of the corneal endothelium. This will be achieved by developing an *in vitro* model of corneal endothelial development and assessing the expression patterns of key function related genes and proteins. This information will contribute to the body of knowledge that exists and perhaps be used to direct the differentiation of induced pluripotent stem cells towards a corneal endothelial phenotype.

Aim 1: To recapitulate the development of the corneal endothelium by determining the endogenous gene and protein expression patterns of key functional genes associated with initiation of differentiation, the differentiated state and the fully functioning endothelium.

Objectives:

- a) To generate presumptive corneal endothelial cell lines from 1: E14.5 and E15.5 embryos and 2. From post natal stage P13 when the eyelids open and the corneal endothelium is functional. Cell lines from earlier developmental stages (E12.5 and E13.5) have already been generated by other members of the laboratory.
- b) To determine the gene expression patterns of *Zo1*, *Aqp1* and *Slc4a4* (markers of differentiated and functional corneal endothelium) at E12.5, E13.5, E14.5, E15.5 and P13

- c) To determine the protein expression patterns of *Zo1* and *Aqp1* at the aforementioned developmental stages.

Preliminary data shows that E12.5 and E13.5 cells are able to form adherens junctions characterised by the presence of *N-cadherin* in the cell membranes. Therefore, confocal microscopy will be used to:

- d) Assess the ability of the cell lines to form tight junctions using *Zo-1* antibodies.  
e) Determine the presence of *Aqp1* proteins to assess the functional capability of the cells.

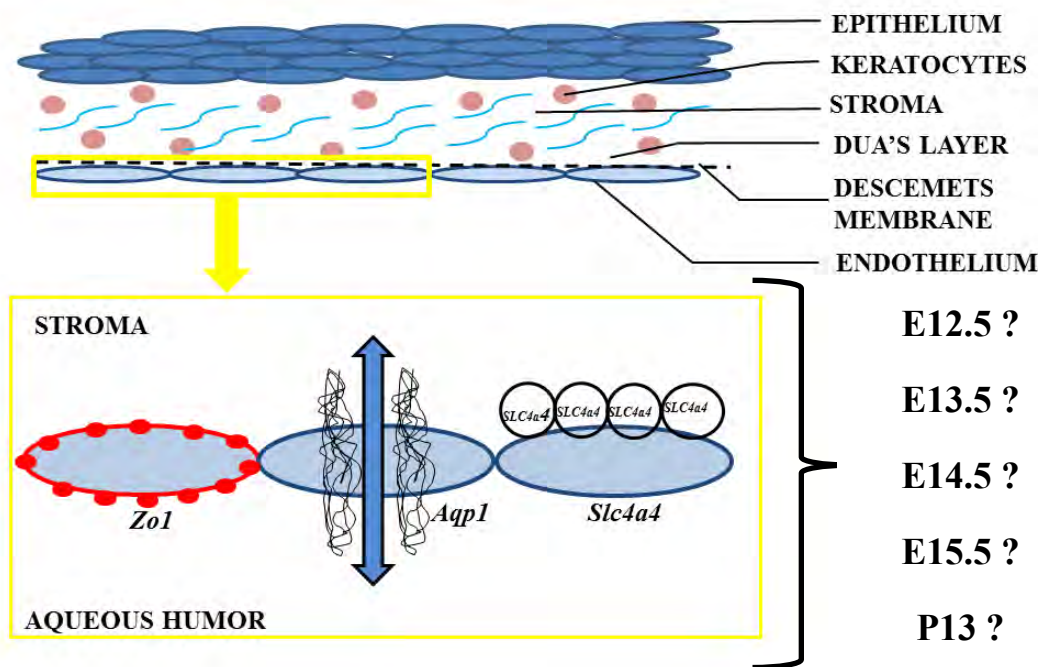


Figure 1.13: Schematic representation of the research aims. *Zo1* is a tight junction protein, expressed corneal endothelial cell membranes, that facilitates the formation of the resilient monolayer that is characteristic of the corneal endothelium. *Aqp1* is a bidirectional water channel protein that mediates transcellular fluid transport across the corneal endothelium, while *Slc4a4* is an ion pump that transports cellular bicarbonate ions across plasma membranes of corneal endothelial cells. The aim of this study is to determine the gene

expression patterns of these functional genes in an *in vitro* model of corneal endothelial development.

Aim 2: To establish a stable *Foxc1* knockdown cell line.

Objectives:

- a) To sub-clone a hairpin siRNA insert targeting murine *Foxc1* expression into a commercial vector for stable knockdown.
- b) To transfect corneal endothelial cells with the siRNA expression vector and assess the effects of *Foxc1* knockdown on the gene expression levels of the functional genes assessed in this study.

It must be noted that, despite numerous attempts to sub-clone the siRNA insert into the expression vector, this was not achieved within the time frame of this research project. However, since an immense amount of work and trouble-shooting was performed, details have been supplied in Appendix 4.

## 2. MATERIALS AND METHODS

### 2.1 Animal handling

The use of the BALB/c mice in this study was approved by the University of KwaZulu-Natal (UKZN) Animal Research Ethics Committee (ethics number 022/15/ANIMAL). The animals were obtained from the Bio-Medical research Unit (BMRU) at UKZN. Animal handling was done in accordance with the UKZN animal experimentation regulations. The mice were fed a constant diet of dry pellets and water in accordance with the UKZN ethical rules and regulations. Human Endpoint observation forms were completed daily to ensure the well-being of the animals as requested by the National Council of societies for the Prevention of Cruelty to Animals (NSCPA).

#### 2.1.1 Timed matings

In order to establish an *in vitro* model of murine corneal endothelial development, timed matings were performed to obtain embryos and mouse pups for dissections at the relevant stages of development (E14.5, E15.5 and P13). Noon on the day of the vaginal plug was considered E0.5 (<http://www.acuc.berkeley.edu/guidelines.html>).

### 2.2 Derivation of primary cultures

Primary cultures of presumptive corneal endothelial cells were derived from wild-type mouse embryos at embryonic day (E) 14.5 and E15.5, and mature corneal endothelial cells were derived from wild-type mouse pups at post-natal day (P) 13 developmental stages. All dissections were performed using a Stemi DV4 stereo microscope (Zeiss, Germany) and tungsten dissecting needles sharpened using electro-chemical etching in KOH solution at 150 V (Appendix 4.1a). All surfaces and dissecting equipment were sterilized with 70% ethanol (Appendix 4.1b). Dissecting needles were sterilized with UV irradiation prior to use and rinsed in 1x phosphate buffer saline (PBS) (Appendix 4.1c), 70% ethanol and heat

sterilized in a glass bead sterilizer (Simon Keller, Switzerland). The dissecting needles were sterilized between uses on each embryo to prevent cross contamination.

Pregnant females and P13 mouse pups were initially euthanized by Halothane exposure and later by exposure to carbon dioxide as per UKZN BRU guidelines. Embryos were harvested by caesarian section. Each embryo or pup was placed in a petri dish on ice containing 1x PBS solution. Corneal endothelial cell derivation was conducted as follows:

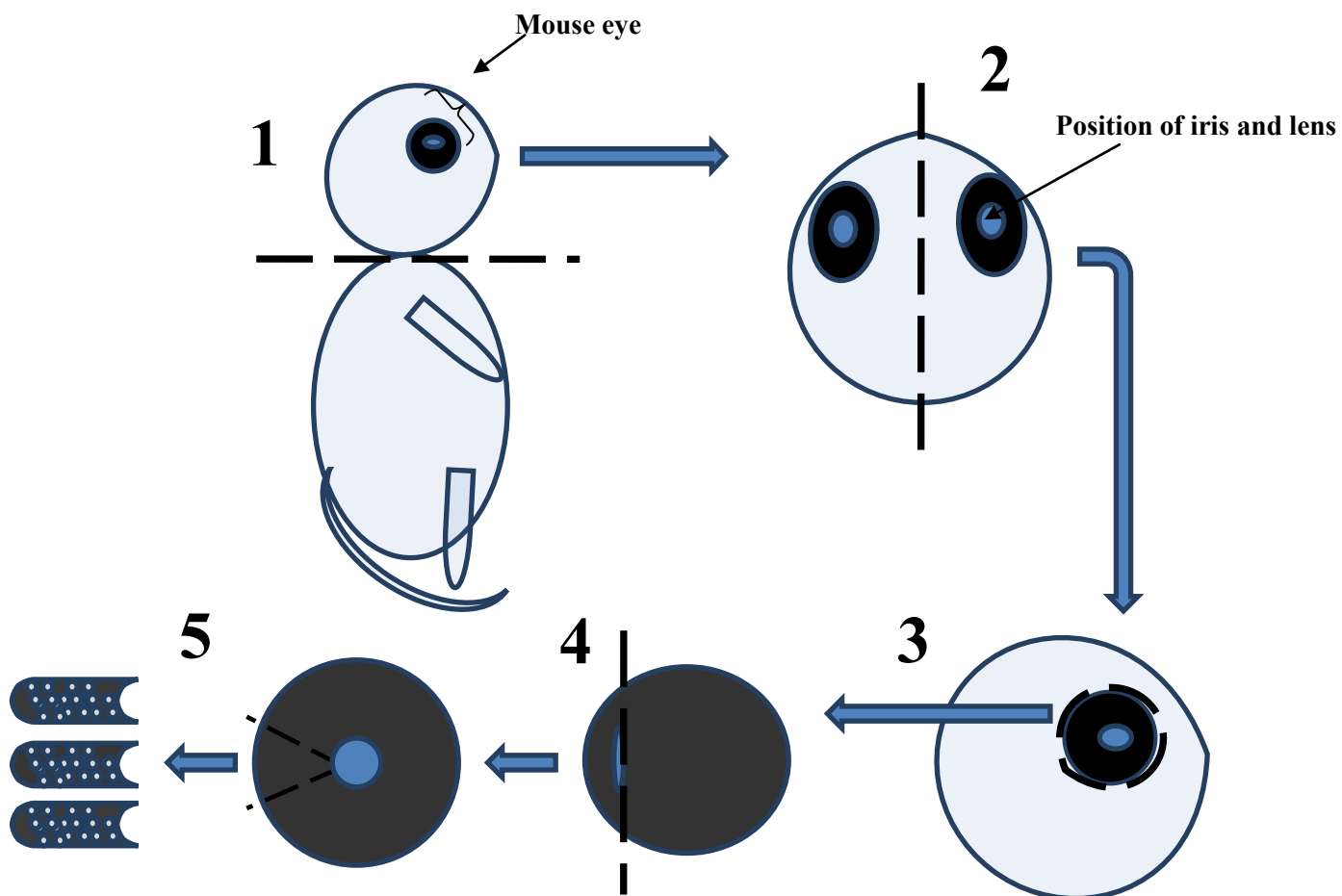


Figure 2.1: The stepwise procedure for the derivation of periocular mesenchyme cells from the eyes of mouse embryos. Black denotes the tissue of the eye, dark blue the position of the iris and lens within the eye and light blue the remainder of the embryo (image obtained from Jerolen Naidoo, MSc thesis 2011).

(1) The head of the embryo or pup was carefully dissected away from the body. (2) The head was bisected longitudinally with each half containing one eye. (3) Each eye was then cut into four wedges using the fine dissecting needles. Careful attention ensured that the fine dissecting needles and all extra ocular head tissue was removed. (4) The wedges were used to separate the anterior and posterior sections of the eye. (5) The anterior regions of the eyes. A mouth pipette was used to transfer the wedges to all wedges to the well of a 24 well plate containing 500µl of DMEM (Invitrogen, USA) supplemented with 20% fetal bovine serum (FBS) (Invitrogen, USA) and 0.5ug/mL penicillin/streptomycin (pen/strep) (Lonza, Germany). Four to five wedges from a single eye were cultured in a single well of a 24 well plate. Primary cultures were allowed to expand for 72 hours and migrate away from the explants before subsequent immortalisation (Figure 2.1).

### 2.3 Immortalisation of primary cultures

Primary cultures of POM cells were immortalised by infection with a temperature sensitive SV40 large T-antigen with Geneticin (G418) (Sigma-Aldrich<sup>®</sup>, USA) resistance as described by Sommer *et al.* (2006). The RV 200 Viraductin<sup>™</sup> Retrovirus Transduction kit (Cell Biolabs Inc., USA) was used to facilitate immortalisation of primary presumptive corneal endothelial cells at E14.5 and E15.5 and mature corneal endothelial cells at P13. The virus was obtained from the conditioned medium of Ψ2 producer cells that were cultured at 37°C in DMEM (Invitrogen, USA) containing 10% FBS (Invitrogen, USA) and 0.5 µg/mL pen/strep (Invitrogen, USA). Conditioned medium was harvested from Ψ2 producer cells 24-48 hours before immortalisation. Harvested medium was centrifuged at

2000 rpm for 1 minute to remove all cellular debris and filter sterilised using a 0.2 micron filter and a sterile syringe.

For a single well in a 24-well plate containing primary cultures, 5  $\mu$ l of 100x Reagent A (Cell Biolabs Inc., USA) were added to 490  $\mu$ l of  $\Psi$ 2 conditioned medium in a sterile micro-centrifuge tube. The mixture was gently inverted several times to mix the solution and 5  $\mu$ l of Reagent B (Cell Biolabs., USA) was added. The solution containing Reagent A,  $\Psi$ 2 conditioned medium and Reagent B was gently inverted several times and incubated at 37°C for 30 minutes. The mixture was then centrifuged at 12 000 x g for 10 minutes at 4°C. Following centrifugation, the supernatant was discarded and the pellet was resuspended in 500  $\mu$ l of fresh antibiotic-free culture medium by vortexing. Culture medium in each well was aspirated and replaced with the mixture containing the pellet of cells. The 24-well plate was then incubated at 37°C overnight. The following day, the mixture was aspirated from each well and replaced with 500  $\mu$ l of a solution containing Reagent C (Cell Biolabs., USA) and normal culture medium in a 1:8 ratio respectively. The 24-well plate was gently swirled for approximately one minute. The solution containing Reagent C was then aspirated and the cells were rinsed twice with 300  $\mu$ l of culture medium containing 20% FBS. 500  $\mu$ l of culture medium was added to each well. The cells were then cultured at 37°C for 48-72 hours before G418 antibiotic selection began. G418 antibiotic pressure was applied to select successfully infected cells. G418 was added to the culture medium at a concentration of 400  $\mu$ g/mL and applied to each well. Antibiotic selection continued for 10-14 days to ensure the selection of immortalised cells. Mouse embryonic fibroblasts dissected from the head region of the embryos and pups were not immortalised and used as controls for antibiotic selection. These untransformed fibroblasts did not survive the antibiotic selection process. Immortalised presumptive and mature corneal endothelial cells were cultured in DMEM containing 20% FBS and 0.5  $\mu$ g/mL pen/strep for approximately 2 weeks, after which DMEM containing 10% FBS and 0.5  $\mu$ g/mL pen/strep was used for all subsequent culturing.

## 2.4 Cell culture

Tissue culture was carried out in a class two, type A2 categorised laminar flow (Logic labconco®). Cells were incubated at 37°C in a humidified Shel Lab 3553 CO<sub>2</sub> incubator (United Scientific (Pty) Ltd) supplemented with 5% CO<sub>2</sub>. Stock cultures of each cell line were maintained in 75 cm<sup>3</sup> tissue culture (T75) flasks (Corning, USA) containing 10 mL DMEM culture medium supplemented with 10% FBS (Invitrogen, USA) and 0.5µg/mL pen/strep (Invitrogen, USA). Working stocks were maintained in 10 cm<sup>3</sup> dishes (Corning, USA) containing 10 mL DMEM culture medium supplemented with 10% FBS (Invitrogen, USA) and 0.5µg/mL pen/strep (Invitrogen, USA). Cell growth was examined using an inverted Nikon TMS-F microscope (Nikon, Japan). Confluent cells were passaged by adding 1 mL of 1x Trypsin-EDTA (PAA) (Appendix 4.1d) to a T75 flask. The flask containing the trypsin-EDTA solution was then incubated at 37°C until the cells detached from the bottom of the flask. 2 mL culture medium was added to the flask to neutralize the trypsin-EDTA solution. Immortalised POM cultures at E12.5 and E13.5 were created by other members of the laboratory and were maintained in 10 cm<sup>3</sup> dishes (Corning, USA) containing 10 mL DMEM culture medium supplemented with 10% FBS and 0.5µg/mL pen/strep (Invitrogen, USA).

All the experiments were performed on passage  $6 \leq p \leq 11$  POM cells at E12.5 and E13.5, and passage  $4 \leq p \leq 9$  presumptive corneal endothelial cells at E14.5 and E15.5, and mature corneal endothelial cells at P13.

Each cell line was regularly tested for *Mycoplasma* infection using a Hoechst nuclear stain (Appendix 4.1e). Stained slides were viewed using a fluorescent microscope. All the cell lines were negative for *Mycoplasma* infection.

## 2.5 RNA extraction

RNA was extracted from cells using a QIAGEN RNeasy Kit according to the manufacturer's instructions for purification of total RNA using spin technology.

Culture medium from selected culture dishes was aspirated and discarded. Expression of adherens and tight junction mRNA transcripts is disrupted by trypsin-EDTA treatment (Zhu *et al.*, 2008), therefore adherent corneal endothelial cells were harvested using a cell scraper (Biologix Research Company) and collected in a sterile 15 mL centrifuge tube. The culture dishes were rinsed with 1x PBS which was collected in the same centrifuge tube. The centrifuge tube was then centrifuged at 1000 x g for 5 minutes at room temperature. The supernatant was discarded and the pellet of cells was re-suspended in 600  $\mu$ l RLT lysis buffer. The cells were homogenised by pipetting and briefly vortexed for 10 seconds. The cell lysate was pipetted into a QIAshredder (QIAGEN) which was centrifuged at 10 000 rpm for 2 minutes at room temperature. The QIAshredder column was discarded and 600  $\mu$ l of 70% ethanol was added to the 2 mL collection tube containing the cell lysate. The solution containing the cell lysate and 70% ethanol was mixed by pipetting and added to an RNeasy spin column placed in a 2mL collection tube. The RNeasy spin column was centrifuged at 10 000 rpm for 15 seconds at room temperature. The flow-through was discarded and 700  $\mu$ l of RW1 buffer was added to the RNeasy spin column which was then centrifuged at 10 000 rpm for 15 seconds at room temperature. The flow-through was discarded and 500  $\mu$ l of RPE buffer was then added to the RNeasy spin column and centrifuged at 10 000 rpm for 15 seconds at room temperature. The flow-through was discarded and the RNeasy spin column was placed in a new 2 mL collection tube. The RNeasy spin column was centrifuged at 10 000 rpm for 1 minute to remove all traces of RPE buffer on the membrane. The RNeasy spin column was placed in a 1.5 mL micro-centrifuge tube and 30  $\mu$ l of nuclease free water was pipetted directly onto the membrane to elute the RNA. The micro-centrifuge tube containing the RNeasy spin column was incubated at room temperature for 5 minutes, after which it was centrifuged at 10 000 rpm for 1 minute. RNA samples were kept on ice and quantified immediately.

### 2.5.1 RNA quantification

Total RNA samples were quantified using a Spectrophotometer ND1000 (NanoDrop technologies) using ND V3.5.2 software in accordance with the MIQE guidelines (Bustin *et al.*, 2009). Readings at  $A_{260}$  indicated the RNA concentration and the  $A_{260/280}$  ratio indicated the RNA purity (pure RNA has an  $A_{260/280}$  ratio between 1.8 and 2.1). RNA samples were aliquoted in volumes equivalent to 2  $\mu\text{g}$  of RNA to ensure that each sample was only subjected to one freeze-thaw cycle. RNA samples were stored at  $-80^{\circ}\text{C}$  immediately after quantification.

### 2.5.2 Validation of RNA integrity

RNA integrity was evaluated by gel electrophoresis. RNA samples were separated on a 1% bleach agarose gel (Appendix 4.1f) containing 5  $\mu\text{g}/\text{mL}$  ethidium bromide. The gels were run in 1x Tris-base-acetate buffer (TAE) running buffer (Appendix 3.1g) by electrophoresis at 100 V for 35 minutes. An O'GeneRuler™ DNA molecular weight marker (MW) (range 100-10 000 bp, Thermo Scientific, USA) was loaded into the first lane of every gel for reference. 2  $\mu\text{l}$  6X loading dye (Thermo Scientific, USA) was added to the equivalent volume of 1  $\mu\text{g}$  of total RNA which was then loaded into a single well in the gel. Gels were visualised and bands were detected under UV light in a Bio-Rad Chemidoc® XRS+ imaging system (Bio-rad, USA). Image Lab™ software version 2.0.1 (Bio-rad, USA) was used to analyse detected bands.

The integrity of the RNA samples was confirmed by the presence of two bands of the 28S and 18S ribosomal subunit RNA (Figure 3.2). As shown in Figure 3.2, the RNA samples used in this study were acceptable for further analysis.

## **2.6 cDNA Synthesis**

The GoScript™ Reverse Transcription System (Promega, USA) was used to synthesise complimentary DNA (cDNA). The kit includes a reverse transcriptase and specialised reagents for efficient synthesis of first-strand cDNA optimised for quantitative PCR analysis. A standard concentration of 2 µg RNA was used for cDNA synthesis in a Bio-Rad My cycler™ thermal cycler.

### **2.6.1 Poly (A) Tailing**

RNA samples were thawed on ice prior to cDNA synthesis. For a single reaction, 2 µg RNA and 1 µl 50 µM Oligo(dT)<sub>15</sub> Primer were added to a sterile PCR tube. Nuclease free water was then added to the reaction to make up a final volume of 10 µl. This solution was incubated for 5 minutes at 70°C, after which it was briefly centrifuged and incubated on ice for additional 5 minutes.

### **2.6.2 First strand cDNA synthesis**

A mastermix containing 4 µl GoScript™ 5x reaction buffer, 2.5 µl 25mM MgCl<sub>2</sub>, 1 µl of GoScript™ random primers (dNTPs), 1 µl Recombinant RNasin® Ribonuclease Inhibitor and 5.5 µl nuclease free water (per reaction) was prepared and added to the RNA solution after the 5 minute incubation period on ice. 14 µl of the mastermix solution was added into each sample. The solution was briefly centrifuged and 1 µl GoScript™ Reverse Transcriptase (RT) was added directly into each sample. The solution was briefly centrifuged and incubated in a Bio-Rad My cycler™ thermal cycler at 25°C for 5 minutes; 42°C for 60 minutes and 70°C for 15 minutes.

A no-reverse transcriptase (no-RT) control and a no-template control (NTC) control (negative controls) was prepared for each RNA sample in which the reverse transcriptase

and template/RNA respectively was replaced by nuclease free water. Fresh cDNA was aliquoted immediately and stored at -80°C. All cDNA samples were synthesised using the same kit to ensure an accurate and comparable representation of subsequent data.

## 2.7 Conventional PCR

Conventional PCR was used to determine the efficacy of the following primer sets (Table 2.1) and the presence of each gene in POM cells at E12.5 and E13.5, presumptive corneal endothelial cells at E14.5, E15.5 and mature corneal endothelium at P13.

Table 2.1: Primer sequences of the genes of interest and reference genes used in this study.

Gene	Orientation	Sequence (5'-3')	Product size (bp)	Source
<i>Zol</i>	Forward	GGCTTAGAGGAAGGTGATCAAA	100	Shei <i>et al.</i> , 2013
	Reverse	CTTAGGGAGGTCAAGGAGGA		
<i>Aqp1</i>	Forward	CTACACTGGCTGCGGTATCA	143	Shei <i>et al.</i> , 2013
	Reverse	GGCCAGGATGAAGTCATAG		
<i>Slc4a4</i>	Forward	TCCCTTCATTGCCTTTGTTC	151	Shei <i>et al.</i> , 2013
	Reverse	CAAGGTGGCGATAGCTCTTC		
<i>Hprt</i>	Forward	GTCCCAGCGTCGTGATTAGCGAT	206	Sommer <i>et al.</i> , 2006
	Reverse	GGCCACAATGTGATGGCCTCC		
$\beta$ -actin	Forward	CTAAGGCCAACCGTGAAAAG	104	Shei <i>et al.</i> , 2013
	Reverse	ACCAGAGGCATACAGGGACA		

The primers for the target genes and *β-actin* were designed by Shei *et al.*, 2013 using Primer 3 primers design software. The forward and reverse primers were designed to be located on separate exons with a large intron in between to exclude amplification of genomic DNA.

The Basic Alignment Search Tool (BLAST) was used to confirm that each primer set was specific to the target mRNA transcript in the *Mus musculus* genome (Appendix 1.7.1). All the primer sets were synthesised by Inqaba biotech.

For all PCR experiments, a 20 µl reaction consisted of 1 µl cDNA; 2 µl *Taq* buffer containing (NH<sub>4</sub>)<sub>2</sub>SO<sub>4</sub> MgCl<sub>2</sub>; 2 µl 2mM dNTPs, 1.8 µl 25mM MgCl<sub>2</sub>, 0.5 µl 10mM forward primer, 0.5 µl 10mM reverse primer (Appendix 1.7), 0.2 µl *Taq* recombinant DNA polymerase (5 units/µl) and 12 µl nuclease free water. A Bio-Rad My cycler™ thermal cycler was used for all PCR experiments with the following cycling parameters: denaturation at 95°C for 3 minutes; followed by 40 cycles of 95°C for 30 seconds; 58°C for 30 seconds; and 73°C for 90 seconds; followed by an additional elongation step of 72°C for 10 minutes.

All PCR reagents were purchased from Thermo Scientific, USA. A NTC control in which cDNA was replaced by nuclease free water was added to each run as a negative control. PCR amplification products were centrifuged briefly and stored at -20°C.

### **2.7.1 Agarose gel electrophoresis**

Agarose gel electrophoresis was used to visualise the PCR products and to confirm the presence of each gene in corneal endothelial cells at various stages of development. PCR products were separated on a 1.5% TopVision agarose gel (Appendix 4.1h) containing 5

$\mu\text{g/mL}$  ethidium bromide. The gels were run in 1x Tris-base EDTA (TBE) running buffer (Appendix 3.1i) by electrophoresis at 85 V for 45 minutes. An O'GeneRuler™ DNA molecular weight marker (MW) (range 100-10 000 bp, Thermo Scientific, USA) was loaded into the first lane of every gel to identify product sizes. 2  $\mu\text{l}$  6X loading dye (Thermo Scientific, USA) was added to 8  $\mu\text{l}$  PCR product which was then loaded into a single well in the gel. Gels were visualised and bands were detected under UV light in a Bio-Rad Chemidoc® XRS+ imaging system (Bio-rad, USA). Image Lab™ software (Bio-rad, USA) was used to analyse detected bands.

## **2.8 Real-time quantitative PCR (qPCR)**

Once the efficacy of the primer sets were evaluated by conventional PCR, qPCR was used to determine the relevant expression levels of the target genes using the Applied Biosystems 7500 Real-Time PCR System with HID Real-Time PCR Analysis Software version 1.2.

SYBR® Green is a commonly used fluorescent dye that binds to double-stranded DNA and can be monitored by measuring an increase in fluorescence. SYBR® green dye for detection was used in a 25  $\mu\text{l}$  reaction that consisted of 12.5  $\mu\text{l}$  SYBR® Green JumpStart™ Taq ReadyMix™ mastermix (Sigma-Aldrich®, USA); 10.5  $\mu\text{l}$  nuclease free water, 0.5  $\mu\text{l}$  10mM forward primer; 0.5  $\mu\text{l}$  10mM reverse primer and 1  $\mu\text{l}$  cDNA. SYBR® Select Master Mix (Applied Biosystems) was later used which required a 20  $\mu\text{l}$  reaction that consisted of 10  $\mu\text{l}$  SYBR select, 8  $\mu\text{l}$  nuclease free water, 0.5  $\mu\text{l}$  10mM forward primer; 0.5  $\mu\text{l}$  10mM reverse primer and 1  $\mu\text{l}$  cDNA. Reactions were transferred into a MicroAmp® Optical 96-well Reaction Plate (Applied Biosystems) in triplicate, which was gently centrifuged at 500 rpm for 1 minute at 4°C and placed in the Real-time PCR System.

The following cycling parameters were used to amplify the target genes: an initial denaturation at 95°C for 10 minutes; followed by 45 cycles of denaturation at 95°C for 30 seconds; annealing at 58°C for 30 seconds; and extension at 72°C for 45 seconds. SYBR Select Master Mix required an additional activation temperature at 50°C for 2 minutes before the initial denaturation at 95°C for 10 minutes. The rest of the cycling parameters remained the same as those used for SYBR<sup>®</sup> Green JumpStart<sup>™</sup> Taq ReadyMix<sup>™</sup>. A melt curve analysis ranged from 50°C to 90°C with 1°C increments and a plate read step was included for 5 seconds after each temperature change (Appendix 1.8).

The expression levels of the target genes were normalised against that of the two reference genes *Hprt* and *β-actin*. Relative quantification using the comparative Ct method was used to analyse the data. Values given are expressed as a fold change relevant to the control cell line (E12.5) as determined by the  $2^{-\Delta\Delta C_t}$  method (Livak and Schmittgen, 2001). All qPCR experimental procedures used in this study were performed in accordance with the MIQE guidelines (Appendix 1).

### **2.8.1 Statistics**

qPCR data were analysed using (IBM) SPSS Statistics Version 21. Differences in expression of the target genes between the different developmental stages were determined using a One Way Analysis of Variance (ANOVA) and a Tukey HSD post-hoc test. All tests for normality were satisfied and significance was determined at  $p < 0.05$ .

## **2.9 Polyacrylamide gel electrophoresis (PAGE) and immunoblot analysis**

### **2.9.1 Protein extraction and sample preparation**

Protein was extracted from E12.5; E13.5; E15.5 and P13 cell lines. Protein could not be extracted from E14.5 cells as the cell line was lost due to failure of the liquid nitrogen stock freezer.

Culture media from selected dishes was aspirated and discarded. Adherent corneal endothelial cells were then harvested from two 10 cm<sup>3</sup> dishes per cell line using a cell scraper (Biologix Research Company). The dishes were rinsed with 1x PBS to collect the cells, which were then transferred into a single sterile 15 mL centrifuge tube per cell line. The 15 mL centrifuge tube was centrifuged at room temperature for 5 minutes at 2000 rpm in an Eppendorf 5810 R centrifuge. The supernatant was discarded and the pellet of cells was re-suspended in 1 mL 1x PBS which was centrifuged for a further 2 minutes at 4°C at 2000 rpm. The supernatant was discarded and the pellet of cells was placed on ice immediately.

Each pellet of cells was resuspended in 50 µl Radio-immunoprecipitation assay (RIPA) buffer (Sigma-Aldrich<sup>®</sup>, USA) and 5 µl of a protease and phosphatase inhibitor cocktail (Sigma-Aldrich<sup>®</sup>, USA), which was then mixed by vortexing at medium speed. The cells were then incubated at room temperature for 5 minutes, followed by a 30 minute incubation period on ice. The tube was centrifuged at 4°C for 15 minutes at 4000 rpm. The quantity of cell lysate removed from each tube was recorded. 10 µl of each lysate was placed in a separate sterile micro-centrifuge tube for protein quantification. An equal volume of reducing sample treatment buffer/protein loading dye (Appendix 4.2a and 4.2b) was added to the remaining cell lysate (1:1 ratio). Protein samples were centrifuged briefly and

incubated at 95°C for 5 minutes. Thereafter the protein samples were vortexed briefly, centrifuged and stored at -80°C.

## **2.9.2 Protein quantification**

A Pierce® Bicinchoninic Acid (BCA) Protein Assay Kit (Thermo Scientific) was used to quantify all protein samples according to the ‘microplate procedure’.

### **2.9.2.1. Preparation of BCA standards**

The BCA kit provides protein standards that can be diluted and used to generate a standard curve of known concentrations. Each ampule provided has a concentration of 2 mg/mL. 300 µl of 2000 µg/mL BCA stock was serially diluted into 7 micro-centrifuge tubes. A blank standard containing ultra-pure water was also prepared.

### **2.9.2.2 Preparation of BCA working reagent (WR)**

The 10 µl lysate dedicated for protein quantification was diluted with nuclease free water in a 1:10 ratio (10 µl lysate in 90 µl nuclease free water). The diluted lysate was centrifuged briefly and kept on ice until needed. The total working reagent (WR) volume required for protein quantification, consisting of Reagent A and Reagent B, was calculated using the following equation:

$$\text{Total WR} = [(\text{number of standards} \times \text{number of replicates}) + (\text{number of samples} \times \text{number of replicates}) + 1 \text{ for pipetting error}] \times 200 \mu\text{l}$$

The total WR was prepared by mixing Reagent A and Reagent B in a 50:1 ratio respectively (50 Reagent A: 1 Reagent B) in a 15 mL centrifuge tube.

### 2.9.2.3 The microplate procedure

The BCA standards and protein lysate samples were thawed on ice and briefly centrifuged. 25  $\mu\text{l}$  of each standard and samples were pipetted into a 96-well microplate (Sero-Well) in duplicate and triplicate respectively. 200  $\mu\text{l}$  of WR was pipetted into each well containing standards or samples and the plate was gently agitated for 30 seconds. The microplate was then sealed and incubated at 37°C for 30 minutes. The microplate was left to cool to room temperature and read on a microplate reader (Powerwave XS plate reader, Bio-Tex<sup>®</sup>) using KC4<sup>™</sup> version 3.2 software. Absorbance readings were measured at 562nm and a standard curve was generated by the software. The unknown protein concentrations were then extrapolated from the standard curve (Figure 2.2)

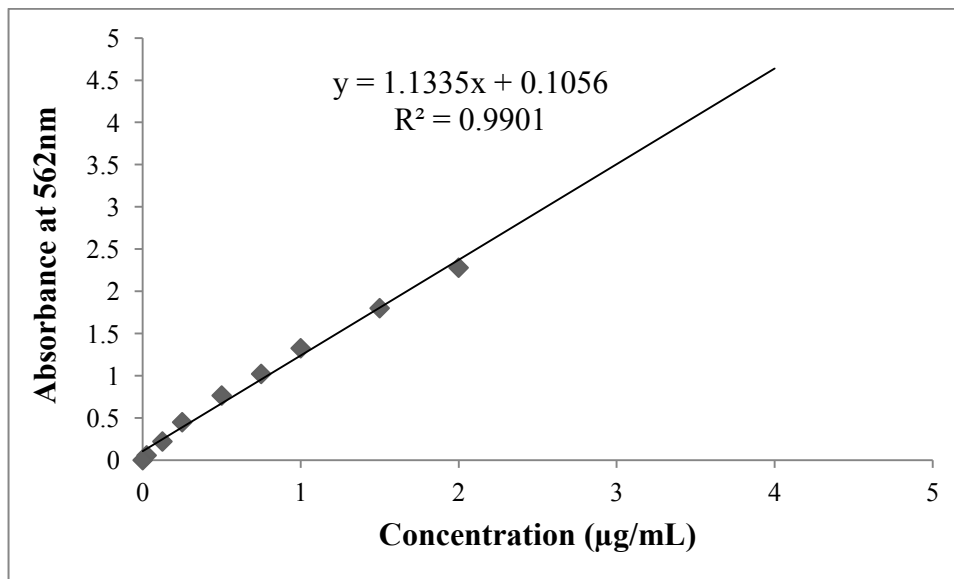


Figure 2.2: BCA standard curve used to extrapolate unknown protein concentrations.

### 2.9.3 Polyacrylamide gel assembly

A Mini-PROTEAN 3 cell system (PowerPac Basic<sup>™</sup>, Bio-Rad) was used for PAGE analysis. Glass plates (1.5 mm) used to assemble the gels were cleaned thoroughly with 70% ethanol. Parafilm (Pechiney Plastic Packaging) was used to seal the glass plates, which were then inserted into a casting frame (Bio-Rad) and secured in a casting stand (Bio-Rad) (Figure 2.3).

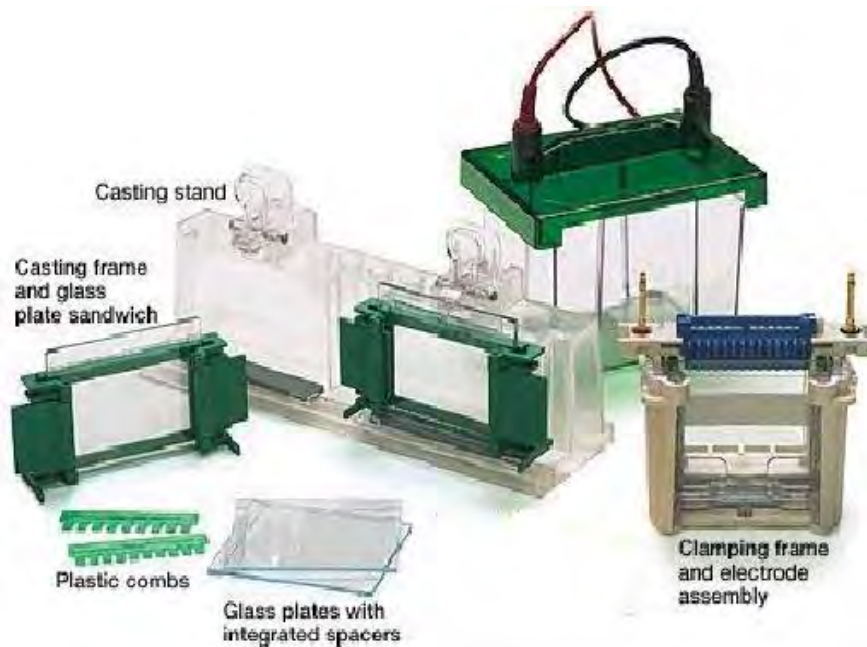


Figure 2.3: Polyacrylamide gel assembly apparatus. Image adapted from [www.bio-rad.com](http://www.bio-rad.com)

12.5 % SDS polyacrylamide gels (Appendix 4.2c) were used to resolve the proteins of interest in this study. The resolving gel components were combined in a 15 mL centrifuge tube and mixed by gently inverting the tube, thus preventing SDS foaming and bubble formation. The resolving gel was promptly loaded between the sealed glass plates using a Gilson pipette. Thereafter, 1 mL of ultra-pure water (Milli-Q<sup>®</sup> Integral 3/5/10/15 system) was gently pipetted in a drop wise manner on top of the resolving gel to form a layer that will trap any air bubbles formed in the resolving gel. The resolving gel was left to set for 25 minutes. Thereafter, the plates were removed from the casting stand and the ultra-pure water was poured off. Residual water was absorbed by a piece of sterile filter paper, paying careful attention not to pierce the resolving gel. The plates and casting frame were secured in the casting stand in preparation for the stacking gel.

4% stacking gels (Appendix 4.2c) were prepared in a 15 mL centrifuge tube. The components were mixed by gently inverting the tube and promptly pipetted onto the solid resolving gel secured in the casting frame. A 15-well comb was inserted into the stacking gel and allowed to set for 25 minutes. Thereafter, the plates were removed from the casting stand and frame, and the parafilm and comb were removed as well. The wells of the gel were gently rinsed with 1x electrode buffer (Appendix 4.2d) using a 1 mL pipette. Excess gel fragments were removed from the surface of the glass plates before they were placed into the electrode assembly apparatus. The entire electrode assembly apparatus was then placed in a tank filled with 1x electrode buffer, with the smaller plate facing inwards. The entire tank was then placed into a Tupperware container that was filled with ice to prevent overheating during electrophoresis.

#### **2.9.3.1 Sample preparation and loading into the gel**

Protein samples were thawed from  $-80^{\circ}\text{C}$  at  $95^{\circ}\text{C}$  for 5 minutes. Thereafter, protein samples were centrifuged at room temperature for 2 minutes at  $2000 \times g$  and allowed to cool to room temperature.  $2.5 \mu\text{l}$  of a PageRuler™ Prestained Protein Ladder (Thermo Scientific) was loaded into the first and last wells in each gel.  $40 \mu\text{g}$  of protein was loaded in duplicate in each gel.

#### **2.9.3.2 PAGE gel electrophoresis and protein transfer**

The protein samples were run through the 4% stacking gel at 90 V for 30 minutes in the Mini-PROTEAN 3 cell system (PowerPac Basic™, Bio-Rad). Thereafter, the protein samples were separated by the resolving gel at 120 V for 60 minutes.

After PAGE gel electrophoresis, the glass plates containing the gels were removed from the tank and placed in a container containing sufficient protein transfer buffer (Appendix 4.2e)

to keep the gels moist. A gel releaser was used to carefully separate the glass plates and loosen the gel. The stacking gel was discarded and the protein transfer cassette was laid out. A foam sponge (Bio-Rad) was soaked in protein transfer buffer and placed on the black side of the protein transfer cassette. Four pieces of pre-cut filter paper were also soaked in protein transfer buffer and placed on the foam sponge individually. A 1 mL pipette tip (TipOne, Starlab) was used to smoothen out the filter paper and remove air bubbles (air bubbles would result in an uneven protein transfer). The gel was carefully placed on top of the fourth piece of filter paper. A pre-cut sheet of Amersham™ Hybond™-ECL nitrocellulose membrane (GE Healthcare) was gently soaked in protein transfer buffer and placed on top of the gel. An additional four pieces of pre-cut paper were soaked in protein transfer buffer and placed on the nitrocellulose membrane to keep the gel and the membrane moist. Air bubbles were smoothened out. Another foam sponge was soaked in protein transfer buffer and placed on the filter paper stack. The protein transfer cassette was closed and placed into the electrode assembly apparatus in the tank filled with protein transfer buffer. A magnetic stirrer was placed in the tank. The entire tank was placed in a Tupperware container which was then placed on an IKA® big-squid stirrer. An ice brick was placed inside the tank, in contact with the protein transfer cassette, and ice was stacked in the Tupperware container around the tank to prevent over-heating. The protein transfer was then run at 100 V for 80 minutes to completely transfer the protein from the gel onto the nitrocellulose membrane.

### **2.9.3.3 Membrane blocking and antibody incubations**

Protein expression could not be determined for Slc4a4 due to the lack of a commercially available antibody specific for mouse Slc4a4. For Zo1, the membrane was probed with a primary polyclonal antibody specific for mouse Zo1, and subsequently probed with a secondary horseradish peroxidase HRP antibody. For Aqp1, the membrane was probed with a primary polyclonal antibody specific for mouse Aqp1, and subsequently probed with a secondary HRP antibody.

After the protein transfer was completed, the protein transfer cassette was dismantled and the nitrocellulose membrane was cut into 3 strips, with first strip containing the Zo1 protein at ~220 kDa, the second strip containing the glycosylated Aqp1 protein at ~35 kDa and the third strip containing the unglycosylated Aqp1 protein at ~35 kDa. A single protein transfer onto 1 nitrocellulose membrane could then be incubated with 3 separate antibodies for different proteins. The strips of nitrocellulose membrane containing each protein were placed in separate containers. The membranes were rinsed twice in Tris-Buffered Saline with tween (TBS-T; Appendix 4.2f) to remove any traces of protein transfer buffer and to keep the membranes moist. The membranes were then incubated in 6% skim milk (Sigma-Aldrich<sup>®</sup>, USA) blocking solution (Appendix 3.2g) for an hour with agitation (MiniMix, Enduro<sup>™</sup>, Labnet). Blocking prevents non-specific primary antibody binding. Thereafter, the membranes were rinsed twice in TBS-T to remove traces of blocking solution. Residual TBS-T was aspirated with a 1 mL pipette.

Following blocking, the membranes were probed with the following primary antibodies:

Table 2.2: Antibodies (AB) used in this study for western blot analysis.

<b>Protein</b>	<b>1° AB Name</b>	<b>1° AB dilution</b>	<b>2° AB Name</b>	<b>2° AB Dilution</b>
Zo1	ZO-1 (H-300): sc-10804 Santa Cruz Biotechnology, Inc	1:1000	Anti-rabbit IgG, HPR-linked. Cell Signaling Technology <sup>®</sup>	1:4000
Aqp1	Anti-AQP1 (#AB2219) Millipore	1:2000	Anti-rabbit IgG, HPR-linked. Cell Signaling Technology <sup>®</sup>	1:4000

\*All primary antibodies were diluted in 6% skim milk (Sigma-Aldrich<sup>®</sup>, USA) and all secondary antibodies were diluted in TBS-T

The membranes were incubated with primary antibodies overnight at 4°C with agitation on an IKA<sup>®</sup> KS 130 Basic at 160 rpm.

The following day, the membranes were rinsed with TBS-T 3 times to remove all traces of the primary antibodies. The membranes were then soaked in TBS-T for 8 minutes on the IKA<sup>®</sup> KS 130 Basic at 320 rpm. These 8 minute washes were repeated 3 times for Zo1 and glycosylated Aqp1, and twice for unglycosylated Aqp1 (more than 2 washes reduced the intensity of the unglycosylated band). In between each wash, the membranes were vigorously rinsed with fresh TBS-T twice. These washes ensure that unbound or non-specifically bound primary antibodies are removed. All the TBS-T was aspirated after the final wash and the membranes were probed with the secondary antibody (Table 2.2) at room temperature for 1 hour with agitation on an IKA<sup>®</sup> KS 130 Basic at 160 rpm.

Following incubation, the secondary antibody was aspirated and the membranes were washed as described for the primary antibody. The 8 minute washes were repeated 3 times for Zo1 and glycosylated Aqp1, and twice for unglycosylated Aqp1 to remove non-specific secondary antibody binding.

#### **2.9.4 Imaging the western blot**

Protein bands were visualised using a Clarity<sup>™</sup> Western ECL Blotting Substrate (Bio-Rad) on the ChemiDoc<sup>™</sup> XRS<sup>+</sup> System using Image lab<sup>™</sup> software version 2.0.1 (Bio-Rad). The Clarity<sup>™</sup> Western ECL Blotting Substrate chemiluminescent detection system (Figure 2.4) is a sensitive kit that is compatible with any HPR-conjugate secondary antibody.

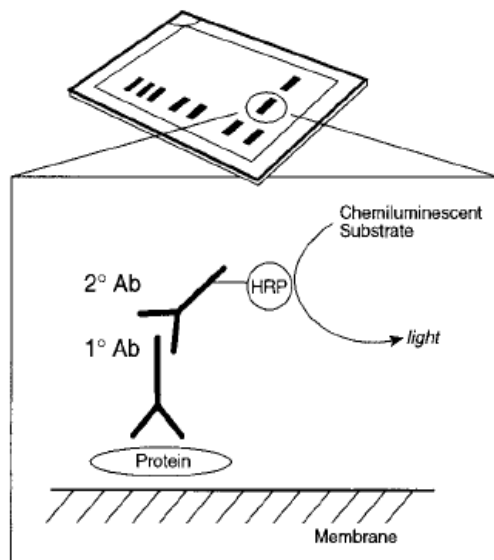


Figure 2.4: The chemiluminescent detection system. After the primary antibody binds to the target protein, a complex with a HRP-linked secondary antibody is formed. The chemiluminescent substrate is added and emits light during enzyme catalysed decomposition. Image obtained from (<http://media.cellsignal.com/pdf/7074.pdf>).

Each membrane was imaged separately. The membrane was dabbed on tissue paper to remove residual TBS-T and placed on a plastic plate. The plate was then placed into the ChemiDoc™ XRS<sup>+</sup> System. A chemiluminescent solution was prepared by adding Clarity™ Western ECL peroxide solution and Clarity™ Western ECL luminol/enhancer solution in a 1:1 ratio (300 µl of each solution was used in this study). 600 µl of the prepared chemiluminescent solution was pipetted onto the membrane in a drop wise manner and the membrane was tilted to ensure an even distribution of the solution. The membranes were imaged using a western blot protocol established in the laboratory. The protein ladder was then imaged using a Molecular Marker protocol as this is not detected by the chemiluminescent signal. The western blot image and the molecular marker image were merged and flipped to yield a single representative image that was in the same orientation as when the protein was loaded. A single representative image was analysed by densitometry. Ponceau S staining was performed to detect total protein on the membrane.

The membranes were stained in 1x Ponceau S stain (Sigma-Aldrich<sup>®</sup>, USA, Appendix 3.2h) for 5 minutes at room temperature with agitation. A Ponceau destain (Appendix 3i) was used to rinse the membranes and remove excess Ponceau S for 30 seconds at room temperature with agitation. Total protein was then detected by imaging the membrane using the Molecular Marker protocol as done for the protein ladder. A single representative Ponceau S image was analysed by densitometry (appendix 2).

### **2.9.5 Densitometry**

Densitometry was performed on the western blot images using the Image lab<sup>™</sup> software version 2.0.1 (Bio-Rad). A rectangle was constructed around each protein band (same size) which allowed the software to calculate the local pixel or band intensity of each band. This was repeated on the Ponceau S image to analyse total protein. The band intensities were exported into Microsoft Excel 2010 and the intensity of the gene of interest (i.e. Zo1 and Aqp1) was calculated relative to the intensity of the total protein (i.e. Ponceau S). The results are expressed as an average with the standard error of the mean (SEM). Densitometric data were analysed using (IBM) SPSS Statistics Version 21. Differences in expression of the target genes between the different developmental stages were determined using a One Way Analysis of Variance (ANOVA) and a Tukey HSD post-hoc test. All tests for normality were satisfied and significance was determined at  $p < 0.05$ .

### **2.10 Immunocytochemistry - confocal microscopy**

Confocal microscopy was performed to evaluate the localisation of Zo1 and Aqp1 protein expression at E12.5, E13.5, E15.5 and P13 cell line in monolayer culture as well as hanging drop culture, simulating the 3-D environment in which corneal endothelial development takes place.

### **2.10.1 Monolayer culture**

The cell lines from each developmental stage were cultured in 10 cm<sup>3</sup> dishes. Culture medium was aspirated and the cells were harvested by gently scraping the cells using a cell scraper (Biologix Research Company). The dishes were rinsed with 1x PBS to collect the cells, which were then transferred into a single sterile 15 mL centrifuge tube. The 15 mL centrifuge tube was centrifuged at room temperature for 5 minutes at 2000 rpm. The supernatant was discarded and the pellet of cells was re-suspended in 1 mL culture medium. Cell counts were performed using a haemocytometer and a Nova compound light microscope (Novatech, USA).  $1 \times 10^3$  cells were seeded onto UV treated 12 mm coverslips placed into each well of a 24-well plate, supplemented with 1 mL of culture medium. Monolayers were cultured under normal cell culture conditions (as described in section 2.5) for 48-72 hours and growth was monitored using a Nikon TMS-F inverted light microscope (Nikon, Japan).

### **2.10.2 Hanging drop culture**

Cells were harvested and counted as described in section 2.10.1. The hanging drops were generated by pipetting 30  $\mu$ l drops of culture medium containing  $1 \times 10^3$  cells on the inverted lid of a 6 cm<sup>3</sup> dish (Corning, USA). 3 mL 1x PBS was added to the culture dish to prevent desiccation of the drops. The lid was then carefully inverted and placed on the base of the dish and the hanging drops were cultured for 72 hours. Cell growth was monitored using a Nikon TMS-F inverted light microscope (Nikon, Japan).

12 mm glass coverslips were coated with 2  $\mu$ l Poly-L-lysine (Sigma-Aldrich<sup>®</sup>, USA) to facilitate cell adhesion of the hanging drops to the coverslips prior to fixation. The hanging drops were gently transferred onto the coated glass coverslips using forceps. The forceps were used to hold the glass coverslips against the lid containing the hanging drops. The

medium containing the hanging drops were gently transferred onto the glass coverslips upon contact. Excess medium around the hanging drops was carefully aspirated by pipetting the medium off the coverslips, paying careful attention not to contact the hanging drops with the pipette tip. The glass coverslips containing the hanging drops were left to air dry for 5 minutes at room temperature and they were placed into each well of a 24-well plate.

### **2.10.3 Immunostaining**

#### **2.10.3.1 Sample preparation of the monolayer and hanging drop cultures**

Culture medium in the wells of the plate was aspirated and discarded. The cells in the wells were gently washed with 200  $\mu$ l 1x PBS using a Pasteur pipette rested against the well wall (to prevent washing the cells off the coverslip). Monolayers and hanging drops were fixed in the wells with 4% paraformaldehyde (Merck, USA, Appendix 3.3a) at room temperature for 10 minutes, followed by 3 washes with 200  $\mu$ l 1x PBS. Thereafter, the cells were blocked in 0.5% bovine serum albumin (BSA) blocking solution (Appendix 4.3b) at room temperature for 1 hour.

#### **2.10.3.2 Antibody incubations**

Following blocking, the cells were probed with the following antibodies:

Table 2.3: Antibodies (AB) used in this study for immunocytochemistry analysis.

<b>Protein</b>	<b>1° AB Name</b>	<b>1° AB dilution</b>	<b>2° AB Name</b>	<b>2° AB Dilution</b>
Zo1	ZO-1 (H-300): sc-10804 Santa Cruz Biotechnology, Inc	1:50	Cy <sup>™</sup> 3-conjugated donkey anti-rabbit IgG. Jackson Immunolabs, USA.	1:1000
Aqp1	Anti-AQP1 (#AB2219) Millipore	1:2000	Cy <sup>™</sup> 3-conjugated donkey anti-rabbit IgG. Jackson Immunolabs, USA.	1:1000

The primary and secondary antibodies were diluted in 0.5% BSA (Sigma-Aldrich<sup>®</sup>, USA) solution.

The cells were incubated in 300 µl primary antibody solution at 4°C overnight. The following day, primary antibody solutions were aspirated and the wells were rinsed with 200 µl of cold 1x PBS 3 times to remove all traces of the primary antibodies. The cells were then incubated with Cy<sup>™</sup>3-conjugated donkey anti-rabbit IgG secondary antibody in the dark for 1 hour at room temperature. Following incubation, the secondary antibody was aspirated and the wells were rinsed with 200 µl 1x PBS 3 times to remove all traces of the secondary antibodies. The cells were then incubated with 300 µl of a 1:50 dilution of 50 µg/mL 4',6-diamidino-2-phenylindole (DAPI) in 1x PBS for 5 minutes at room temperature to stain the nuclei. The cells were then rinsed once with 200 µl 1x PBS and the coverslips were mounted on glass slides using a drop of mowial with 1,4-diazabicyclo [2.2.2]octane (DABCO) mounting medium (Appendix 4.3c and 4.3d). Mounted slides were stored in the dark at 4°C.

For the negative controls, primary and secondary antibodies were substituted by 1x PBS in no-primary controls and no-secondary controls respectively, to identify non-specific binding of each antibody (appendix 3).

#### **2.10.4 Visualisation**

Zo1 and Aqp1 monolayers and hanging drops were analysed by confocal microscopy using a Zeiss LSM 710 Laser Scanning Confocal Microscope (Zeiss, Germany) at the UKZN Centre for electron microscopy (UKZN Pietermaritzburg campus). Images were captured using ZEN Efficient Navigation 2010 software (Zeiss, Germany). The slides were viewed under Lcl PlanNeoFluar 25x/0.8 1 mm Korr DIC M27 and 63x/1.3 1 mm Korr DIC M27 objectives. The frame size maintained at 1024 x 1024 and images were taken at speed 3 with an averaging of 4. The pin hole was maintained at 1 airy unit. The laser intensity for DAPI and Cy3 was maintained at 4 and 20 respectively to ensure that images between developmental stages were comparable.

### **2.11 *Foxc1* knockdown using the *pSilencer*<sup>TM</sup> hygro kit.**

#### **2.11.1 Overview**

Previously in the laboratory, we generated a shRNA targeting *Foxc1* that was shown to knock down *Foxc1* expression by 99% (Silla *et al.*, 2014). The siRNA was cloned into pGEMTeasy and therefore can only be used for transient transfections. One of the aims of this study (although not achieved) was to clone the siRNA sequence into a vector that allows for stable knockdown. We chose the *pSilencer*<sup>®</sup>2.1-U6 hygro vector (Figure 2.5) that uses RNA polymerase III (pol III) promoters which produce large amounts of small RNA using promoter and terminator sequences. The plasmid used in this study includes both Hygromycin and Ampicillin antibiotic resistance genes for selection (Figure 2.5). The plasmid is also linearised with both *BamH* 1 and *Hind* III restriction sites to facilitate directional cloning (Figure 2.6).



### 2.11.2 *Foxc1*-shRNA sequence

Previously, with the aid of Prof. Marco Weinberg from The University of Witwatersrand, we designed an shRNA that targets *Foxc1* and knocks down its expression effectively (Figure 2.7) (Silla *et al.*, 2014). These oligonucleotide sequences were modified to incorporate additional sequences for *BamH* I and *Hind* III on the 5' and 3' ends of the siRNA sequence respectively, synthesised and PAGE purified. The total length of the modified oligonucleotides was 65bp.

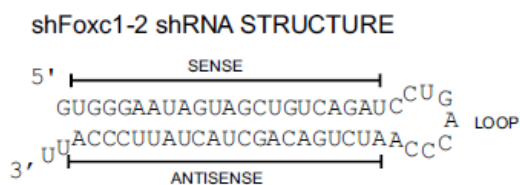


Figure 2.7: shRNA-2-*Foxc1*.

### 2.11.3 Cloning hairpin siRNA inserts into the *pSilencer* vector

#### 2.11.3.1 Oligonucleotide annealing and ligation

Sense and antisense siRNA template oligonucleotides were dissolved in nuclease free water to yield a 100  $\mu$ M stock solution. The concentration of each oligonucleotide was quantified using a Spectrophotometer ND1000 (NanoDrop technologies). Each oligonucleotide was then diluted to prepare a 1  $\mu$ g/ $\mu$ l solution in nuclease free water. An annealing mixture was prepared by mixing 2  $\mu$ l of each oligonucleotide in 46  $\mu$ l 1x DNA Annealing solution (*pSilencer*<sup>TM</sup> hygro kit) in a sterile 1.5 mL micro-centrifuge tube. The annealing mixture was heated to 90°C for 3 minutes in a dry bath incubator, after which it was incubated at 37°C for 1 hour. The annealed siRNA hairpin template was then ligated into the *pSilencer* vector as follows: 5  $\mu$ l of the annealed siRNA hairpin template insert was diluted in 45  $\mu$ l nuclease free water for a final concentration of 8 ng/ $\mu$ l. A 10  $\mu$ l plus-insert ligation reaction was set up in a micro-centrifuge by mixing 1  $\mu$ l of the diluted annealed siRNA insert, 6  $\mu$ l nuclease free water, 1  $\mu$ l 10x T4 DNA ligase buffer (Promega), 1  $\mu$ l *pSilencer* vector and

1.7  $\mu\text{l}$  T4 DNA ligase (3 u/ $\mu\text{l}$ ) (Promega). A 10  $\mu\text{l}$  minus-insert ligation reaction was set up as a negative control by replacing the diluted annealed siRNA insert with 1x DNA Annealing solution. The plus and minus insert ligation reactions were incubated overnight at 16°C to facilitate a very high ligation efficiency.

### **2.11.3.2 Plasmid transformation**

DH5a Z-Competent™ *Escherichia Coli* (*E.coli*) cells (Zymo Research) that were stored at -80°C were briefly thawed on ice. A 50  $\mu\text{l}$  aliquot of competent *E.coli* cells was transformed with 5  $\mu\text{l}$  minus-insert ligation product in a 1.5 mL microcentrifuge tube. A second aliquot of competent *E.coli* cells was transformed with 5  $\mu\text{l}$  plus-insert ligation product in a 1.5 mL microcentrifuge tube. The tubes were gently flicked to mix the cells which were then pipetted onto the centre of pre-warmed ampicillin-containing Luria broth (LB) agar plates (Appendix 4.4a) (1 plate per treatment) and spread using the aseptic technique. The minus-insert ligation product was plated first to avoid cross contamination from the plus-insert ligation product. The ampicillin agar plates were incubated at 37°C overnight to facilitate cell transformation. The following day, individual colonies were isolated by gently scraping them off the agar with a pipette tip. The selected colonies were grown in 10 mL LB broth (Appendix 4.4b) containing ampicillin (1  $\mu\text{l}$  of 100 mg/ml ampicillin per 1 mL LB broth) in a 50 mL centrifuge tube (Corning, USA) overnight at 37°C with agitation in a shaking incubator (225 rpm). The following day, 1 mL glycerol stocks of each colony was prepared and stored at -20°C (Appendix 4.4c). This ensured that samples that contained the positive insert could be propagated later. Plasmid DNA was then purified.

### **2.11.3.3 Plasmid mini-prep**

Plasmid DNA was initially purified from transformed *E.coli* cells using a QIAprep Spin Miniprep kit (QIAGEN, Germany). The 50 mL centrifuge tubes containing the colonies in LB broth were removed from the shaking incubator and cells were harvested by

centrifugation at 1 000 x g for 10 minutes at 4°C in an Eppendorf 5218R centrifuge. The supernatant was discarded and the pellet of cells was re-suspended in 250 µl buffer P1 supplemented with RNase A and LyseBlue. The solution was mixed by pipetting and transferred into a sterile 1.5 mL micro-centrifuge tube. The micro-centrifuge tube was inverted several times to homogenise the solution. The cell suspension turned blue which indicated a homogeneous solution. 250 µl buffer P2 was added to the solution and mixed by inverting the tube 4-6 times. 350 µl buffer N3 was added and the tube was inverted 4-6 times to thoroughly mix the solution. The tube was then centrifuged at room temperature at 10 000 rpm for 10 minutes to yield a compact white pellet. The supernatant was aspirated and added directly into a QIAprep spin column by pipetting. The QIAprep spin column was briefly centrifuged at room temperature at 10 000 rpm for 30 seconds and the flow-through was discarded. 750 µl buffer PE (wash buffer) was added to the QIAprep spin column, which was then centrifuged at room temperature at 10 000 rpm for 30 seconds to wash the spin column. The flow-through was discarded and the spin column was centrifuged at room temperature at 10 000 rpm for 1 minute to remove residual wash buffer. The flow-through and collection tube were discarded and the spin column was placed in a sterile 1.5 mL micro-centrifuge tube. To elute the DNA, 30 µl TE buffer (Appendix 4.4d) was pipetted directly onto the membrane in the centre of the spin column. This was left to stand at room temperature for 5 minutes. Thereafter the spin column was centrifuged at room temperature at 10 000 rpm for 1 minute. The spin column was then discarded and the purified plasmid DNA was stored on ice until it was quantified using a Spectrophotometer ND1000 (NanoDrop technologies). The plasmid DNA was then stored at -20°C.

#### **2.11.3.4 PCR amplification to verify that the clones contained the siRNA insert**

T7 sequencing primers were used for conventional PCR to verify that the clones contained the siRNA insert (Appendix 4.4e). The primer sequences were as follows: forward 5'-GTA ATA CGA CTC ACT ATA GGG-3'; reverse 5'-AGG CGA TTA AGT TGG GTA-3'. A

temperature gradient PCR was performed to optimise the melting temperature of the T7 primers (Figure 2.8).

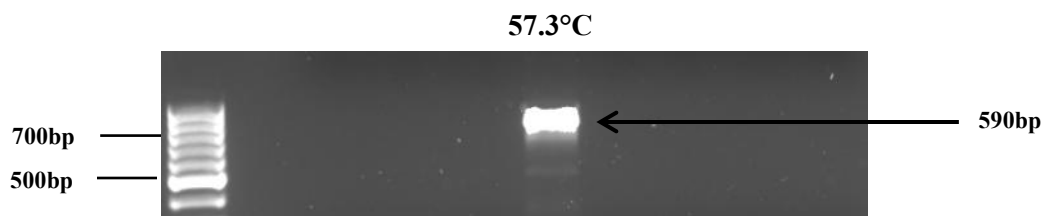


Figure 2.8: A temperature gradient PCR of the T7 primers showing the optimal melting temperature at 57.3°C.

A 20  $\mu$ l reaction consisted of 1  $\mu$ l plasmid DNA; 2  $\mu$ l *Taq* buffer containing  $(\text{NH}_4)_2\text{SO}_4$   $\text{MgCl}_2$ ; 2  $\mu$ l 2mM dNTPs, 1.8  $\mu$ l 25mM  $\text{MgCl}_2$ , 0.5  $\mu$ l 10mM forward primer, 0.5  $\mu$ l 10mM reverse primer, 0.2  $\mu$ l *Taq* recombinant DNA polymerase (5 units/ $\mu$ l) and 12  $\mu$ l nuclease free water. A Bio-Rad My cycler™ thermal cycler with the following cycling parameters: denaturation at 95°C for 3 minutes; followed by 40 cycles of 95°C for 30 seconds; 57.3°C for 30 seconds; and 73°C for 90 seconds; followed by an additional elongation step of 72°C for 10 minutes. PCR products were analysed by agarose gel electrophoresis as explained in section 2.7.1 of the materials and methods.

### 2.11.3.5 Digestion of purified plasmid DNA

The purified plasmid DNA was digested with restriction enzymes to verify that the clones contained the plasmid insert. Each DNA sample was prepared for digestion as follows: 1  $\mu$ g plasmid DNA; 1  $\mu$ l *BamH* I restriction enzyme (10 u/ $\mu$ l) (Thermo Scientific); 1  $\mu$ l *Hind* III restriction enzyme (10 u/ $\mu$ l) (Thermo Scientific) and 2  $\mu$ l 10x Tango buffer (Thermo Scientific) was added to a 1.5 mL micro-centrifuge tube. Nuclease free water was then added to the reaction to make up a final volume of 20  $\mu$ l. The tube was then incubated in a dry bath incubator at 37°C for 2 hours to facilitate the restriction digest. Following

incubation, the tubes were centrifuged briefly and the restriction products were separated on a 1.5% agarose gel by electrophoresis as described in section 2.7.1. The presence of 2 bands should indicate that the clones contain the siRNA insert. A band at approximately 4900bp would represent the vector and a 65bp band would represent the insert.

#### **2.11.4 Troubling shooting**

Due to the small size of the siRNA insert (65bp) and the low concentration of the plasmid DNA obtained from a mini-prep, further trouble shooting was performed to distinguish the presence of the small siRNA insert.

##### **2.11.4.1 Native polyacrylamide gel electrophoresis (PAGE)**

Despite numerous attempts, the siRNA insert (65bp) could not be detected by agarose gel electrophoresis following digestion with restriction enzymes. Therefore, native polyacrylamide gel electrophoresis was performed to resolve the restriction products. Native PAGE gels resolve DNA instead of protein and differ from conventional PAGE gels as SDS is replaced by water (Appendix 4.4f). The restriction products were separated on an 8% native PAGE gel run in 1x TBE buffer at 100V for 80 minutes. Clones that contained the siRNA insert were subjected to midi-prep purification to yield a greater concentration of plasmid DNA.

##### **2.11.4.2 Plasmid midi-prep**

Super Optimal Broth (SOB) with catabolite repression (SOC) (i.e. SOB with added glucose) is a nutrient rich medium that was used to increase the yield of the microbial culture.

A starter culture of 100 mL SOC medium (Appendix 4.4g) was transferred into a 200 mL glass Schott bottle. 10 µl of the plasmid from the glycerol stock was added to the culture, which was then incubated at 37°C overnight with agitation in a shaking incubator (225 rpm). The following day, 50 mL of the culture was transferred into a 50 mL centrifuge tube (Corning, USA) and centrifuged at 10 000 rpm for 30 minutes at 4°C to pellet the cells. The supernatant containing the SOC medium was discarded and the remaining 50 mL of culture was added into the same centrifuge tube that contains the cell pellet. The tube was centrifuged again at 10 000 rpm for 30 minutes at 4°C to pellet the cells in the remaining culture. The supernatant containing the SOC medium was discarded and the pellet was purified using a QIAGEN midi-prep kit (QIAGEN, Germany).

The pellet was re-suspended in 4 mL buffer P1 containing RNase A and LyseBlue. The solution was mixed by pipetting and transferred into a sterile 15 mL centrifuge tube. The centrifuge tube was vigorously inverted several times to homogenise the solution. The cell suspension turned blue which indicated a homogeneous solution. Thereafter, 4 mL buffer P2 was added to the solution and mixed by inverting the tube 4-6 times until the solution turned white. Thereafter, 4 mL buffer P3 was added and the tube was vigorously inverted 4-6 times to thoroughly mix the solution. The tube was incubated on ice for 15 minutes, followed by centrifugation at 4°C at 10 000 rpm for 30 minutes to yield a compact white pellet containing cellular debris. A layer of cell debris was carefully removed and the supernatant containing the plasmid DNA was aspirated promptly and added directly into a QIAGEN-tip 100 that had been equilibrated with 4 mL buffer QBT. The QIAGEN-tip 100 containing the supernatant was balanced over a glass beaker to filter the supernatant through the membrane by gravity flow. The QIAGEN-tip 100 membrane was washed twice with 10 mL buffer QC. The QIAGEN-tip 100 was placed into a sterile 15 mL centrifuge tube and the plasmid DNA was eluted from the QIAGEN-tip 100 membrane by adding 5 mL buffer QF directly onto the membrane. The plasmid DNA was then precipitated by adding 3.5 mL of room temperature isopropanol (Merck), followed by centrifugation at 10 000 rpm at 4°C for 30 minutes. The supernatant was carefully aspirated and discarded. 2

mL 70% ethanol was added to wash the cell pellet which was then centrifuged at 10 000 rpm at 4°C for 10 minutes. The supernatant was carefully aspirated and discarded, and the cell pellet was left to air dry for 5 minutes. The cell pellet was dissolved in 30 µl TE buffer and stored on ice until it was quantified using a Spectrophotometer ND1000 (NanoDrop technologies). The plasmid DNA was then stored at -20°C.

### **2.11.5 Sequencing**

Clones containing the siRNA insert were verified by Sanger sequencing (Inqaba Biotec™, South Africa) using T7 primers (Appendix 4.4e). BiQ Analyzer Software version 2.00 was used to compare the clonal sequences to the oligonucleotide design to determine sequence homology between the two (Bock *et al.*, 2005). Despite numerous attempts to sub-clone the siRNA sequence into p*Silencer*, this was not achieved within the time frame of this research project. The results have therefore been supplied in Appendix 5.

### 3. RESULTS

#### 3.1 Establishment of immortalised murine corneal endothelial cultures at various stages of development

Mesenchyme cells, derived from predominantly neural crest with contributions from lateral plate mesoderm, are collectively known as periocular mesenchyme (POM) (Beebe and Coats, 2000, Langenberg *et al.*, 2008). Fate mapping studies have shown that these POM cells contribute to the development of the corneal endothelium as well as other key structures in the anterior segment of the eye during embryogenesis (Ittner *et al.*, 2005).

In the mouse, the corneal endothelium develops from a population of POM cells that migrate into the region between the surface ectoderm and the lens vesicle in the anterior segment of the eye at E12.5 (Kidson *et al.*, 1999, Ittner *et al.*, 2005). From E12.5, the POM cells undergo a mesenchyme to endothelial transition (MET), finally differentiating into an adherent corneal endothelial monolayer at E15.5.

Immortalised POM cultures at E12.5 and E13.5 were successfully established by another member of the laboratory. These cell lines have been verified (Silla *et al.*, 2014). In this study, immortalised cell lines representing presumptive corneal endothelium (E14.5), differentiated corneal endothelium (E15.5) and functional corneal endothelium (P13) were created.

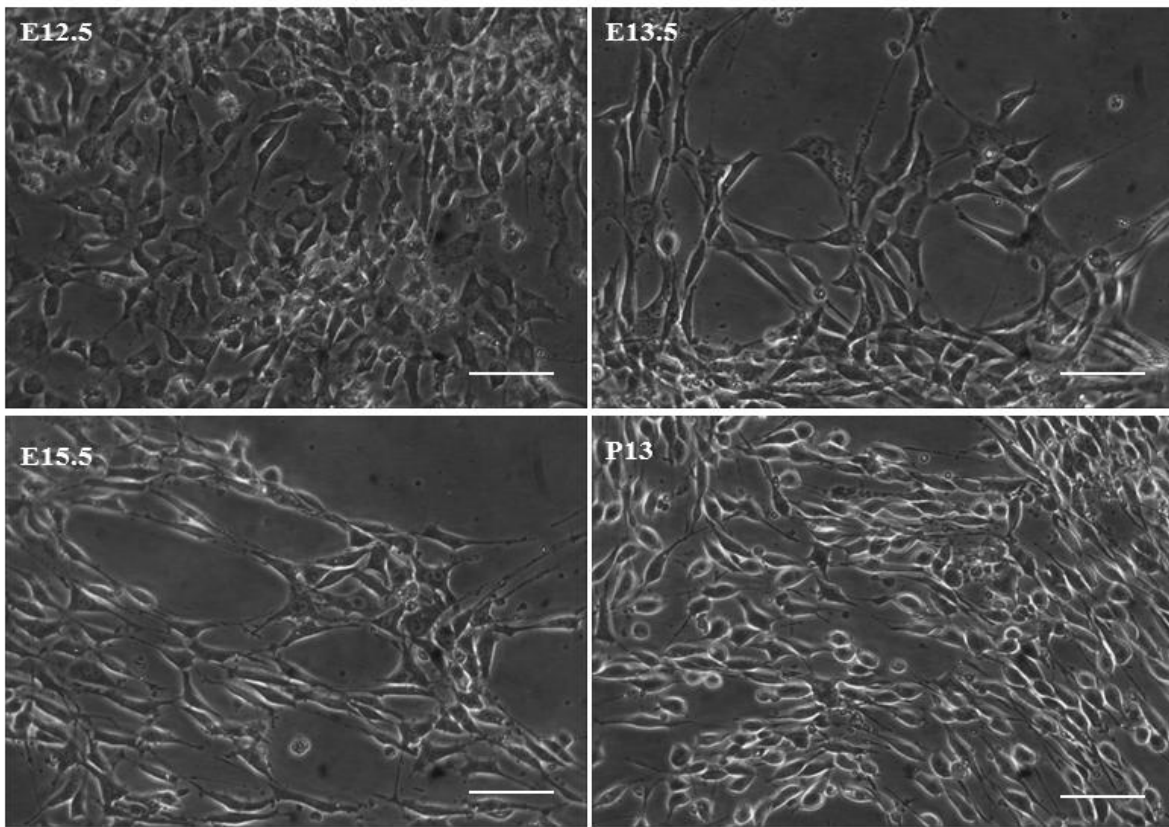


Figure 3.1: Cell morphology at each stage of development in this model (400x). Scale bar is 16  $\mu\text{m}$ .

The cells maintained a stellate morphology throughout development in this model. POM cells at E12.5 and E13.5 grew in dense layers or clumps of cells. Presumptive corneal endothelial cells at E14.5 also grew in dense layers. An image of the cells at E14.5 was not obtained as the cell line was lost due to failure of the liquid nitrogen freezer. Differentiated corneal endothelial cells at E15.5 and functional corneal endothelial cells grew in tightly-packed monolayers (Figure 3.1).

## 3.2 Gene expression analysis

### 3.2.1 Validation of RNA integrity

The cell lines described in section 3.1 were used in gene expression analyses. Total RNA was extracted from the cells and reverse transcribed into cDNA that was used for all subsequent PCR and qPCR reactions. In accordance with MIQE guidelines (Bustin *et al.*, 2009), the integrity of the RNA samples were validated by gel electrophoresis before use in qPCR analyses. RNA aliquots equivalent to 2  $\mu$ g were separated on a 1% bleach agarose gel (Aranda *et al.*, 2012) supplemented with ethidium bromide. A 1Kb DNA molecular weight marker (MW) was loaded into the first well of each gel for reference. The integrity of the RNA samples was confirmed by the presence of two distinct bands of 28S and 18S murine ribosomal subunit RNA (Figure 3.2). The RNA gel shows that the samples used in this study were acceptable for further analysis.

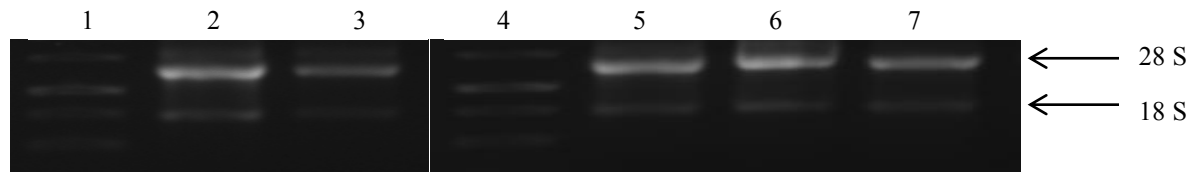


Figure 3.2: RNA integrity of samples extracted from the cells at each stage of development. 1) MW; 2) E12.5; 3) E13.5; 4) MW; 5) E14.5; 6) E15.5; 7) P13. RNA extracted for the first biological repeat is shown as a representative image for all the biological replicates.

### 3.2.2 Efficacy of primer sets confirmed by conventional PCR

Conventional PCR was used to determine the efficacy of the primer sets and the melting temperature (58°C) for *Zol1*, *Aqp1* and *Slc4a4* before use in subsequent qPCR analyses. Total RNA was extracted from cells and reverse transcribed into cDNA. PCR products were separated by electrophoresis as described in the materials and methods section 2.8.1.

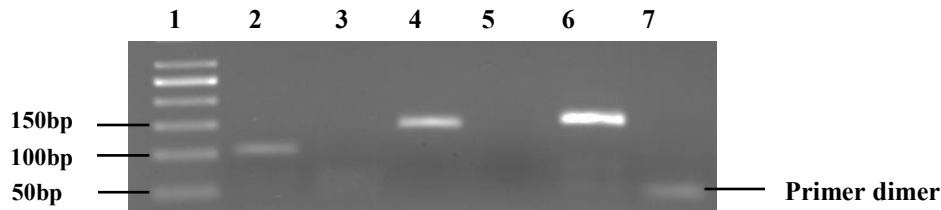


Figure 3.3: PCR amplicons showing the efficacy of the primer sets used in this study. 1) MW, 2) *Zo1* (100bp), 3) *Zo1* No template control (NTC), 4) *Aqp1* (143bp), 5) *Aqp1* NTC, 6) *Slc4a4* (151bp), 7) *Slc4a4* NTC. cDNA synthesised from E15.5 cells is shown as a representative image for all the cell lines.

The conventional PCR results shown in figure 3.3 validate the efficacy of the primer sets used in this study. The *Slc4a4* (no template control) NTC control resulted in primer dimers which occur when the primer sets anneal. The primer sets for these target genes were considered to be suitable for subsequent qPCR analyses.

### 3.2.3 mRNA expression patterns of key functional genes expressed in immortalised murine corneal endothelial cultures at various stages of development

To establish gene expression profiles of key functional genes during corneal endothelial development total RNA was extracted from the cells, reverse transcribed into cDNA and qPCR was performed. The expression levels of the target genes were normalised against that of two reference genes, *Hprt* and  $\beta$ -*actin*. Relative quantification using the comparative Ct method was used to analyse the data. Values given are expressed as a fold change relevant to E12.5 (reference point) as determined by the  $2^{-\Delta\Delta C_t}$  method (Livak and Schmittgen, 2001). All qPCR experimental procedures used in this study were performed in accordance with the MIQE guidelines (Appendix 1). qPCR reaction efficiencies, presented in Appendix 1.10, were shown to be comparable thus allowing for comparison of subsequent data. Data analyses are presented in Appendix 1.11.

### 3.2.3.1 Characterisation of *Zo1* mRNA expression levels

*Zo1* is a tight junction protein that facilitates the formation of the resilient monolayer that is characteristic of the corneal endothelium. Previous studies have shown that *Zo1* is expressed very early in embryonic development as it is required for morula to blastocyst transformation in the mouse (Wang *et al.*, 2008). *Zo1* mRNA expression is a known functional marker of mature corneal endothelium (Zhu *et al.*, 2008, Fan *et al.*, 2011, Ju *et al.*, 2012).

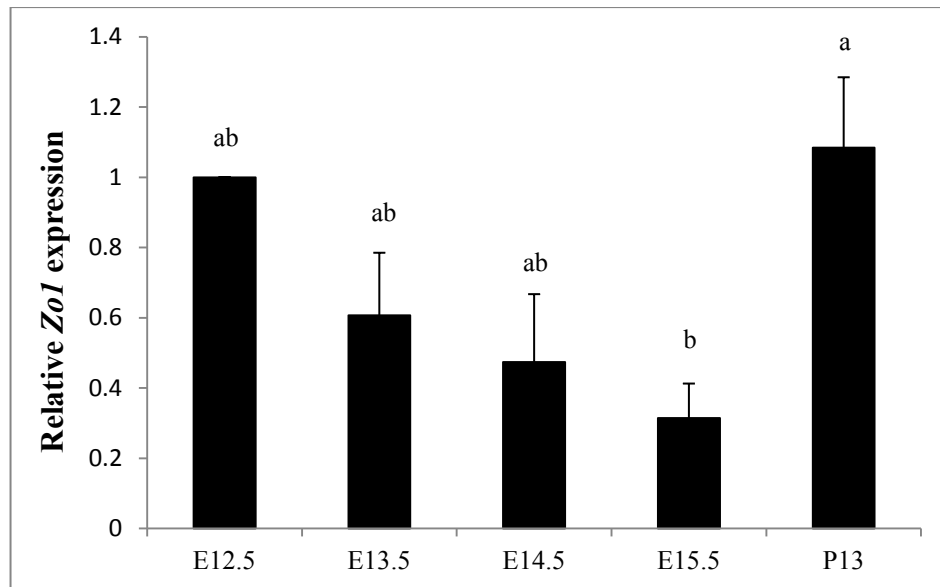


Figure 3.4: The relative fold change in *Zo1* mRNA expression in corneal endothelial cells at various stages of development. *Zo1* was normalised to the geometric mean of two reference genes, *Hprt* and  $\beta$ -*actin*. Expression values are normalised to E12.5 which is set at 1. Values are presented as the mean  $\pm$  SEM. A dissimilar character (a/b) denotes statistical significance ( $p < 0.05$ ;  $n = 3$ ).

*Zo1* mRNA levels decrease gradually, but not significantly, from E12.5 to E15.5. *Zo1* is then highly re-expressed at P13 ( $p < 0.05$  with respect to E15.5) (Figure 3.4).

### 3.2.3.2 Characterisation of *Aqp1* mRNA expression levels

*Aqp1* is a water channel protein that mediates transcellular fluid transport. Knockout models, as reviewed in chapter 1 (Table 1.1), have provided sufficient evidence for the roles of *Aqp1* in transcellular fluid transport. Various studies have used *Aqp1* expression to assess the functional capability of corneal endothelial cells (reviewed by Verkman, 2009).

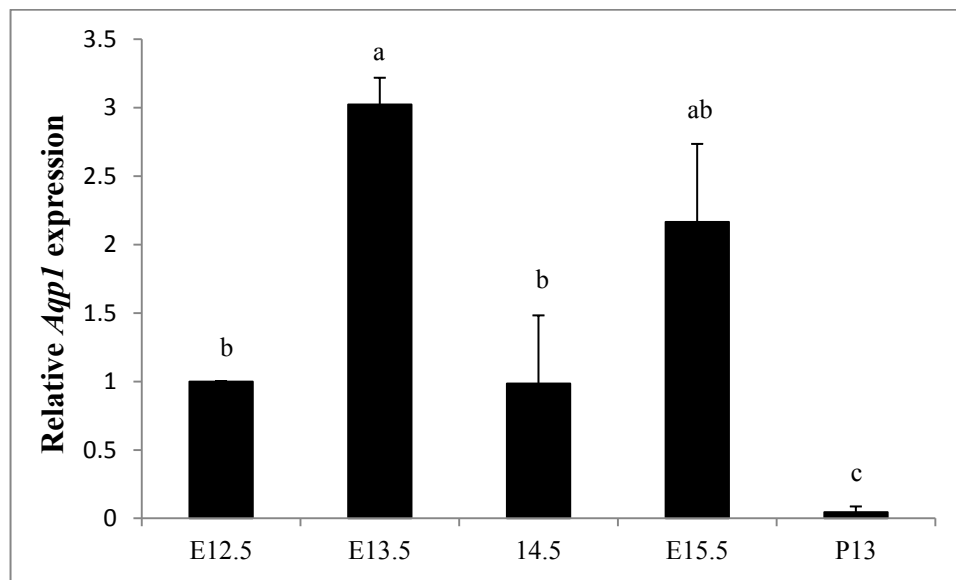


Figure 3.5: The relative fold change in *Aqp1* mRNA expression in corneal endothelial cells at various stages of development. *Aqp1* was normalised to the geometric mean of two reference genes, *Hprt* and  $\beta$ -*actin*. Expression values are normalised to E12.5 which is set at 1. Values are presented as the mean  $\pm$  SEM. A dissimilar character (a/b/c) denotes statistical significance ( $p < 0.05$ ;  $n = 3$ ).

The expression of *Aqp1* was significantly up-regulated (by 2-fold) at E13.5 compared to E12.5 ( $p < 0.05$ ). By E14.5, levels of *Aqp1* are then restored to levels similar to those at E12.5. *Aqp1* expression levels increase by E15.5, and then decrease significantly by P13 ( $p < 0.05$  when compared to all other cell lines) (Figure 3.5).

### 3.2.3.3 Characterisation of *SLC4a4* mRNA expression levels

*Slc4a4* is an ion pump that transports cellular bicarbonate ions across plasma membranes. A study by Shei *et al.* (2013) characterised the expression of several Slc4 members in adult corneal endothelial cells and reported that *Slc4a4* was highly expressed.

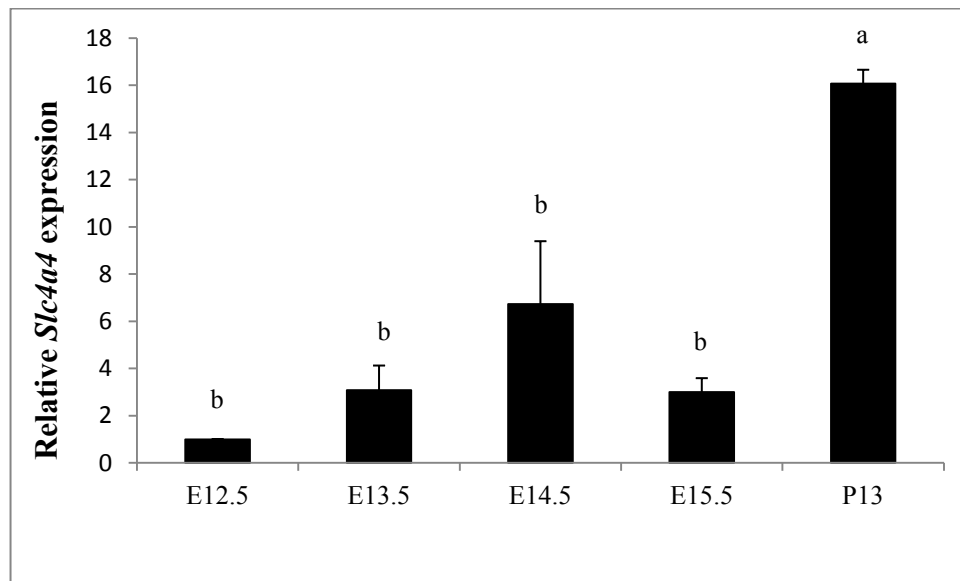


Figure 3.6: The relative fold change in *Slc4a4* mRNA expression in corneal endothelial cells at various stages of development. *Slc4a4* was normalised to the geometric mean of two reference genes, *Hprt* and  $\beta$ -*actin*. Expression values are normalised to E12.5 which is set at 1. Values are presented as the mean  $\pm$  SEM. A dissimilar character (a/b) denotes statistical significance ( $p < 0.05$ ;  $n = 3$ ).

*Slc4a4* is expressed at low levels during corneal endothelial development. However, it is highly expressed at P13 ( $p < 0.05$  when compared to all other cell lines) in the model of functional endothelium (Figure 3.6).

### 3.2.3.4 Verification of the qPCR results obtained for the immortalised cell lines used in this study.

Although all experiments were performed at low and similar passages, we wanted to verify that immortalisation did not have an effect on target gene expression. To determine this, we performed the same qPCR experiments on primary, non-immortalised cells at E14.5, E15.5 and P13. *Aqp1* expression was used as a representative of all the cell lines.

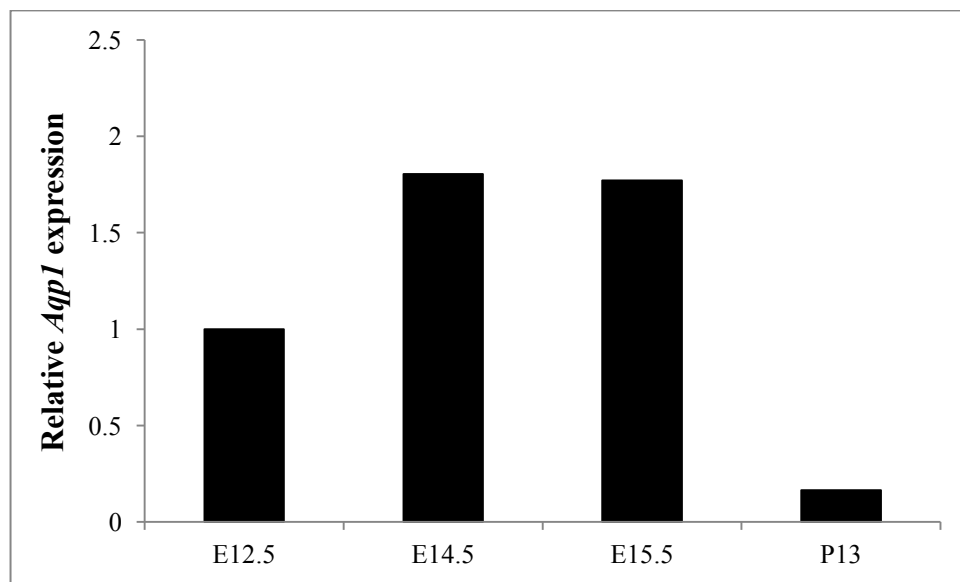


Figure 3.7: The relative fold change in *Aqp1* mRNA expression in non-immortalised corneal endothelial cells at various stages of development. *Aqp1* was normalised to the geometric mean of two reference genes, *Hprt* and  $\beta$ -actin. Expression values are normalised to E12.5 which is set at 1. The results depicted represent one experiment.

The gene expression pattern of *Aqp1* in non-immortalised cells is similar to immortalised cells given that these are primary cells and there was no opportunity to obtain another biological replicate [Figure 3.5 (expression in immortalised cells) and 3.7 (expression in primary cells)]. It seems, therefore, that immortalisation has little effect on the endogenous

expression of *Aqp1* at low passage (Figure 3.7). We have previously shown that gene expression in low passage immortalised E12.5 and E13.5 cells appear unaffected by immortalisation (Silla *et al.*, 2014).

### 3.3 Protein expression analysis

#### 3.3.1 Protein expression patterns of Zo1 and Aqp1 determined by western blot analysis

Western blot analysis was performed to establish protein expression profiles of two key functional genes during corneal endothelial development. Protein expression could not be determined for *Slc4a4* due to the lack of a commercially available antibody specific for mouse *Slc4a4*. Furthermore, the E14.5 cell line was lost due to failure of the liquid nitrogen stock freezer before protein was extracted from the cells. Consequently, the results of this study do not include a protein expression profile for Zo1 and Aqp1 at E14.5.

Protein was extracted and separated on a 12.5% SDS PAGE gel, then transferred onto a nitrocellulose membrane. For Zo1, the membrane was probed with a primary polyclonal antibody specific for mouse Zo1, and subsequently probed with a secondary HRP antibody. For Aqp1, the membrane was probed with a primary polyclonal antibody specific for mouse Aqp1, and subsequently probed with a secondary HRP antibody.

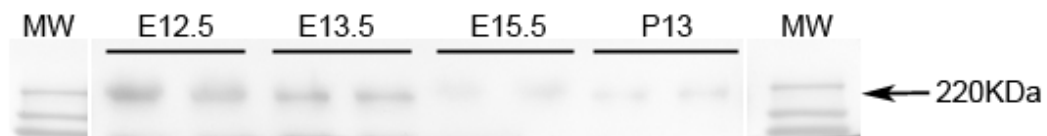


Figure 3.8: Western blot image of Zo1 protein expression at different stages of corneal endothelial development. This is a representative image (n=3).

A distinct band detected at ~ 220 kDa (Figure 3.8) represents the Zo1 protein found in each cell line. Zo1 protein is therefore expressed throughout corneal endothelial development in this model, although at different levels.

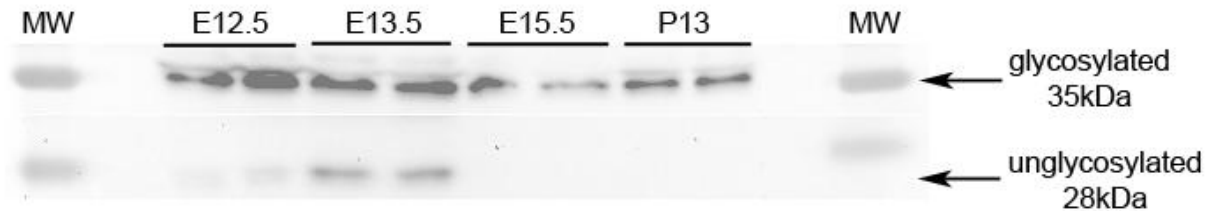


Figure 3.9: Western blot image of glycosylated and unglycosylated Aqp1 protein expression at different stages of corneal endothelial development. This is a representative image (n=3).

Two distinct bands detected at ~35 kDa and ~28 kDa represent the glycosylated and unglycosylated Aqp1 isoforms found in each cell line respectively (Figure 3.9).

A study by Hendriks *et al.* (2004) reported that protein glycosylation, a post-translational modification, is a requirement for Aqp2 transport from the golgi complex to post-golgi compartments such as cell membranes. Hendriks *et al.* (2004) demonstrate that glycosylation is required for Aqp2 cell surface expression in kidney type 1 (MDCK-1) cells expressing human wild-type Aqp2, and that unglycosylated Aqp2 is localized intracellularly (Hendriks *et al.*, 2004).

Given that *Aqp1* and *Aqp2* have the same substoichiometric glycosylation (Smith *et al.*, 1994, Hendriks *et al.*, 2004), the structure and function of these two homologs are comparable. In this study, unglycosylated Aqp1 protein was only expressed at E12.5 and

E13.5, while glycosylated Aqp1 protein was expressed at each developmental stage shown in Figure 3.9. This result suggests that the Aqp1 proteins expressed in the presumptive corneal endothelial cells at E15.5 and mature corneal endothelial cells at P13 have undergone post-translational modification and have been translocated from the golgi complex to post-golgi compartments.

Densitometry was performed on the western blot images to quantitate the band intensity which is indicative of the protein expression. Other members of the laboratory attempted to use Gapdh as a reference protein. However, Gapdh showed variation in expression between the different cell lines and perhaps is not suitable in the developmental context. Therefore, Ponceau S staining was performed in this study to detect total protein on the membrane.

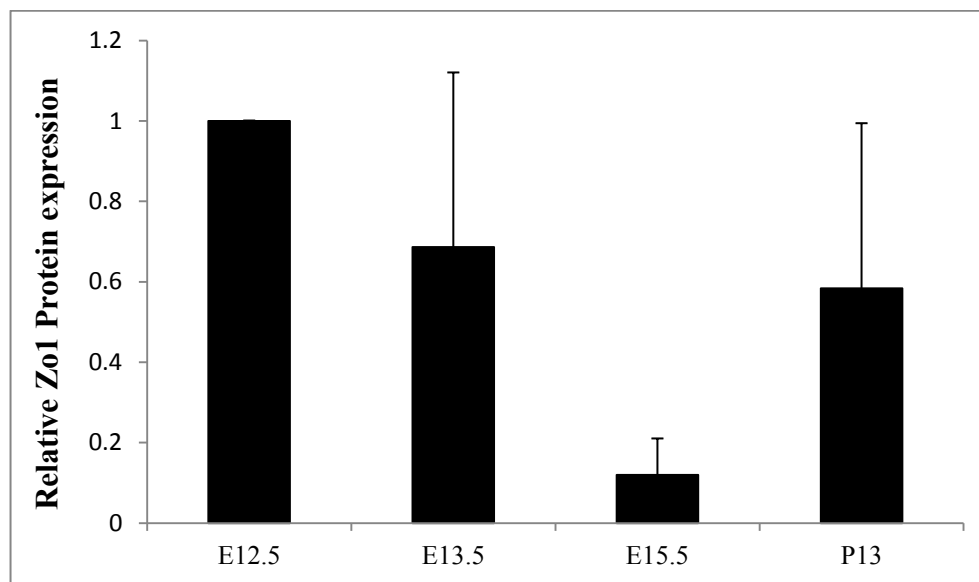


Figure 3.10: Densitometric analysis of Zo1 protein expression relative to the total protein extracted. Expression values are normalised to E12.5 which is set at 1. Values are presented as the mean  $\pm$  SEM (n=3).

Although not significant, Zo1 protein levels decrease from E12.5 to E15.5. Zo1 protein expression then increases again at P13 (Figure 3.10).

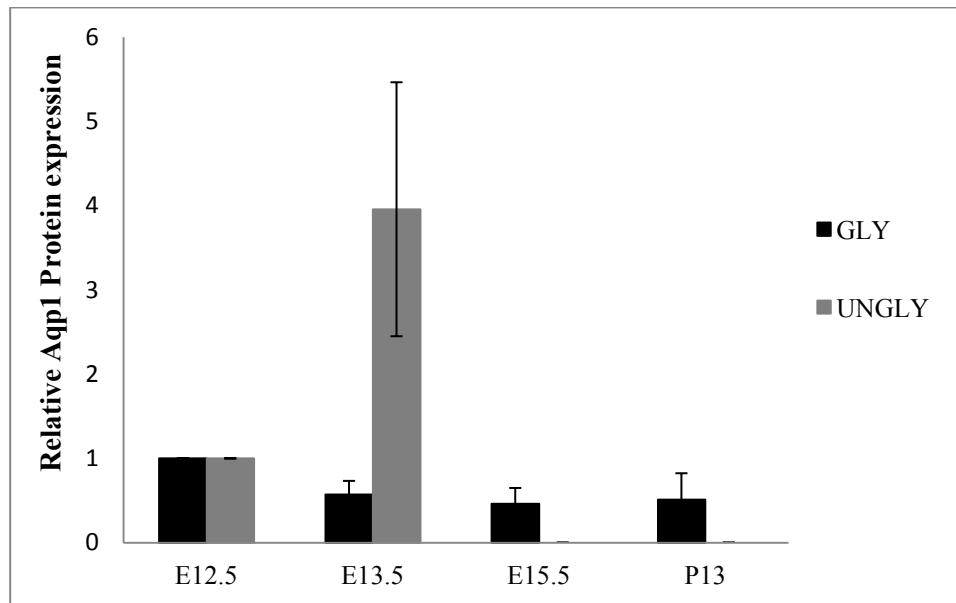


Figure 3.11: Densitometric analysis of glycosylated and unglycosylated Aqp1 protein expression relative to the total protein extracted. Expression values are normalised to E12.5 which is set at 1. Values are presented as the mean  $\pm$  SEM (n=3).

Glycosylated Aqp1 protein expression levels decrease gradually from E12.5 to P13. Unglycosylated Aqp1 protein was only expressed at E12.5 and E13.5, and increased at E13.5 compared to E12.5 (Figure 3.11).

### 3.3.2 Protein localisation patterns of Zo1 and Aqp1 determined by immunocytochemistry

Confocal microscopy was performed to evaluate the protein localisation patterns of Zo1 and Aqp1 at E12.5, E13.5, E15.5 and P13 developmental stages in monolayer culture as

well as hanging drop culture, mimicking the 3D environment in which corneal endothelial development takes place. Settings were kept identical to allow for comparison between the images. Images for the no-primary and no-secondary antibody controls are shown in Appendix 2.

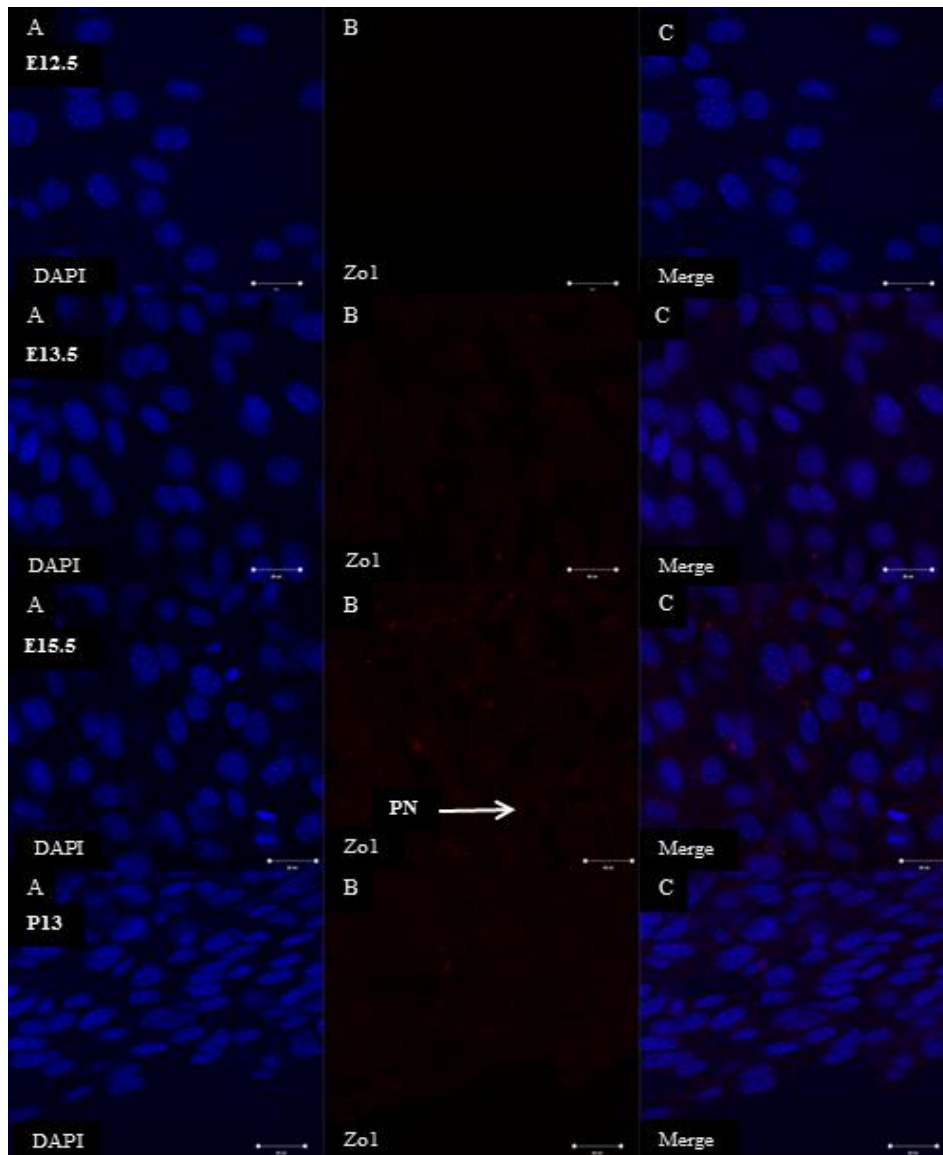


Figure 3.12: 63x confocal microscopy image of monolayer cultures for ZO1. A) DAPI stained cells B) ZO1 stained cells C) Merged DAPI and ZO1 image. PN= perinuclear localisation of ZO1. Scale bar is 20  $\mu\text{m}$ .

Zo1 protein localisation was difficult to detect in monolayer culture in this model, despite the repeated attempts to optimise the staining protocol using this Zo1 antibody. Dilution series and time series experiments were conducted in which different concentrations of the antibody and different incubation times were assessed for optimal Zo1 staining. Monolayer cultures were also grown in serum free media to assess whether protein factors in the serum affected Zo1 expression (Appendix 3b). However, despite this, very little Zo1 staining was seen in monolayer (Figure 3.12).

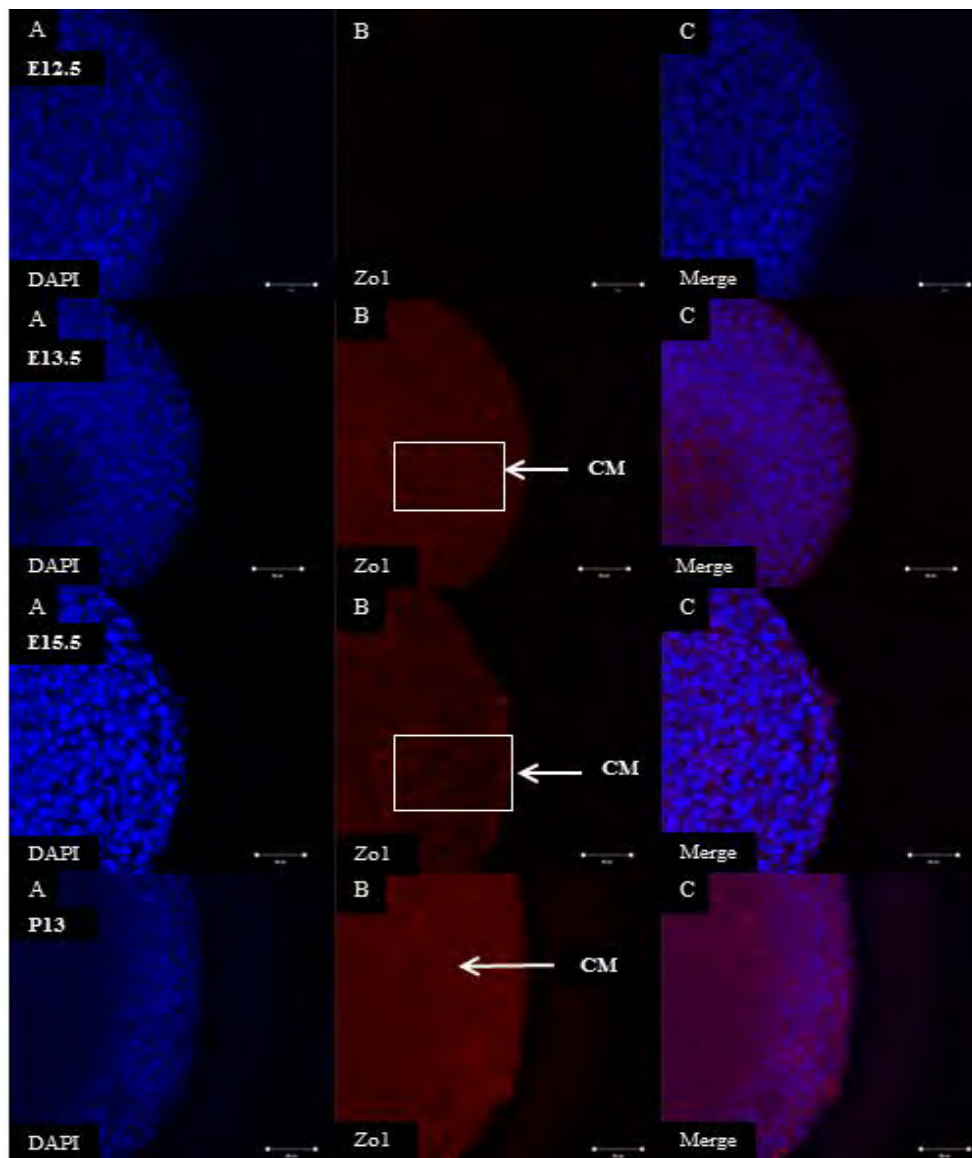


Figure 3.13: 25x confocal microscopy image of hanging drop cultures for ZO1. A) DAPI stained cells B) ZO1 stained cells C) Merged DAPI and ZO1 image. CM= membrane localisation of ZO1. Scale bar is 50  $\mu\text{m}$ .

ZO1 staining was not detected at E12.5 in this model. A perinuclear lattice of ZO1 staining was observed in the cell membrane from E13.5 to P13 in this model of corneal endothelial

development. Although faint, it appears that Zo1 has localised to the cell membrane at E13.5 and E15.5. The images show high expression of Zo1 at P13 (Figure 3.13).

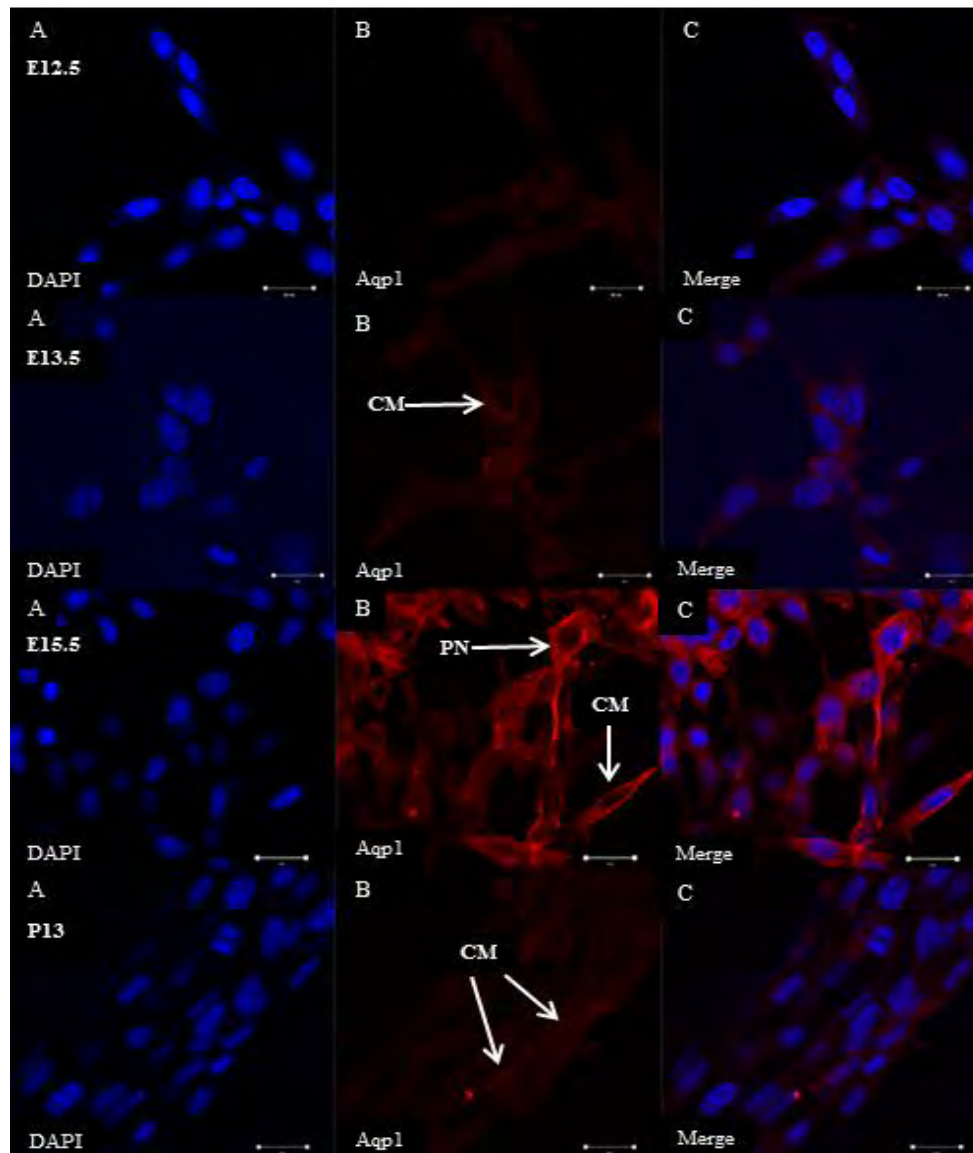


Figure 3.14: 63x confocal microscopy image of monolayer cultures for Aqp1. A) DAPI stained cells B) Aqp1 stained cells C) Merged DAPI and Aqp1 image. The antibody recognises both glycosylated and unglycosylated protein. PN= perinuclear localisation of Aqp1. CM= membrane localisation of Aqp1. Scale bar is 20  $\mu\text{m}$ .

Aqp1 was homogenously distributed in the cytoplasm in POM cells at E12.5 and E13.5. Although there was still cytoplasmic expression, perinuclear Aqp1 staining was distinct in differentiated corneal endothelial cells at E15.5. Some Aqp1 has also localized to the membrane at E15.5. Although faint, at P13, Aqp1 has localized to the membrane where there is distinct presence (Figure 3.14).

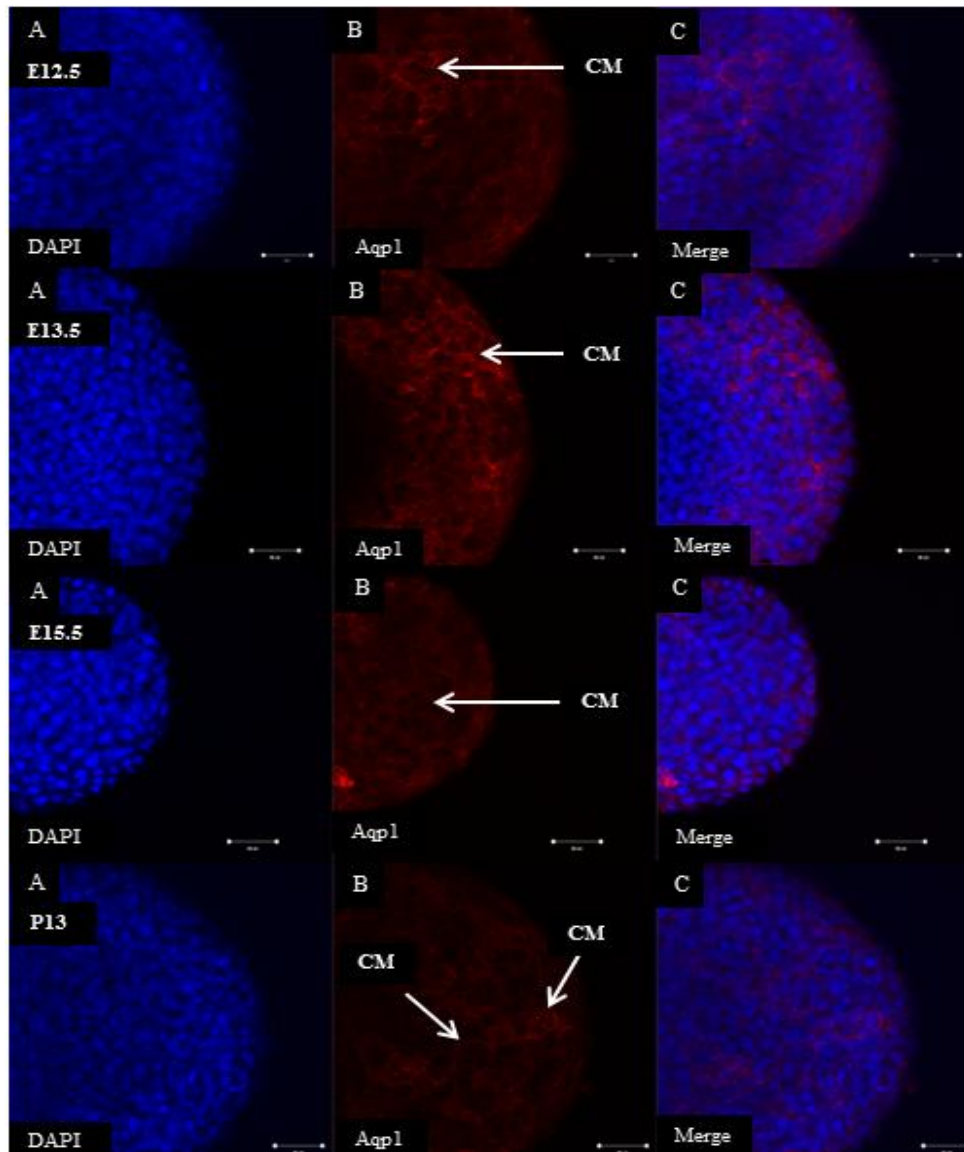


Figure 3.15: 25x confocal microscopy image of hanging drop cultures for Aqp1. A) DAPI stained cells B) Aqp1 stained cells C) Merged DAPI and Aqp1 image. CM= membrane localisation of Aqp1. Scale bar is 50  $\mu$ m.

A perinuclear lattice of Aqp1 staining was observed from E12.5 to P13 in this model of corneal endothelial development. Aqp1 localisation in the membrane was more distinct at

E13.5 compared to E12.5, and more distinct at P13 compared to E15.5. The images show high expression levels of Aqp1 at E13.5 (Figure 3.15).

### **3.4 Establishment of a stable *Foxc1* knockdown cell line**

Despite numerous attempts to sub-clone the siRNA insert into the expression vector, this was not achieved within the time frame of this research project. However, an immense amount of work and troubleshooting was performed, details have been supplied in Appendix 4.

## 4. DISCUSSION

The mammalian eye is a specialised organ whose function depends on co-ordinated interactions between the structures of the anterior and posterior segments. Embryonic development of the anterior segment of the eye is a multifaceted process that requires precise molecular cues. Disrupted morphogenesis of the anterior segment initiates a cascade of developmental disorders that can result in anterior segment dysgenesis (ASD) (Ito and Walter, 2014). Axenfeld-Rieger Syndrome (ARS) and Peters Anomaly are the two most prevalent and well-studied developmental eye disorders that are associated with abnormal development of the anterior segment. Both conditions are characterized by overlapping phenotypes that include iris hypoplasia, corectopia (iris rupture), prominent Schwalbe's line or iridocorneal synechiae in which the cornea fails to separate from the lens or the iris. The most important feature of these phenotypes is the increased risk of developing glaucoma which is the second leading cause of blindness worldwide (Kidson *et al.*, 1999, Alward, 2000, Reneker *et al.*, 2000, Nishimura *et al.*, 2001).

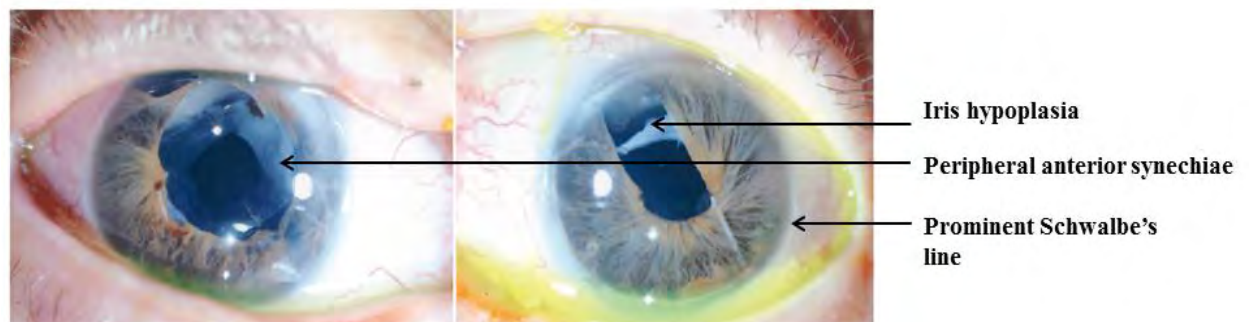


Figure 4.1: A patient presenting with a severe form of ARS with iris hypoplasia, peripheral anterior synechiae and a prominent Schwalbe's line. Image obtained from Ito and Walter 2014.

The cornea, a layered structure, is an integral component of the anterior segment of the eye. Bullous Keratoplasty and Fuchs' endothelial dystrophy are two common clinical conditions that involve corneal endothelial damage and progressive corneal edema. They are the two leading causes of corneal transplant surgery (keratoplasty) in the United States (Macnamara *et al.*, 2004, Besharse *et al.*, 2010). Other disorders closely related to Fuchs' dystrophy include posterior polymorphous dystrophy (PPMD) and congenital hereditary endothelial dystrophy (CHED). Fuch's dystrophy is characterized by a thinning of corneal endothelial cells, while CHED is characterized by a loss of endothelial cells (Besharse *et al.*, 2010).

Keratoplasty is currently the only option available to treat corneal dysfunction caused by aging (Peh *et al.*, 2011), genetic disorders (Liu *et al.*, 2010), intraocular surgery, laser procedures (Fan *et al.*, 2011), trauma/injury or disease (Du *et al.*, 2009, Makgotloe and Carmichael, 2009, Schwartzkopff *et al.*, 2010). Cadaver tissue is currently the only source of donor graft tissue that can be used to surgically repair damaged corneas (Peh *et al.*, 2011). Although keratoplasty has a high success rate (Schwartzkopff *et al.*, 2010), corneal donations have decreased worldwide (Meyer, 2007, Liu *et al.*, 2010, Peh *et al.*, 2011). Furthermore, modern medicine has facilitated an increase in the ageing population and general life expectancy of the population (Araujo Silva *et al.*, 2011). Consequently, the demand for corneal transplants exceeds the number of corneal donations (Peh *et al.*, 2011).

Although considerable research has been directed towards developing alternate donor graft tissue through tissue engineering, producing functional corneal endothelial tissue remains a formidable task as these cells do not proliferate *in vivo* (Peh *et al.*, 2011).

Current literature, as reviewed in chapter 1, provides compelling evidence for the importance of the functional genes *Zo1*, *Aqp1* and *Slc4a4* in corneal endothelial physiology. However, there is a major gap in the literature with regards to the expression patterns of

these genes throughout development. These studies generally characterise the expression of these functional genes in adult corneal endothelium and assess the effects of gene knockdown. Whilst this information is undoubtedly valuable, we need to further our understanding of the developmental expression patterns of these functional genes in order to produce viable tissue alternatives. Comprehensive studies mapping gene expression patterns at key stages in corneal endothelial development will provide the baseline values needed for further studies such as stem cell based tissue engineering. As we are unable to access developing corneas *in vivo*, the best alternative is to use an *in vitro* model of corneal endothelial development.

#### **4.1 Establishing an *in vitro* model of murine corneal endothelial development**

In this study, we created an *in vitro* model of murine corneal endothelial development by immortalising endothelial cells at significant stages in corneal endothelial morphogenesis. Presumptive corneal endothelial cells were immortalised from E14.5 and E15.5 wild-type mouse embryos and mature endothelial cells were immortalised from P13 wild-type mouse pups.

These immortalised cell lines, together with already established cell lines at earlier stages in corneal endothelial development (E12.5 and E13.5), were used to map the expression patterns of three functional genes associated with corneal endothelial function, *Zo1*, *Aqp1* and *Slc4a4*.

POM cells differentiate into both the corneal endothelium and the stroma during embryonic eye development (Cvekl and Tamm, 2004, Gage *et al.*, 2005). The cell lines express all the tested corneal endothelial markers, however, none of the cell lines exhibit stromal markers (unpublished data from another member of the laboratory), possibly because they have been cultured predominantly in monolayer. The cells may have exhibited stromal markers

if they were grown on a matrix that mimics the stroma, consequently altering the results obtained in this study. This could be taken into account in future developmental studies.

To determine whether the procedure used to immortalise the cell lines had effects on the endogenous gene expression patterns of these genes, quantitative real-time PCR (qPCR) was performed on non-immortalised cells at E14.5, E15.5 and P13. *Aqp1* expression was used as a representative of all the cell lines. The gene expression pattern of *Aqp1* in non-immortalised cells was similar to immortalised cells at the various stages (Figure 3.5). Therefore, the procedure used to immortalise the cell lines did not affect the gene expression pattern of *Aqp1* (Figure 3.7) at low passages used in this study. Previously we showed that immortalisation did not affect the endogenous expression of *Foxc1* at E12.5 and E13.5 (Silla *et al.*, 2014).

Cell culture and *in vitro* expansion is known to affect gene expression patterns, and this was shown for *Slc4* genes (Shei *et al.*, 2013). For this reason, caution was taken in the experimental design of this study to ensure that the biological replicates of each cell line were at the same passage for all qPCR and western blot analyses.

#### **4.2 Characterising intercellular junctions present in the corneal endothelium by assessing *Zo1* gene and protein expression at various stages of development**

Intercellular junctions, namely gap, adherens and tight junctions, play an important role in maintaining cell-cell adhesion and communication between adjacent cells. Tight junctions play a particularly important role in cellular communication by controlling the movement of small molecules across apical and basolateral compartments of the plasma membranes between adjacent cells, thereby controlling the permeability of the para-cellular pathway (Ying-Ting *et al.*, 2008, Kojima *et al.*, 2009).

Zo1 was the first tight junction protein studied (Stevenson *et al.*, 1986). It is a selectively semipermeable protein that acts as a scaffold to which other intercellular junctions bind. Claudin, occludin and JAM proteins bind to Zo1 and collectively form the structural components of the tight junctions that join adjacent cells (Stevenson *et al.*, 1986, Sugrue and Zieske, 1997, Ban *et al.*, 2003, Kojima *et al.*, 2009).

Zo1 expression has been observed very early in development. A study by Wang *et al.* (2008) analysed the effects of Zo1 knockdown in the process of morula to blastocyst formation in the mouse and found that Zo1 expression is required for initiating blastocyst formation from the morula (Wang *et al.*, 2008). These results support the importance of Zo1 expression during all stages of development. Zo1 expression is particularly important during wound healing (Cao *et al.*, 2002, Stepp *et al.*, 2002, Lu *et al.*, 2012).

The corneal endothelium is a monolayer of cells joined by tight junctions that form a barrier between the stroma and aqueous humor in the anterior chamber of the eye. The ability of corneal endothelial cells to maintain a tightly packed monolayer is imperative to its function. Without tight junctions, the monolayer would be disrupted and its function would be impaired. Fluid would flow into the stroma unrestricted and stromal hydration would increase, thus causing loss of stromal proteoglycans, disorder of collagen fibrils and subsequent loss of transparency (Hemmavanh *et al.*, 2013). Given its role in tight junction formation, Zo1 is therefore a predominant function related marker of tight junction formation in corneal endothelial cells.

qPCR and western blot analysis showed that *Zo1* was expressed at both mRNA and protein level and that *Zo1* gene expression patterns correlated with protein expression patterns. *Zo1* gene expression was progressively down-regulated from E12.5, when the corneal endothelium begins to differentiate, to E15.5 when the corneal endothelium is completely

differentiated (Figure 3.4). Postnatal corneal endothelial cells (at P13) express significantly higher levels of *Zo1* mRNA relative to presumptive corneal endothelium at E15.5 (Figure 3.4).

Western blot analysis demonstrated a single protein band (~220 kDa) at each stage of development that represents *Zo1* expression (Figure 3.8). Densitometric results demonstrate that the protein expression pattern obtained for *Zo1* from E12.5 to P13 ( $p > 0.05$ ) (Figure 3.10) is similar to the gene expression pattern in this study (Figure 3.4). The results show that the up-regulation of this tight junction protein, at both mRNA and protein level, coincides with corneal endothelial maturity at P13. The mature corneal endothelium at P13 is a fully functional monolayer which explains the requirement for greater levels of this tight junction protein when compared to earlier developmental stages.

It is important to note that a sonication step was not included during the protein extraction protocol. This may account for a possible loss of membrane-bound proteins. Although a sonication step was not included in this study, it should be taken into account in future studies that aim to analyse the expression patterns of membrane bound proteins such as *Zo1*.

Confocal microscopy was performed to evaluate the protein localisation patterns of *Zo1* at E12.5, E13.5, E15.5 and P13 in monolayer culture as well as hanging drop culture, mimicking the 3D environment in which corneal endothelial development takes place. *Zo1* protein localisation was difficult to detect in monolayer culture. Although faint, some perinuclear *Zo1* staining was detected in monolayer culture at E13.5, E15.5 and P13 (Figure 3.12). In hanging drop culture, *Zo1* was clearly localised to the cell membrane at E13.5, E15.5 and P13 in this model of corneal endothelial development. A perinuclear lattice of *Zo1* staining was detected at these stages, with high expression of *Zo1* at P13 (Figure 3.13). The presence of continuous *Zo1* protein staining was detected at the cell

borders between adjacent cells in hanging drop culture, suggesting the ability of these cells to form an intact monolayer.

Endothelial cell-cell junctions, extensively reviewed by Bazzoni and Dejana (2004), are continuously translocated between intracellular compartments and the cell membrane, but the underlying mechanisms that drive this translocation are not well characterised. Zo1 localisation is therefore a dynamic process whereby Zo1 is translocated between the cytoplasm and nucleus (Bauer *et al.*, 2010). The correlation between Zo1 protein expression and culture confluency in endothelial cells was established by Li and Poznansky (1990) who found that Zo1 was only expressed in the cell membranes when the cells were in direct contact with each other. Zo1 has been shown to localise to the nucleus on sub-confluent epithelial cells before tight junction maturation (Bauer *et al.*, 2010). Therefore Zo1 nuclear localisation is more likely to relate to the extent or maturity of cell to cell contacts.

Although confocal analysis did not detect distinct Zo1 localisation in monolayer culture, it did detect Zo1 in hanging drop culture where the cells are in 3D contact with one another. The mRNA and protein for qPCR and western blot analysis was harvested from cells in monolayer culture. Therefore, gene and protein expression patterns of cells grown in hanging drop culture may yield different Zo1 expression patterns compared to the Zo1 expression patterns presented in this study. Clearly, the different methods have different levels of detection. It is therefore very clear that culturing the cells in a more 3D environment has an effect on Zo1 expression and localisation. It would be interesting to analyse Zo1 protein and mRNA in the hanging drops but the tiny nature of the drops does not allow for this. It is possible that cell to cell contact in a 3D environment configuration is necessary to stimulate the correct production and trafficking of Zo1.

Calcium ions are necessary for the formation of the protein complex associated with tight junction formation (between adherens and tight junction proteins) (Ju *et al.*, 2012, Silla *et al.*, 2014). It is possible that the calcium in the medium may have been a factor that resulted in faint Zo1 staining in monolayer culture. It is important to note that the cells were also grown in serum-free media in monolayer culture in an attempt to optimise the protocol to detect Zo1 expression. However, there was no visible difference in Zo1 staining in the cells grown in serum-free media (images not shown).

Zo1 is a phosphoprotein (Sugrue and Zieske, 1997, Ban *et al.*, 2003), and therefore post-translational phosphorylation may play a role in its cellular localisation. Zo1 expression is regulated by phosphorylation, but it is unknown whether phosphorylation is required for translocation to a post-golgi compartment such as the cell membrane. Sugrue and Zieske (1997) suggested that Zo1 expression in the cell membrane is regulated by reversible phosphorylation. Ulluwishewa *et al.* (2011) reported that reduced Zo1 phosphorylation was associated with increased transendothelial electrical resistance (a measure of tight junction resistance) in canine kidney cells type 1 (MDCK-1) epithelial cells in monolayer culture. Zo1 phosphorylation must therefore be regulated for expression and function in the cell membrane. Zo1 localisation in this model, shown in the confocal images, may have been affected by the phosphorylation state of the cells at these developmental stages.

Corneal endothelial cells undergo mesenchyme-epithelial transition (MET) during early stages of development (i.e. E12.5 to E15.5) whereby the cells change from a motile phenotype to an ordered cohesive structure. MET is characterised by a gain of cell junctions and up-regulation of the factors that promote cell-cell adhesion (Thiery, 2003, Baum *et al.*, 2008, Silla *et al.*, 2014). The progressive down-regulation of *Zo1* at these stages is therefore an unexpected result. A possible explanation may be that the cells generate a large reserve of *Zo1* mRNA and proteins at the proliferative stages of development (i.e. E12.5) and no longer need to generate large amounts of *Zo1* until the

endothelial layer is completely functional at P13. The statistically significant up-regulation from E15.5 to P13 is suggestive of a maturation of the barrier function from the differentiated state at E15.5 to the more mature functional state at P13.

Confocal microscopy of mouse corneal tissue at P4, P14 and P30 show that Zo1 expression is diffuse and localized to both the apical and basolateral membranes of the corneal endothelial cells. The Zo1 expression pattern was irregularly spaced (Hemmavanh *et al.*, 2013).

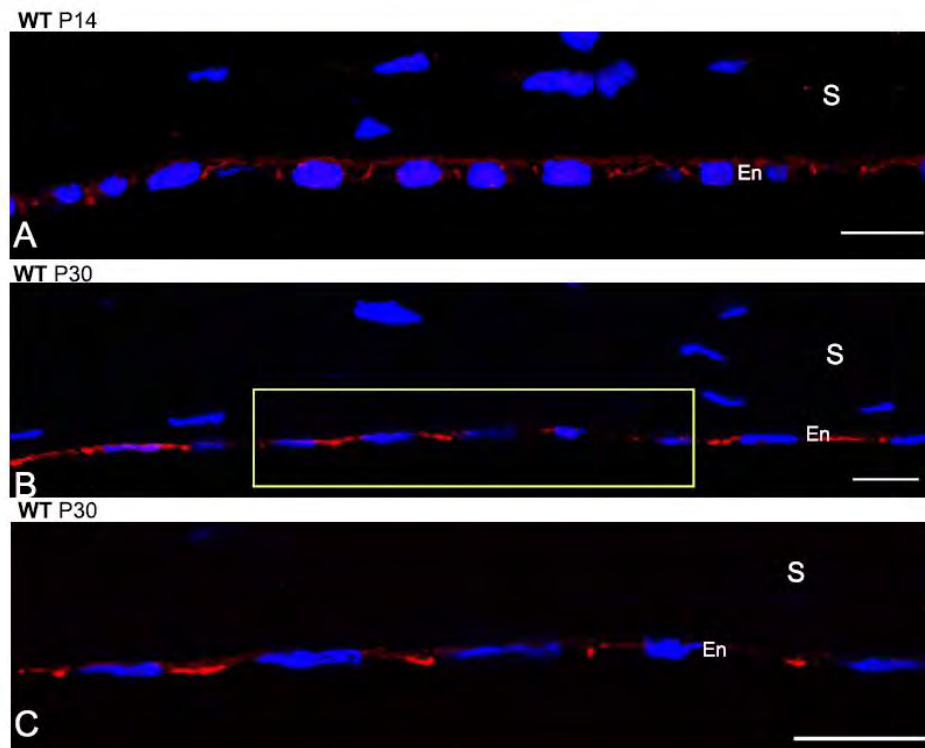


Figure 4.2: Endothelial junction maturation in WT mice at P14 and P30. Red staining represents Zo1 expression in the corneal endothelium of WT mouse corneas. (A) Zo1 is expressed in the apical and lateral corneal endothelial membrane at P14. (B, C) Zo1 expression becomes localised to the lateral membrane at P30. The yellow box in (B) outlines the area in (C). Scale bar is 40  $\mu\text{m}$ . Image obtained from Hemmavanh *et al.* (2012).

Hemmavanh *et al.* (2012) demonstrate that Zo1 expression becomes more regularly spaced as the endothelium matures at P30 (Hemmavanh *et al.*, 2013). It is clear from these images that tight junctions mature over time. The tight junctions in the endothelium at P13 are, therefore, immature relative to P30.

Kidson *et al.* (1999) examined normal and mutant (*Foxc1*<sup>-/-</sup>) whole corneas under the confocal microscope for the presence of Zo1 protein. The results of this study concluded that the mutant cornea lacked the presence of continuous bands of tight junctions that are present between the posterior endothelial cells in normal corneas. Occasional Zo1 staining was attributed to the stromal layer, whose cells are able to synthesize some Zo1, but fail to form the continuous bands that are required for to form a monolayer (Kidson *et al.*, 1999).

Although the importance of tight junctions is well-known, the regulatory mechanisms that underlie tight junction formation are not completely understood (Ramachandran and Srinivas, 2010). Corneal endothelial cells contain a dense band of actin cytoskeleton which is referred to as the perijunctional actomyosin ring (PAMR). Tight junctions bind to the PAMR through tight junction proteins, such as Zo1, facilitating cell signaling, particularly signaling that involves the Rho family of small GTPases (Ramachandran and Srinivas, 2010). Zo1 is therefore required to regulate the connection between the PAMR of adjacent cells and tight junction complexes. The loss of corneal endothelial cells and consequent edema through ageing, disease or trauma is characterised by the loss of tight junctions. Understanding the regulatory mechanisms that underlie tight junction formation may provide the insight required to develop pharmacological strategies against corneal dystrophies that are characterised by corneal edema (Ramachandran and Srinivas, 2010).

The cornea, located in the anterior segment of the eye, is exposed to various environmental factors including physical and chemical injuries, and microbial infections. The corneal epithelium is the outermost layer of the cornea and is therefore the first layer to be exposed to the external environment. Given its position, the corneal epithelium has a remarkable ability to continuously undergo self-renewal and wound healing. Epithelial cells undergo a remarkable rate of proliferation; migration and differentiation to maintain renewal and wound healing. Essentially epithelial cells at the wound edge begin to migrate to cover the denuded area. Once the epithelial layer has been restored at the wound area, the cells differentiate to form tight junctions and re-establish the barrier function (Lu *et al.*, 2012). Although the molecular cues that direct wound healing are beyond the scope of this study, the functional importance of *Zo1* in other corneal layers warrants mention as the barrier function of the corneal epithelium and endothelium is critical for corneal integrity and normal vision (Lu *et al.*, 2012).

Adherens junctions maintain cell-cell contact in addition to tight junctions. *Cadherens*, which are essentially specific adherens junctions, are calcium ion ( $\text{Ca}^{2+}$ ) dependent proteins that facilitate cell-cell adhesion between adjacent cells (Reneker *et al.*, 2000). *N-cadherin* (*N-cad*) is widely expressed in many tissues and is often used as a marker of cell differentiation. *N-cad* expression coincides with corneal endothelial differentiation (Ju *et al.*, 2012, Silla *et al.*, 2014). Owing to the fact that *N-cad* is widely expressed in many cell types and that *Zo1* is also expressed in stromal cells (Kidson *et al.*, 1999), relying on one cell contact marker could lead to misleading results. Therefore, the use of multiple differentiation and function-related protein markers can strengthen the results of future studies that aim to characterise corneal endothelial cells (Ju *et al.*, 2012). Both *N-cad* and *Zo1*, among other markers, were used to identify the induction of corneal endothelial cells from neural crest cells in a study conducted Ju *et al.* (2012). Future studies could include more than one marker to strengthen the results of the study.

The expression of *Zo1* mRNA and protein in this study is suggestive of a mature functional endothelium that is able to maintain corneal deturgescence, thus adding to the value of this *in vitro* model of corneal endothelial development.

### **4.3 Characterising the pump function of the corneal endothelium**

Corneal deturgescence is actively maintained by the pump function of the corneal endothelium. With the exception of oxygen, all the nutrients required for corneal transparency are transported from the aqueous humor through the corneal endothelium into the corneal stroma and epithelium. The accepted pump-leak hypothesis (Maurice, 1981) states that there is a fluid balance between the stroma and the aqueous humor, where fluid is ‘pumped’ out of the stroma into the aqueous humor while fluid ‘leaks’ into the stroma from the aqueous humor. The corneal stroma has a high concentration of glycosaminoglycans that create an osmotic driving force for the accumulation of fluid in the stroma. The corneal endothelium is thus responsible for actively pumping fluid out of the stroma into the aqueous humor, to essentially counteract the continuous leak of fluid into the stroma. The constant pump-leak action across the corneal endothelium is responsible for maintaining a relatively dehydrated stroma, a requirement for corneal transparency (Bonanno, 2012). The corneal endothelium relies on various transporters and channels to maintain its pump-leak function.

#### **4.3.1 Characterising the water channels present in corneal endothelial cells by assessing *Aqp1* gene and protein expression at various stages of development**

*Aqp1* is a water channel protein that mediates transcellular fluid transport across plasma membranes of tissues that depend on water/fluid transport.

AQPs are ubiquitously expressed in extra-ocular tissues involved in fluid transport. Mice lacking *Aqp1* manifest defective urinary-concentrating and lung water permeability (Thiagarajah and Verkman, 2002). Mice lacking *Aqp5* manifest defective fluid secretion by

salivary and airway glands, and reduced alveolar water permeability in the lungs (Thiagarajah and Verkman, 2002).

Although the physiology of AQP-mediated water transport is not fully understood, progress has been made in understanding the intracellular transport of AQP proteins. Hendriks *et al.* (2003) studied Aqp2 protein expression in canine kidney cells type 1 (MDCK-1) cells and reported that N-linked glycosylation is important for its transport from the golgi-complex to post golgi-compartments such as the plasma membrane. They reported that both glycosylated and unglycosylated Aqp2 proteins are stable, indicating that glycosylation is not required for stability of the wild-type protein. Both glycosylated and unglycosylated Aqp2 proteins yielded similar water permeability which demonstrates that glycosylation is not required for the ability of the proteins to act as functional water channels. To determine if glycosylation is N-linked, they removed the N-linked glycosylation consensus site and reported that this removal did not affect the expression of the unglycosylated protein but did diminish the expression of the glycosylated protein. Aqp2 glycosylation is therefore N-linked. Their results also demonstrated that a mutant Aqp2 protein that did not contain an N-linked consensus site was not present on the cell surface, which suggests that the mutant was unable to undergo glycosylation and was therefore retained on the endoplasmic reticulum or another intracellular compartment. Overall the results of this study demonstrate that glycosylation is required for Aqp2 cell surface expression and that the absence of glycosylation induces intracellular retention (Hendriks *et al.*, 2004). To the best of my knowledge this is the most comprehensive study on Aqp glycosylation published to date. Given that *Aqp1* and *Aqp2* have the same substoichiometric glycosylation (Smith *et al.*, 1994, Hendriks *et al.*, 2004), the structure and function of these two homologs are comparable.

qPCR and western blot analysis showed that *Aqp1* was expressed at both mRNA and protein level. Unlike *Zo1*, *Aqp1* gene expression patterns in this study do not correlate with

protein expression patterns. *Aqp1* gene expression was significantly up-regulated from E12.5, when the corneal endothelium begins to differentiate, to E13.5 as differentiation continues (Figure 3.5). *Aqp1* gene expression was then significantly down-regulated from E13.5 to E14.5 when the corneal endothelium is almost completely differentiated, followed by an up-regulation at E15.5 when the corneal endothelium is completely differentiated (Figure 3.5). Postnatal corneal endothelial cells (at P13) express significantly lower levels of *Aqp1* mRNA relative to presumptive corneal endothelium at E15.5 (Figure 3.5). Interestingly, *Aqp1* mRNA levels were the highest at E13.5 when the corneal endothelium is still differentiating. A similar result was observed for *Zo1* mRNA expression, whereby the endothelial cells appear to be producing more *Zo1* and *Aqp1* mRNA transcripts at the earlier proliferative stages in development. Unlike *Zo1* expression at P13, *Aqp1* gene expression is significantly reduced at P13 which suggests that the cells do not require additional mRNA transcripts at this stage of development. Although not statistically significant, the up-regulation of *Aqp1* mRNA transcripts at E15.5 may have biological significance by serving as a large enough reserve to sustain the water channels at P13 when the corneal endothelium is completely functional.

Western blot analysis demonstrated two protein bands at each stage of development that represent Aqp1 expression (~35kDa for glycosylated Aqp1 and ~28kDa for unglycosylated Aqp1) (Figure 3.9). Unglycosylated Aqp1 was only detected at the early proliferative stages of development (E12.5 and E13.5). Glycosylated Aqp1 was detected at each stage of development (Figure 3.9). This suggests that Aqp1 proteins at E15.5, when the corneal endothelium is completely differentiated, have undergone post-translational modification and have been translocated from the golgi-complex to the cell surface. A strict experimental design, whereby RNA and protein were extracted from the cells at the same passage for each biological replicate, ensures that the results are comparable. Consequently, this result remained consistent for three biological replicates.

Aqp1 protein expression in the anterior epithelial cells of the mouse lens also show a band at ~28 kDa corresponding to the unglycosylated Aqp1 protein and a band at ~34kDa corresponding to the glycosylated Aqp1 protein (Ruiz-Ederra and Verkman, 2006).

Densitometric results demonstrated that the protein expression pattern obtained for Aqp1 from E12.5 to P13 ( $p>0.05$ ) (Figure 3.11) does not follow the gene expression pattern in this study (Figure 3.5). The results show that unglycosylated Aqp1 was up-regulated from E12.5 to E13.5, although not statistically significantly. Glycosylated Aqp1 expression was slightly down-regulated from E12.5 to E13.5, but remained relatively constant thereafter at both E15.5 and P13 ( $p>0.05$ ). This result suggests that protein expression of this water channel protein is stable and that expression levels at E15.5 is presumably adequate for its function at P13 when the pump function of the corneal endothelium is fully functional. Clearly, gene expression analyses do not distinguish between these two forms of post-translational modifications. Elevated *Aqp1* mRNA transcript levels at E13.5, shown in Figure 3.5, therefore represent both glycosylated and unglycosylated forms of this protein.

Aqp1 is the most abundantly expressed AQP isoform in humans, rats and mice. Its expression has been documented in cardiac tissue, particularly in endothelial and vascular muscle cells that are key regulators of transcellular fluid transport (Montiel *et al.*, 2014). Montiel *et al.* (2013) reported several Aqp1 protein bands from total protein extracts of the heart, aorta and mesenteric artery. These bands were attributed to the differential migration of glycosylated AQP proteins. They reported that *Aqp1* deletion affected the expression of other aquaporin isoforms, for example, over-expression of *Aqp4*, *Aqp7*, and *Aqp8* was detected in *Aqp1* null mice. Given the wide expression of all the AQP isoforms in ocular tissue (reviewed in Table 1), it would be interesting to characterise the effects of *Aqp1* knockdown on other AQPs in the eye.

Confocal microscopy demonstrated that Aqp1 expression was homogeneously distributed in POM cells at E12.5 and E13.5 in monolayer culture. Perinuclear staining was distinct at E15.5 when the corneal endothelial cells are fully differentiated. Some Aqp1 was also localised to the cell membrane at E15.5. At P13, Aqp1 has localised to the cell membrane in monolayer culture (Figure 3.14). In hanging drop culture, a distinct perinuclear lattice of Aqp1 staining was observed from E12.5 to P13 in this model of corneal endothelial development. The images show Aqp1 localisation at the cell membrane was more distinct at E13.5 and P13 (Figure 3.15). A polyclonal Aqp1 antibody, that detects both glycosylated and unglycosylated Aqp1 proteins, was used in this study. As shown in Figure 3.11, unglycosylated Aqp1 levels are elevated at E13.5. This result may account for the intense Aqp1 staining detected in hanging drop culture at E13.5 (Figure 3.15).

Macnamara *et al.* (2004) studied *Aqp1* expression in human and mouse corneal endothelial dysfunction. Tissue samples were obtained from 18 patients undergoing corneal transplantation surgery. Of these, 4 patients had Fuch's dystrophy, 5 had Bullous Keratopathy (BK), 1 had a corneal graft failure due to endothelial decompensation, 2 had keratoconus (non-corneal endothelial disease) and 6 had corneal scarring from trauma or infection (non-corneal endothelial trauma). Additionally, 3 normal corneas from donor tissue were analysed. A mouse model of corneal injury was induced with injection of sterile hot water in the anterior chamber of the eye in wild-type mice. The results demonstrated that *Aqp1* expression was diminished in the human corneal tissue with corneal endothelial disease (i.e. Fuchs dystrophy, BK, graft endothelial failure) and in the animal model of corneal endothelial injury. *Aqp1* expression was unchanged in human corneal tissue with non-corneal endothelial disease (i.e. keratoconus and corneal scarring). Although the results of this study provide compelling evidence of the importance of *Aqp1* expression in corneal endothelial cells, it is not clear whether reduced *Aqp1* expression is a cause or effect of corneal endothelial disease. Future studies are needed to determine the key regulators of AQPs and to determine if *Aqp1* up-regulation in the corneal endothelium may facilitate rehabilitation of swollen and diseased corneas (Macnamara *et al.*, 2004). A clinical

manifestation of these corneal endothelial diseases is chronic corneal edema, which essentially leads to loss of transparency and subsequent vision loss. The results of future 'cause and effect' studies of disease target genes such as *Aqp1* may provide effective treatment strategies aimed at managing these pathological diseases affecting the eye.

#### **4.3.2 Characterising the ion pumps present in corneal endothelial cells by assessing *Slc4a4* gene expression at various stages of development**

*Slc4a4* is an ion pump, present in the basolateral membrane of corneal endothelial cells, which transports cellular bicarbonate ions across plasma membranes. Bicarbonate ions play an important role in the pump function of corneal endothelial cells. Carbonic anhydrase (enzyme that converts carbon dioxide and water to bicarbonate ions) inhibitors prevent the process of fluid reabsorption across the endothelium, thus reiterating the role of bicarbonate ions in corneal deturgescence (Bonanno, 2012, Suzuki *et al.*, 2012).

A recent study by Shei *et al.* (2013) characterised the relative expression levels of all the solute carrier 4 family members in adult murine corneal endothelial cells. The study also analysed the effects of cell culture and *in vitro* expansion on baseline expression levels by comparing the gene expression levels at different passages (passage 2 and 7). The results of the study demonstrate that cell culture does affect the expression levels of Slc4 genes. Mesenchymal markers such as *Coll1a1* were detected at the later passage, which suggests that the phenotype of the endothelial cells were changing. Further studies could include a mesenchymal marker as a check point to determine if the endothelial cells in culture have undergone phenotypic changes as these changes would affect gene expression (Shei *et al.*, 2013).

qPCR analysis showed that *Slc4a4* gene expression was progressively up-regulated from E12.5, when the corneal endothelium begins to differentiate, to E14.5 when the corneal endothelium is almost completely differentiated (Figure 3.6). Interestingly, *Slc4a4* gene

expression is down-regulated from E14.5 to E15.5 when the corneal endothelium is completely differentiated. This result suggests that the ion pump function may not yet fully be established at this stage of development or that sufficient mRNA is present to produce protein. Postnatal corneal endothelial cells (at P13) express significantly higher levels of *Slc4a4* mRNA relative to presumptive corneal endothelium at E15.5 (Figure 3.6). *Slc4a4* is highly expressed at P13, indicative of an established pump function at this stage of development. The significant up-regulation of this ion pump, at mRNA level, coincides with corneal endothelial maturity at P13. The mature corneal endothelium is an active functional monolayer which explains the requirement for greater levels of this ion pump protein when compared to earlier developmental stages. A limitation of this study is the lack of *Slc4a4* protein expression data, which could not be determined due to the lack of a commercially available antibody specific for mouse *Slc4a4*.

Among the *Slc4* members assessed by Shei *et al.* (2013), *Slc4a11* was the most highly expressed isoform in corneal endothelial cells, followed by *Slc4a4*, *Slc4a2* and *Slc4a7* (Shei *et al.*, 2013). A limitation of the Shei *et al.* (2013) study is that gene expression was only assessed in adult corneal endothelial cells. The results of the current study provide a developmental pattern, which given for the other highly expressed *Slc4* members, could provide valuable insight into corneal dystrophies related to these members. Several members of the *Slc4* family have been linked to ocular diseases, particularly corneal dystrophies. *Slc4a11* mutations are associated with corneal dystrophies including late-onset CHED. A study by Chen *et al.* (2013) analysed several novel molecular markers in human fetal and adult corneal endothelial cells. They identified 284 signature genes that are highly expressed in human corneal endothelial cells. Among these genes, they identified *Slc4a11* as one of the top-ranking genes, thus supporting the use of *Slc4* members as markers of function in corneal endothelial cells. *Slc4a4* and *Slc4a11* are both well-established disease target genes which is indicative of their functional significance in corneal endothelial physiology (Chen *et al.*, 2013, Shei *et al.*, 2013). Future studies could include *Slc4a11* throughout development to contribute to the mapping of disease target genes associated

with the development of the corneal endothelium. Although the precise function of each Slc4 member is unknown, their wide expression in corneal endothelial cells and the known importance of bicarbonate ions in the pump function of corneal endothelial cells, strongly suggests that they are of great importance in corneal endothelial physiology.

#### **4.4 Conclusion and future considerations**

Optimal functioning of the corneal endothelium depends on cell features that include its cytoskeleton, signaling cascades and a host of regulatory membrane proteins (Fischbarg, 1997). Failure of any of these elements could result in corneal endothelial decompensation, which is the most documented reason for corneal endothelial dysfunction. Endothelial decompensation occurs as surviving cells spread out over the denuded surface, essentially changing their shape and volume which alters their function (Fischbarg, 1997).

The genes expressed in this model are associated with key corneal endothelial functions. The barrier function is well established at P13, which correlates well with the increased *Zo1* mRNA and protein expression in mature corneal endothelial cells. *Aqp1* and *Slc4a4*, both part of the pump function of these cells, are differentially expressed throughout development.

Cell junctions, water channels, ion pumps and transporters function together to drive ion-coupled fluid absorption across the corneal endothelium. They essentially facilitate the pump-leak function of the corneal endothelium that is required to nourish the cornea and maintain corneal deturgescence and transparency required for vision. The studies reviewed in this chapter have highlighted the importance of these functional genes in corneal physiology. Developmental gene and protein expression patterns of these genes will provide the baseline values needed to direct stem cells into a corneal endothelial phenotype. Stem cell therapy has gained the attention of research groups worldwide. Takahashi and Yamanaka 2006 demonstrated that pluripotent stem (iPS) cells can be generated from

fibroblast cultures by the addition of four inducing factors, Oct3/4, Sox2, c-Myc and Klf4 (Takahashi and Yamanaka, 2006). In theory, iPS cells can then be directed to multiple phenotypes.

The first corneal transplant was performed in 1905 and this technique is still the most effective way for treating corneal blindness. This alone highlights the need for innovative tissue regenerative techniques that could replace conventional transplantation. In developing countries, trachoma is the most cited cause of corneal blindness as hygiene and public health services are often inadequate (Liu *et al.*, 2010). In South Africa, five regional eye banks harvest and supply corneal tissue to ophthalmic surgeons. The availability of corneal tissue in South Africa has declined due to various reasons. Government legislation has placed restrictions on access to information on the deceased. Before 2006, the South African Police Service forensic mortuaries allowed eye banks to access information on those who died of natural causes. Since then, the Department of Health has restricted access to this information owing to the confidential nature of this information. Consequently, eye banks have lost a source of information that could lead to potential donors. Furthermore, tissue from donors positive for HIV, hepatitis b or c is not safe for transplantation. Consequently, the number of suitable corneas that are safe for transplantation have declined drastically (Meyer, 2007, Makgotloe and Carmichael, 2009). These issues highlight the need for alternative graft tissue that can replace cadaver corneas for transplantation.

Tissue engineered corneas, and perhaps personalised cell therapy, would supplement the supplies of donor corneal tissue. Furthermore, corneal equivalents could serve as a model for toxicological screening of drugs to treat corneal diseases (Ju *et al.*, 2012). Comprehensive studies mapping gene and protein expression patterns at key stages in corneal endothelial development will provide extremely important information needed for further studies such as stem cell based tissue engineering.



## 5. APPENDIX

### 1. The Minimum Information for Publication of Quantitative Real-time PCR Experiments (MIQE)

MIQE is a set of guidelines that describes the information required for assessing qPCR experiments. They were established to promote consistency between all qPCR experiments to ensure that they are reliable and the results are reproducible. Reviewers rely on the MIQE guidelines to assess the validity of protocols used in publications based on the relevant experimental conditions and assay characteristics (Bustin *et al.*, 2009). All qPCR experimental procedures used in this study were performed in accordance with the MIQE guidelines.

#### 1.1 Experimental design

The relative expression of the target genes *Zol*, *Aqp1* and *Slc4a4* in POM cells at E12.5 and E13.5, and presumptive corneal endothelium at E14.5 and E15.5, as well as mature corneal endothelium at P13 were evaluated by qPCR. RNA was extracted from the corneal endothelial cells cultured in a single T75 flask or 10 cm<sup>3</sup>dish. The cells were harvested by cell scraping as expression of adherens and tight junction mRNA transcripts is disrupted by trypsin-EDTA treatment (Ying-Ting *et al.*, 2008). RNA was extracted from fully confluent flasks or dishes in which cell-cell contacts were visible under an inverted microscope. This ensured that tight junction mRNA transcripts were present. RNA integrity was evaluated by gel electrophoresis prior to cDNA synthesis. cDNA was synthesised using the GoScript™ Reverse Transcription System (Promega, USA). Two biological repeats were performed per developmental stage, with two technical repeats per biological and individual samples were performed in triplicate.

All qPCR experiments and analyses were performed by myself at the research laboratory of Dr. Paula Sommer at the School of Life Sciences, Biological and Conservation Sciences Building, UKZN.

## **1.2 Sample Information**

Cells were incubated at 37°C in a humidified Shel Lab 3553 CO<sub>2</sub> incubator supplemented with 5% CO<sub>2</sub>. Stock cultures were maintained in T75 flasks containing 10 mL DMEM culture medium supplemented with 10% FBS and 0.5µg/mL pen/strep. Sub-cultures were maintained in 10 cm<sup>3</sup> dishes containing 10 mL DMEM culture medium supplemented with 10% FBS and 0.5µg/mL pen/strep. Cell growth was examined using an inverted Nikon TMS-F microscope and confluent cells were passaged by Trypsin-EDTA treatment as described in section 2.5 of the materials and methods.

Stock cultures of each cell line were frozen down from confluent flasks or dishes. Stock cultures were stored in cryovials (Corning<sup>®</sup>) in 1 mL culture medium supplemented with 10% dimethyl sulfoxide (DMSO). The cryovials were then flash dried in liquid nitrogen and stored in a liquid nitrogen dewar at -196°C.

## **1.3 RNA extraction**

Total RNA was extracted using the QIAGEN RNeasy Kit according to the manufacturer's instructions for purification of total RNA using spin technology as described in section 2.6 of the materials and methods. The RNA samples were not DNase treated as this degrades the RNA. Instead, genomic DNA contamination was assessed by including a no-RT control and a NTC control (negative controls) in which the reverse transcriptase and template/RNA was replaced by nuclease free water respectively. Genomic DNA was also assessed by bleach agarose gel electrophoresis as described in Appendix 1.5 below. RNA samples were

aliquoted in volumes equivalent to 2  $\mu\text{g}$  of RNA to ensure that each sample was only subjected to one freeze-thaw cycle. RNA aliquots were stored at  $-80^{\circ}\text{C}$ .

#### 1.4 RNA quantification

RNA samples were quantified using a Spectrophotometer ND1000 (NanoDrop technologies) using ND V3.5.2 software. Readings at  $A_{260}$  indicated the RNA concentration and the  $A_{260/280}$  ratio indicated the RNA purity (pure RNA has an  $A_{260/280}$  ratio between 1.8 and 2.1) (Figure 5.1).

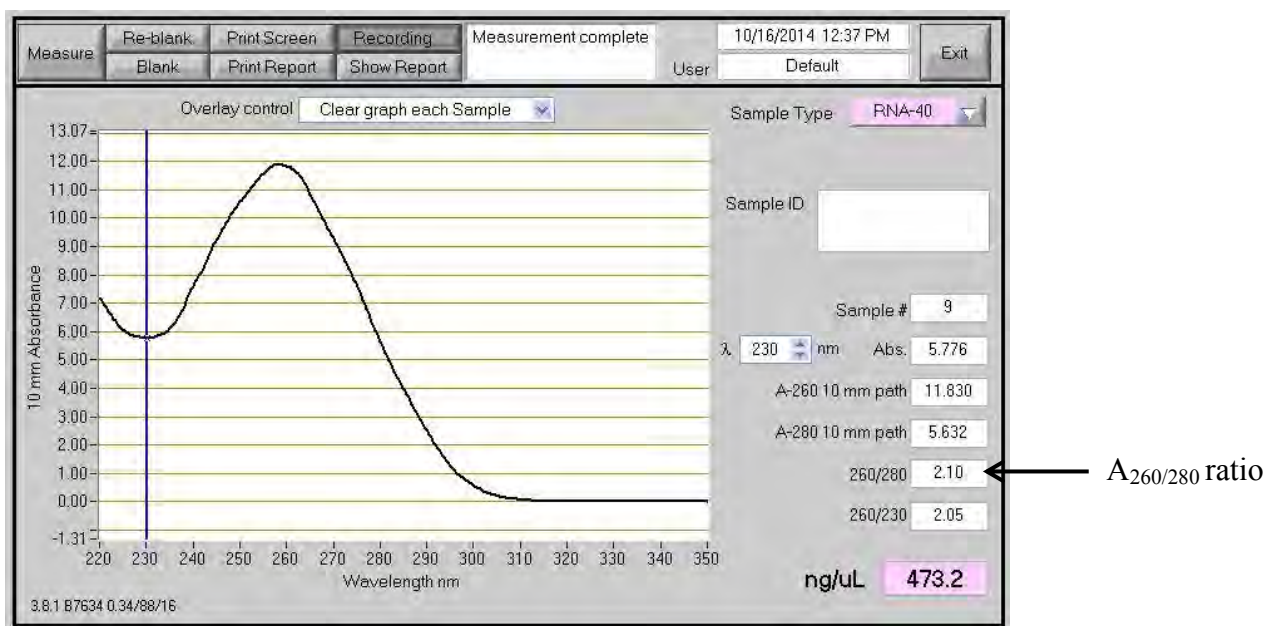


Figure 5.1: *In silico* screen of RNA quantification using a Spectrophotometer ND1000 (V3.5.2 software).

### **1.5 RNA gel electrophoresis**

RNA integrity was assessed by gel electrophoresis. RNA samples were separated on a 1% bleach agarose gel as described in section 2.6.2 of the materials and methods. Gels were visualised and bands were detected under UV light in a Bio-Rad Chemidoc® XRS+ imaging system (Bio-rad, USA). Image Lab™ software version 2.0.1 (Bio-rad, USA) was used to analyse detected bands.

The integrity of the RNA samples was confirmed by the presence of two bands of the 28S and 18S ribosomal subunits (Figure 3.2).

### **1.6 Reverse transcription**

The GoScript™ Reverse Transcription System (Promega, USA) was used to synthesise complimentary DNA (cDNA). The kit includes a reverse transcriptase and specialised reagents for efficient synthesis of first-strand cDNA optimised for quantitative PCR analysis. The presence of the specialised RNase inhibitor reduces RNA degradation, thus increasing the overall yield and quality of the resultant cDNA. A standard concentration of 2 µg RNA was used for cDNA synthesis in a Bio-Rad My cycler™ thermal cycler. The precise cDNA reactions and cycling conditions are described in section 2.7 of the materials and methods.

### **1.7 Primer information**

Table 2.1 provided in section 2.7 of the materials and methods describe the primer sets for both target and reference genes used in this study. The primer sets, synthesised by Inqaba biotech, were diluted to 100 µM stock solutions according to the manufacturer's instructions. Stock solutions were then diluted to a 10 µM working solution with nuclease free water. Primer stocks and working solutions were stored at -20°C.

### 1.7.1 The Basic Alignment Search Tool (BLAST)

The Primer BLAST tool (<http://www.ncbi.nlm.nih.gov/tools/primer-blast/>) was used to confirm that each primer set was specific to the target mRNA transcript in the *Mus musculus* genome available in the NCBI database ([www.ncbi.nlm.nih.gov](http://www.ncbi.nlm.nih.gov)).

Primer-BLAST Primer-Blast results

▶ NCBI/ Primer-BLAST: results: Job id=4vkYVURf7XvSVtZYt3bkJqxb1je\_RMsy [more...](#)

Input PCR template: none  
 Specificity of primers: Target templates were found in selected database: Refseq mRNA (Organism limited to Mus musculus)  
 Other reports: [▶ Search Summary](#)

☏ Detailed primer reports

**Primer pair 1**

	Sequence (5'->3')	Length	Tm	GC%	Self complementarity	Self 3' complementarity
Forward primer	GGCTTAGAGGAAGGTGATCAAA	22	57.78	45.45	6.00	2.00
Reverse primer	CTTTAGGGAGGTC AAGGAGGA	21	58.17	52.38	3.00	0.00

**Products on target templates**

>XM\_011250844.1 PREDICTED: Mus musculus tight junction protein 1 (Tjp1), transcript variant X11, mRNA

product length = 100

Forward primer	1	GGCTTAGAGGAAGGTGATCAAA	22
Template	2223	.....	2244
Reverse primer	1	CTTTAGGGAGGTC AAGGAGGA	21
Template	2322	.....	2302

Figure 5.2: *In silico* screen of the *Zol* primer BLAST against the *Mus musculus* genome. *Zol* is also referred to as tight junction protein (*Tjp1*).

Primer-BLAST Primer-Blast results

▶ NCBI/ Primer-BLAST : results: Job id=dm2PXMZWb3JQQFRONWBmMC5NVCE9Ukkk [more...](#)

Input PCR template none  
 Specificity of primers Target templates were found in selected database: Refseq mRNA (Organism limited to Mus musculus)  
 Other reports ▶ [Search Summary](#)

☰ Detailed primer reports

**Primer pair 1**

	Sequence (5'->3')	Length	Tm	GC%	Self complementarity	Self 3' complementarity
Forward primer	CTACTGGCTGCGGTATCA	20	59.54	55.00	3.00	1.00
Reverse primer	GGCCAGGATGAAGTCATAG	20	57.44	55.00	6.00	2.00

**Products on target templates**  
 >[NM\\_007472.2](#) Mus musculus aquaporin 1 (Aqp1), mRNA

product length = 143

Forward primer	1	CTACTGGCTGCGGTATCA	20
Template	747	.....	766
Reverse primer	1	GGCCAGGATGAAGTCATAG	20
Template	889	.....	870

Figure 5.3: *In silico* screen of the *Aqp1* primer BLAST against the *Mus musculus* genome.

Primer-BLAST Primer-Blast results

▶ NCBI/ Primer-BLAST : results: Job id=c2iJHQwXpTOei5qF-6uo--CGmurzmYfv [more...](#)

Input PCR template none  
 Specificity of primers Target templates were found in selected database: Refseq mRNA (Organism limited to Mus musculus)  
 Other reports ▶ [Search Summary](#)

☰ Detailed primer reports

**Primer pair 1**

	Sequence (5'->3')	Length	Tm	GC%	Self complementarity	Self 3' complementarity
Forward primer	TCCCTTCATTGCCTTTGTTC	20	56.21	45.00	3.00	0.00
Reverse primer	CAAGGTGGCGATAGCTCTTC	20	58.42	55.00	4.00	2.00

**Products on target templates**  
 >[XM\\_006535139.2](#) PREDICTED: Mus musculus solute carrier family 4 (anion exchanger), member 4 (Slc4a4), transcript variant X6, mRNA

product length = 151

Forward primer	1	TCCCTTCATTGCCTTTGTTC	20
Template	884	.....	903
Reverse primer	1	CAAGGTGGCGATAGCTCTTC	20
Template	1034	.....	1015

Figure 5.4: *In silico* screen of the *Slc4a4* primer BLAST against the *Mus musculus* genome.

Primer-BLAST Primer-Blast results

▶ NCBI/ Primer-BLAST : results: Job id=aXKTBwwNpSmekZqf-7Go4eCcmvDzg4f1 [more...](#)

Input PCR template none  
 Specificity of primers Target templates were found in selected database: Refseq mRNA (Organism limited to Mus musculus)  
 Other reports ▶ [Search Summary](#)

☰ Detailed primer reports

**Primer pair 1**

	Sequence (5'->3')	Length	Tm	GC%	Self complementarity	Self 3' complementarity
Forward primer	GTCCCAGCGTCGTGATTAGCGAT	23	64.99	56.52	4.00	2.00
Reverse primer	GGGCCACAATGTGATGGCCTCC	22	66.03	63.64	8.00	4.00

**Products on target templates**

> [NM\\_013556.2](#) Mus musculus hypoxanthine guanine phosphoribosyl transferase (Hprt), mRNA

product length = 180

Forward primer	1	GTCCCAGCGTCGTGATTAGCGAT	23
Template	160	.....	182
Reverse primer	1	GGGCCACAATGTGATGGCCTCC	22
Template	339	.....	318

Figure 5.5: *In silico* screen of the *Hprt* primer BLAST against the *Mus musculus* genome.

Primer-BLAST Primer-Blast results

▶ NCBI/ Primer-BLAST : results: Job id=EwjppESu7YrSp9apt4fk16yq1sa\_tcvD [more...](#)

Input PCR template none  
 Specificity of primers Target templates were found in selected database: Refseq mRNA (Organism limited to Mus musculus)  
 Other reports ▶ [Search Summary](#)

☰ Detailed primer reports

**Primer pair 1**

	Sequence (5'->3')	Length	Tm	GC%	Self complementarity	Self 3' complementarity
Forward primer	CTAAGGCCAACCGTGAAAAG	20	57.01	50.00	4.00	0.00
Reverse primer	ACCAGAGGCATACAGGGACA	20	60.25	55.00	2.00	0.00

**Products on target templates**

> [NM\\_007393.4](#) Mus musculus actin, beta (Actb), mRNA

product length = 104

Forward primer	1	CTAAGGCCAACCGTGAAAAG	20
Template	444	.....	463
Reverse primer	1	ACCAGAGGCATACAGGGACA	20
Template	547	.....	528

Figure 5.6: *In silico* screen of the  $\beta$ -actin primer BLAST against the *Mus musculus* genome.

The specificity of each primer set was also analysed by agarose gel electrophoresis of the PCR products (Figure 3.4) and qPCR products (Appendix 1.9).

## **1.8 qPCR Protocol**

The qPCR protocol used in this study was sourced from Shei *et al.*, 2013. SYBR<sup>®</sup> Green JumpStart<sup>™</sup> Taq ReadyMix<sup>™</sup> mastermix (Sigma-Aldrich<sup>®</sup>, USA) and SYBR<sup>®</sup> Select Master Mix (Applied Biosystems) were both used in this study. Although both reagents are fluorescent dyes that essentially work the same way, they do require slightly different reaction protocols and SYBR<sup>®</sup> Select Master Mix (Applied Biosystems) requires an additional activation temperature at 50°C for 2 minutes before the initial denaturation.

### **1.8.1 SYBR<sup>®</sup> Green JumpStart<sup>™</sup> Taq ReadyMix<sup>™</sup> mastermix (Sigma-Aldrich<sup>®</sup>, USA)**

A 25 µl reaction consisted of 12.5 µl SYBR<sup>®</sup> Green JumpStart<sup>™</sup> Taq ReadyMix<sup>™</sup> mastermix (Sigma-Aldrich<sup>®</sup>, USA); 10.5 µl nuclease free water, 0.5 µl 10mM forward primer, 0.5 µl 10mM reverse primer and 1 µl cDNA. Reactions were transferred into a MicroAmp<sup>®</sup> Optical 96-well Reaction Plate (Applied Biosystems) in triplicate, which was gently centrifuged at 500 rpm for 1 minute at 4°C and placed in the Applied Biosystems 7500 Real-Time PCR System with HID Real-time PCR Analysis Software version 1.2.

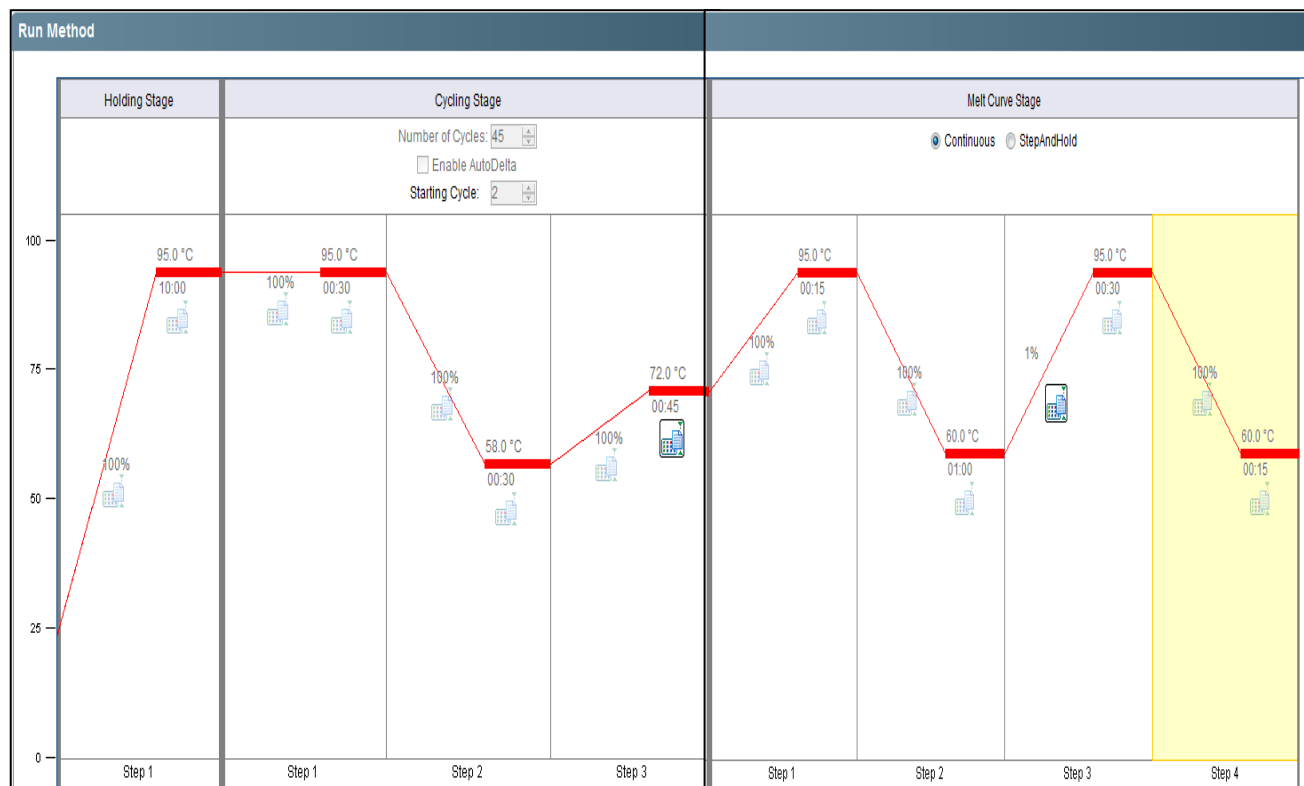


Figure 5.7: The qPCR cycling protocol using SYBR<sup>®</sup> Green JumpStart<sup>™</sup> Taq ReadyMix<sup>™</sup> mastermix (Sigma-Aldrich<sup>®</sup>, USA).

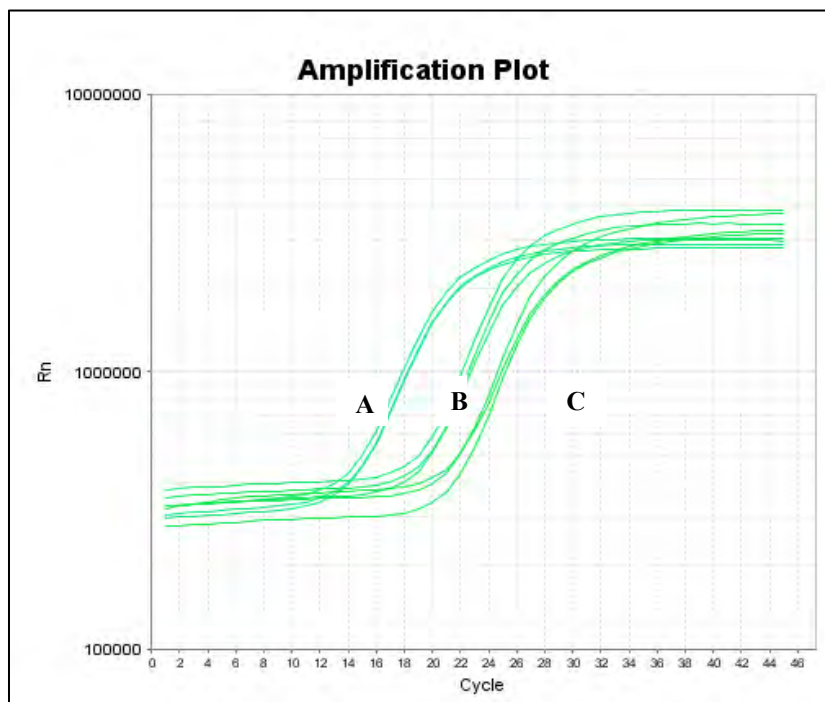


Figure 5.8: Amplification curves of *βactin* (A); *Hprt* (B) and *Slc4a4* (C) amplified with SYBR<sup>®</sup> Green JumpStart<sup>™</sup> Taq ReadyMix<sup>™</sup> mastermix.

### 1.8.2 SYBR<sup>®</sup> Select Master Mix (Applied Biosystems)

A 20  $\mu$ l reaction consisted of 10  $\mu$ l SYBR select, 8  $\mu$ l nuclease free water, 0.5  $\mu$ l 10mM forward primer; 0.5  $\mu$ l 10mM reverse primer and 1  $\mu$ l cDNA. Reactions were transferred into a MicroAmp<sup>®</sup> Optical 96-well Reaction Plate (Applied Biosystems) in triplicate, which was gently centrifuged at 500 rpm for 1 minute at 4°C and placed in the Applied Biosystems 7500 Real-Time PCR System with HID Real-Time PCR Analysis Software version 1.2

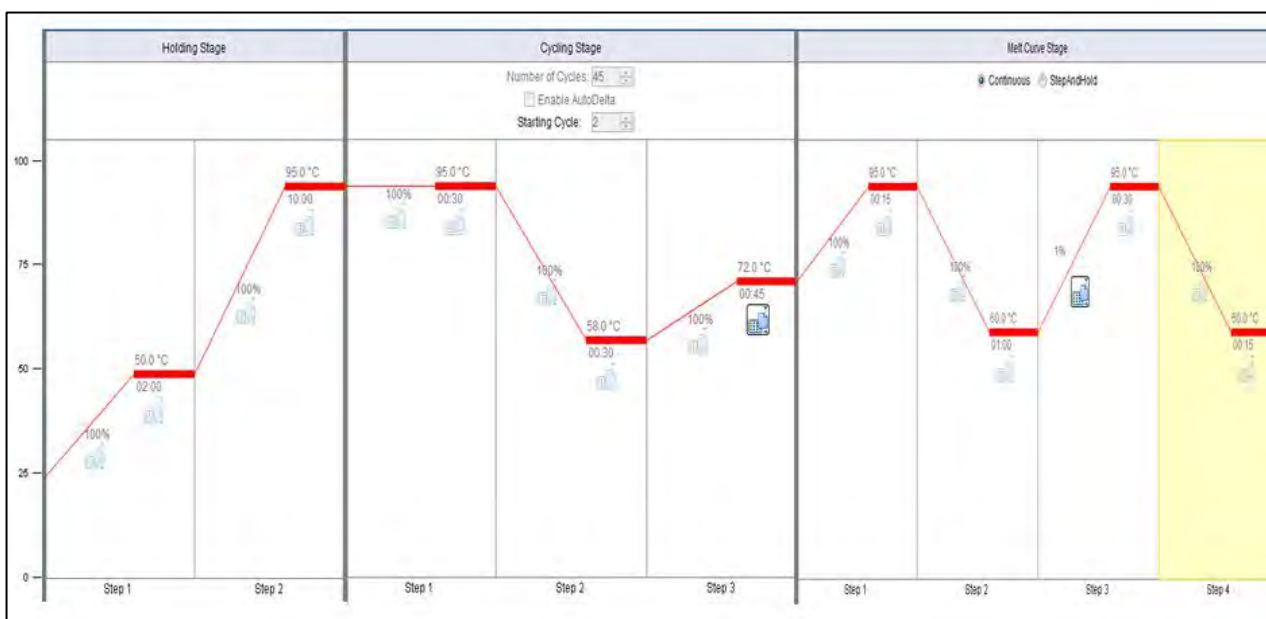


Figure 5.9: The qPCR cycling protocol using SYBR<sup>®</sup> Select Master Mix (Applied Biosystems), which requires an additional activation temperature at 50°C for 2 minutes before the initial denaturation.

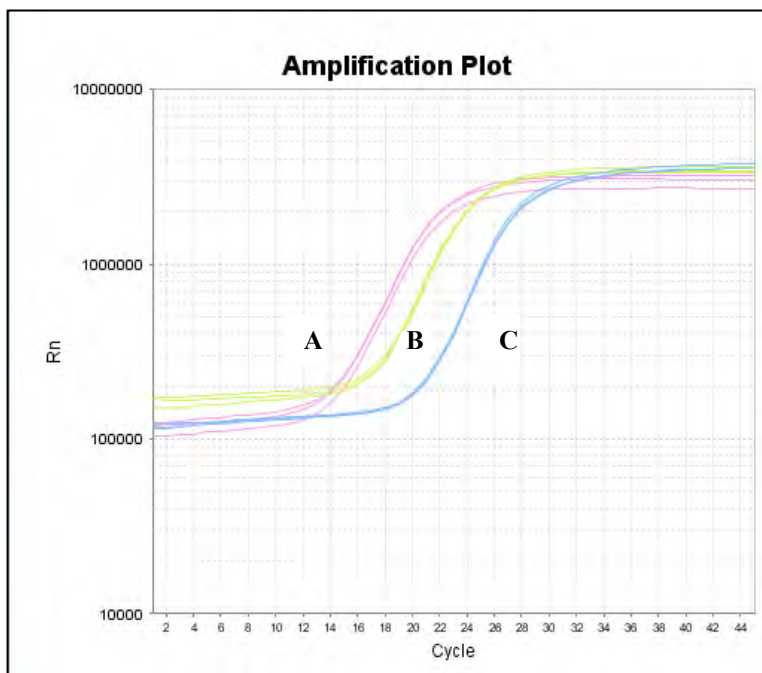


Figure 5.10: Amplification curves of  $\beta$ -actin (A); *Hprt* (B) and *SLC4a4* (C) amplified with SYBR select mastermix.

The MicroAmp<sup>®</sup> Optical 96-well Reaction Plate (Applied Biosystems) used in this study is free of DNase, RNase and PCR inhibitors. Gilson Pipetman starter kit micropipettes (Gilson) were used to manually set up all qPCR reactions. Dedicated sterile TipOne beveled filter tips (Starlab) were used for reactions. All qPCR reagents and cDNA samples were kept on ice for the duration of the experiment.

### 1.9 qPCR Melt analysis

A melt curve analysis, generated by the HID Real-Time PCR Analysis software, provides another tool to determine the specificity of the primer sets and the protocol used in this study. The melt curve analysis ranged from 50°C to 90°C with 1°C increments and a plate read step was included for 5 seconds after each temperature change. A single peak in the

sample (representing a single melting temperature) and multiple peaks in the NTC control of the same sample indicate a single amplicon for the primer set. The correct size of the amplicon was verified by gel electrophoresis (1% agarose gel as described in section 2.7.1 of the materials and methods).

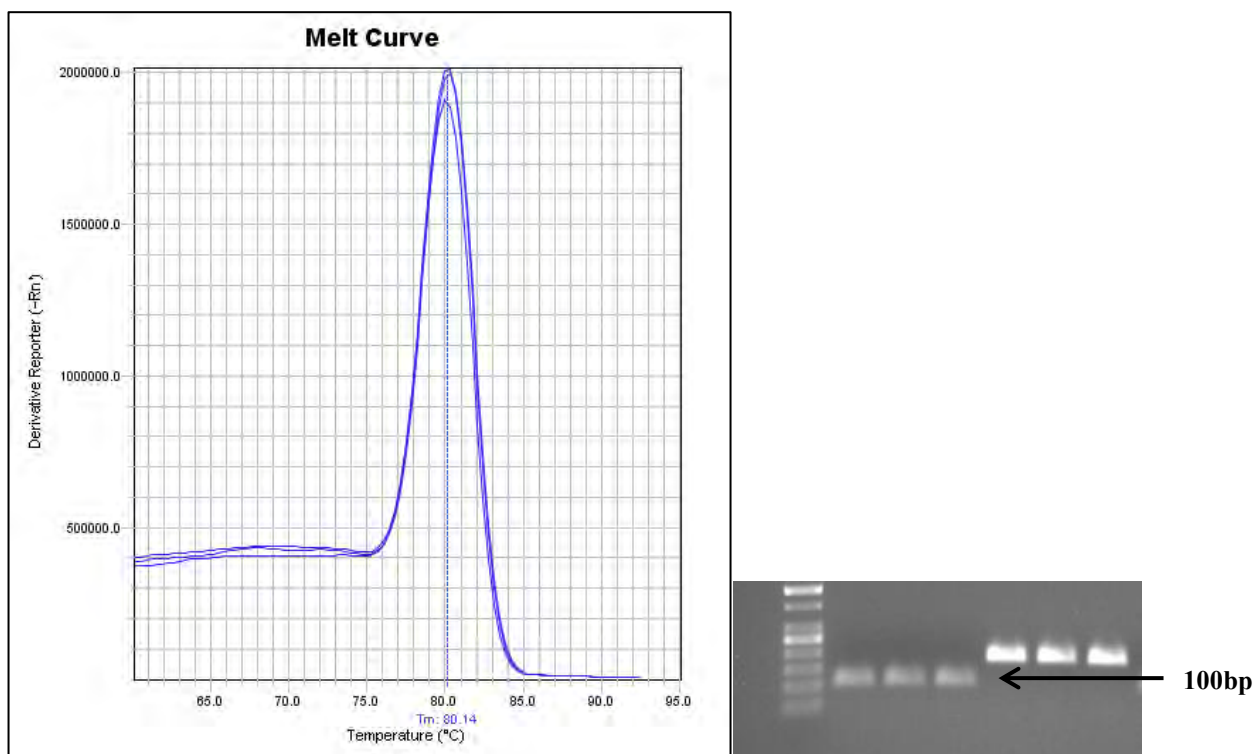


Figure 5.11: Melt curve analysis and agarose gel verification of the *Zol* primer set. *Zol* qPCR melting temperature at 80.14°C and a product size of 100bp.

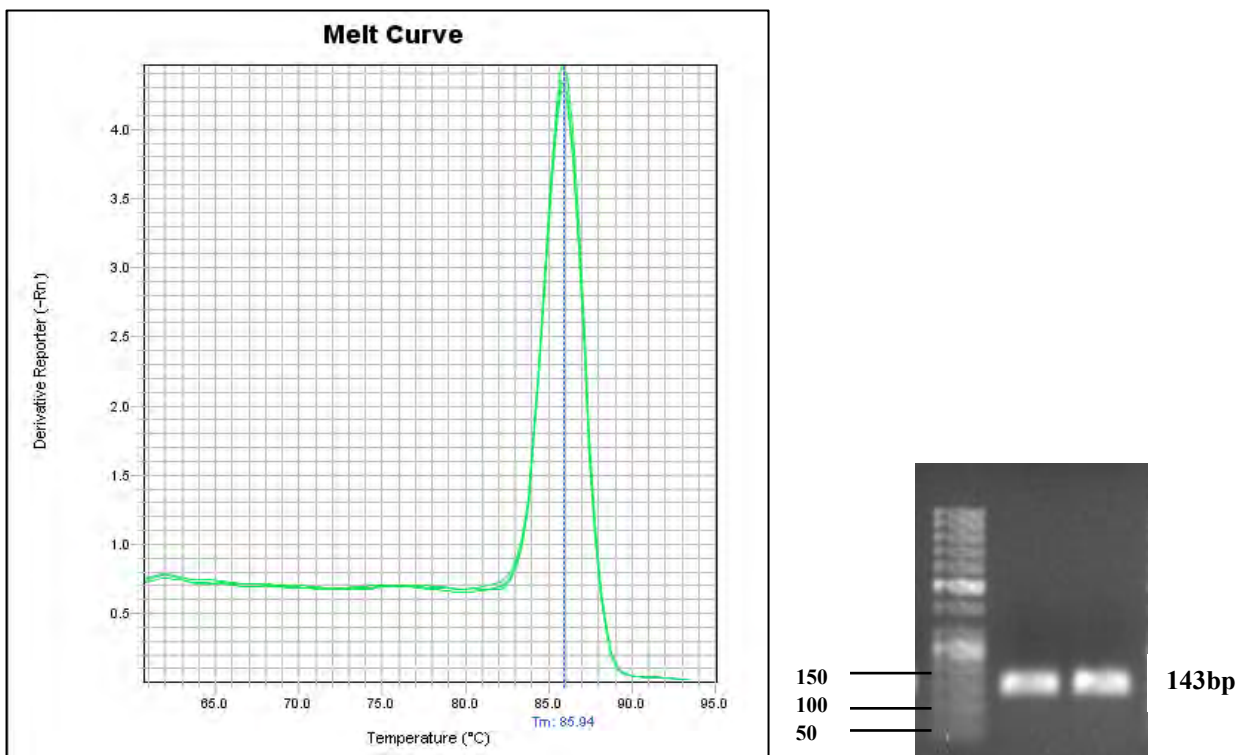


Figure 5.12: Melt curve analysis and agarose gel verification of the *Aqp1* primer set. *Aqp1* qPCR melting temperature at 85.94°C and a product size of 143bp

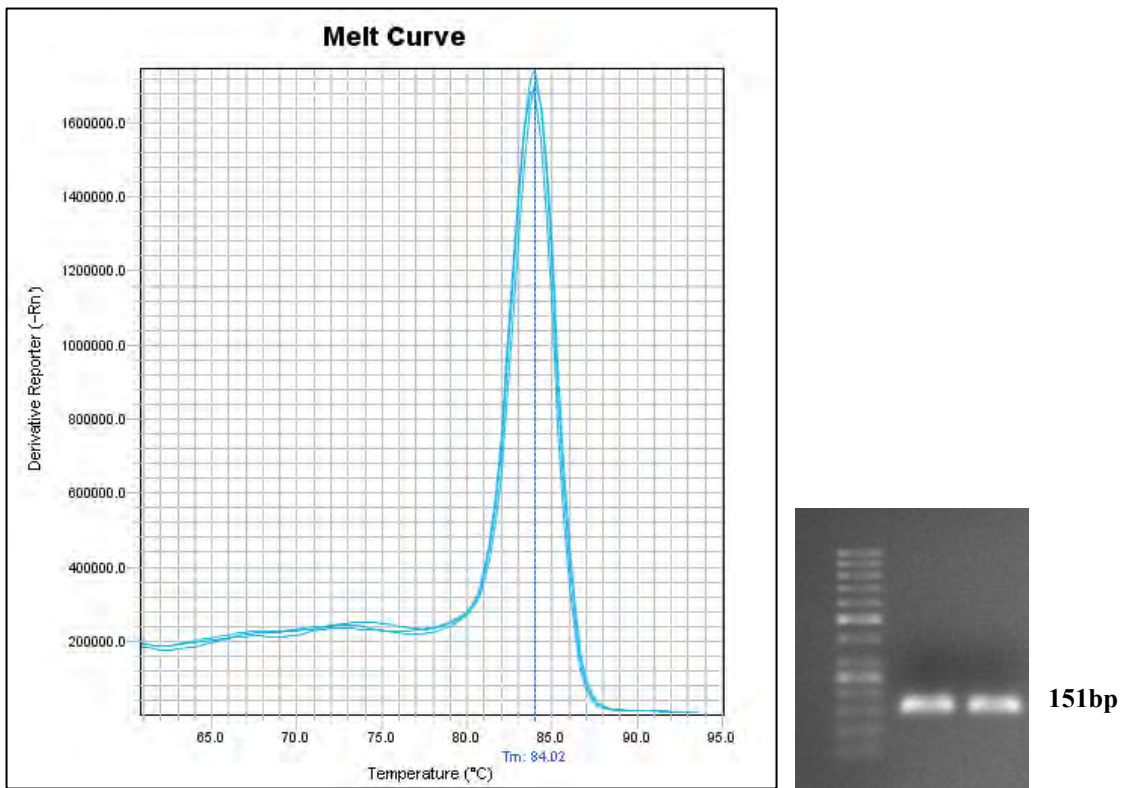


Figure 5.13: Melt curve analysis and agarose gel verification of the *Slc4a4* primer set. *Slc4a4* qPCR melting temperature at 84.02°C and a product size of 151bp.

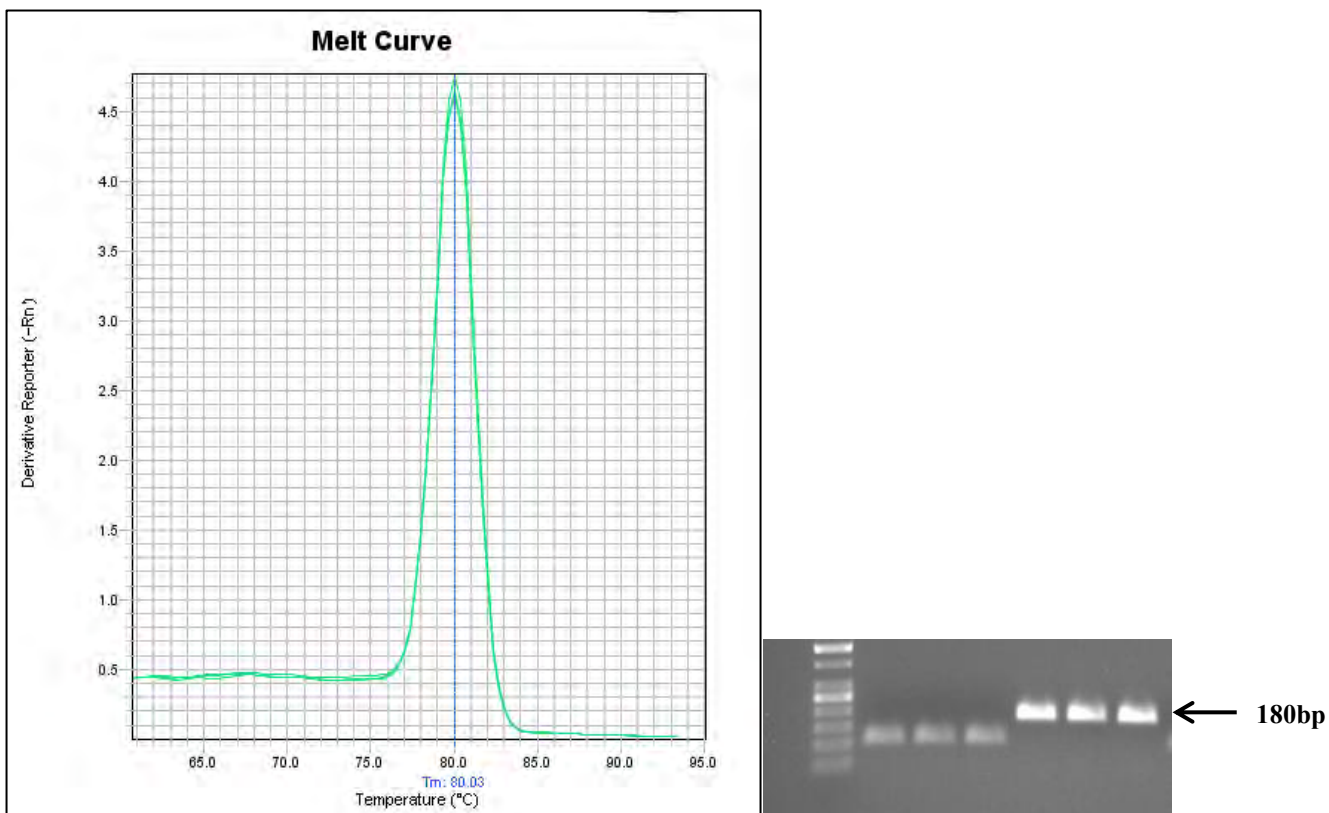


Figure 5.14: Melt curve analysis and agarose gel verification of the *Hprt* primer set. *Hprt* qPCR melting temperature at 80.03°C and a product size of 180bp.

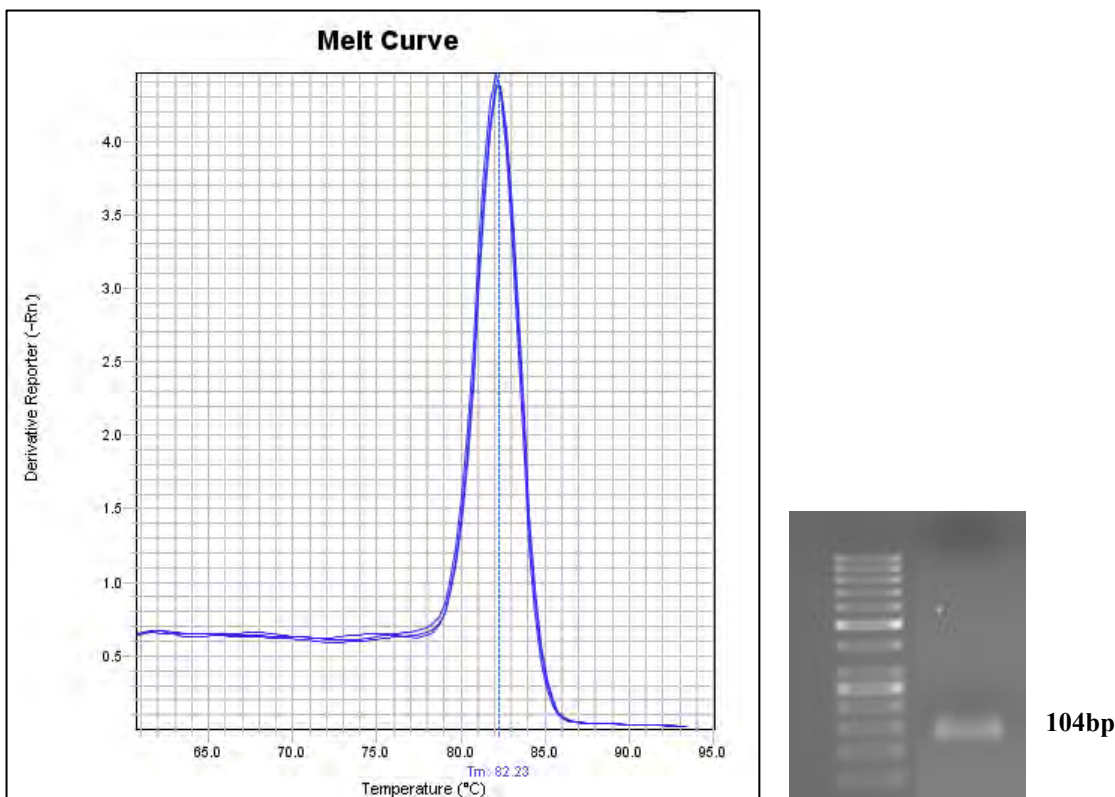


Figure 5.15: Melt curve analysis and agarose gel verification of the  $\beta$ -actin primer set. *B-actin* qPCR melting temperature at 82.23°C and a product size of 104bp.

### 1.10 Evaluation of qPCR reaction efficiency

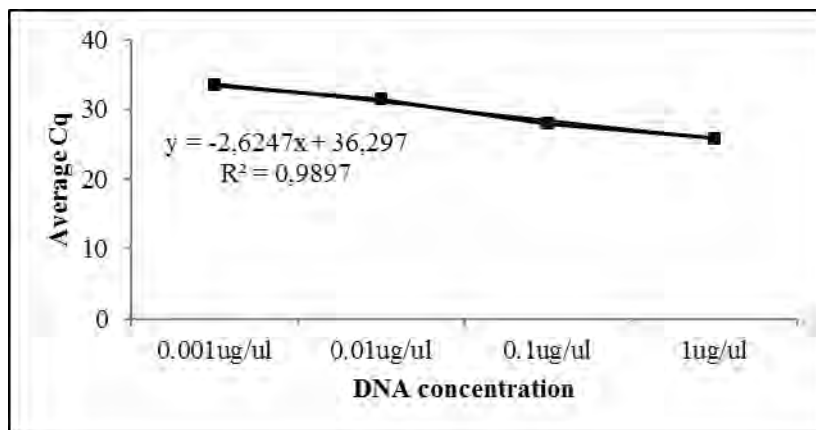
To accurately quantify the relative expression of the target genes using the comparative Ct method, the amplification efficiencies between the target genes and the reference genes must be very similar (between 90-100%) with an  $r^2$  value greater than 0.98 (Livak and Schmittgen, 2001).

A 10x serial dilution of template cDNA was used to determine the reaction efficiencies of the primer sets of the genes of interest used in this study. Each sample in the dilution series was then analysed by qPCR as previously described in appendix 1.8. The Ct values for the target and reference genes were averaged and the delta-Ct value was calculated as follows:

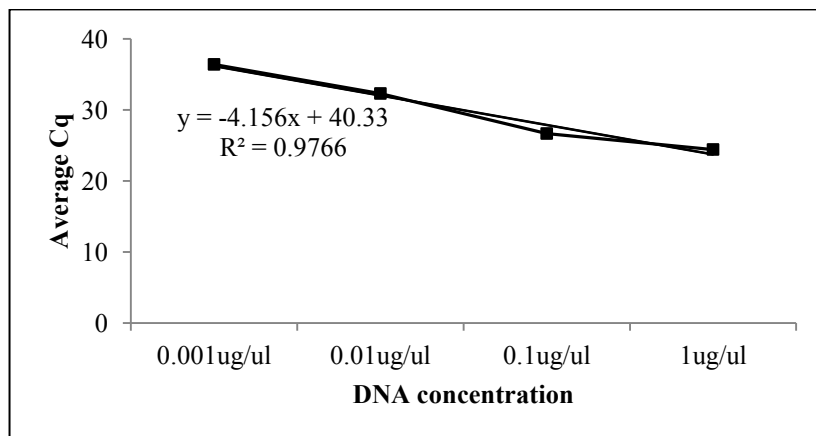
$Ct_{\text{target gene}} - Ct_{\text{reference gene}}$ ). The delta-Ct value was then plotted against the cDNA dilution range. For the comparative Ct method to be applicable in this study, the slope of the regression line must be close to zero (Livak and Schmittgen, 2001).

The qPCR Standard Curve Slope to Efficiency Calculator software (<http://www.genomics.agilent.com/CalculatorPopupWindow.aspx?CallID=8>) was used to calculate the reaction efficiencies of the primer sets used in this study.

a)



b)



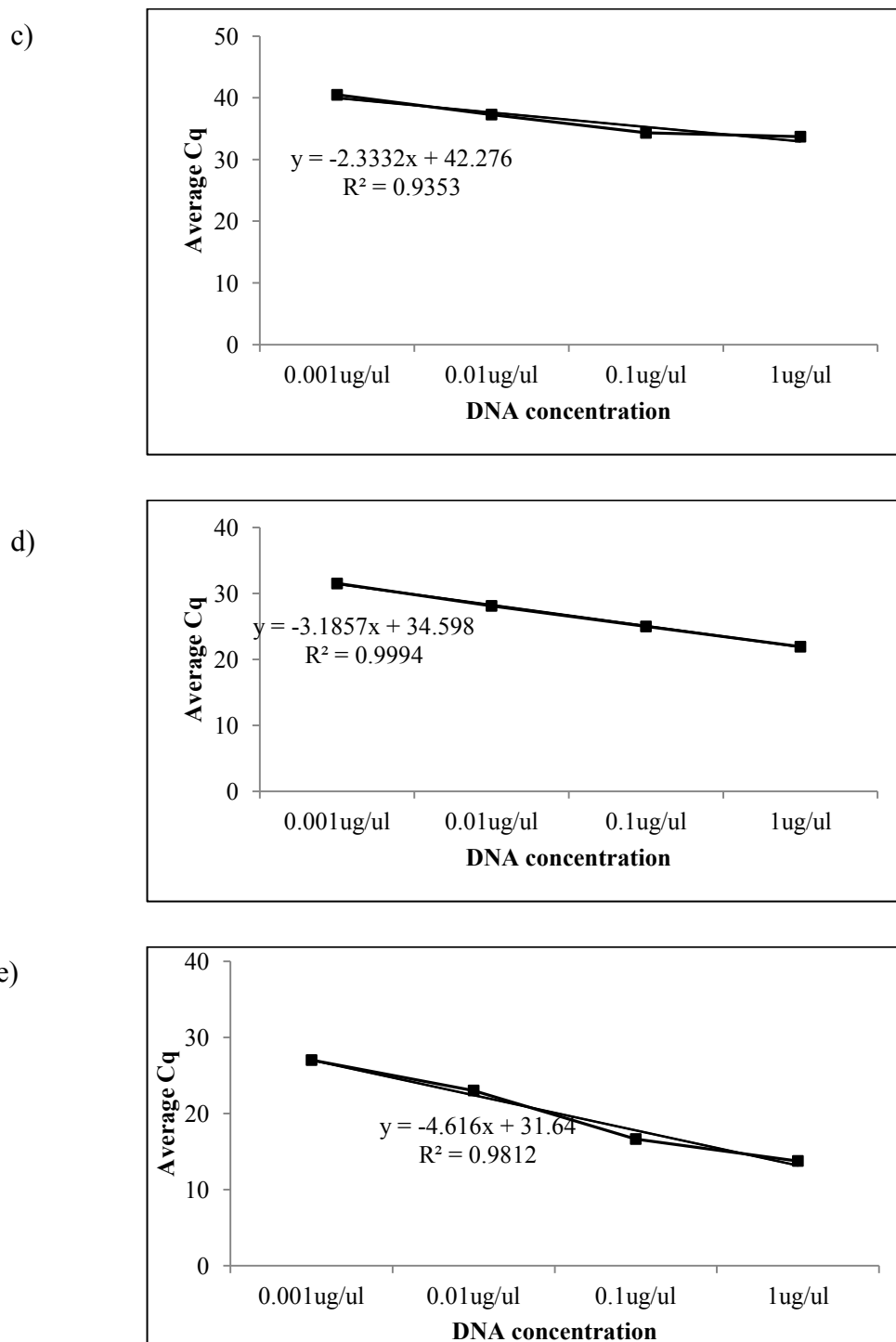


Figure 5.16: Linear analysis of a) *Zol* ( $r^2 = 0.9897$ ; reaction efficiency = 140.41%,  $n=3$ ), b) *Aqp1* ( $r^2 = 0.9766$ ; reaction efficiency = 73.94%,  $n=3$ ), c) *Slc4a4* ( $r^2 = 0.9353$ ; reaction

efficiency = 168.31%, n=3), d) *Hprt* ( $r^2 = 0.9994$ ; reaction efficiency = 106%, n=3), e)  *$\beta$ -actin* ( $r^2 = 0.9812$ ; reaction efficiency = 64.68%, n=3).

### **1.11 Data analysis**

HID Real-Time PCR Analysis Software version 1.2 (Applied Biosystems) was used to analyse all the qPCR data presented in this study. A custom assay was designed using the HID Real-Time software package. The custom assay option allows the user to define the qPCR reaction parameters and provides a quality control (QC) summary that indicates which reactions should be excluded from the analysis (figure 5.17). Quantification cycle ( $C_q$ ) readings were determined using an automatic threshold determined by the HID software package. The SYBR channel was used to measure fluorescence in the absence of a passive dye reference.

QC Summary			
<b>Flag Summary</b>			
Total Wells: 96	Processed Wel... 36	Manually Omitted Wel... 0	Targets Used: 3
Wells Set ... 36	Flagged Wells: 1	Analysis Omitted Wells: 0	Samples Us... 2
Flag Details			
Flag:	Name	Frequency	Wells
AMPNC	Amplification in negative control	0	
BADROX	Bad passive reference signal	0	
OFFSCALE	Fluorescence is offscale	0	
HIGHSD	High standard deviation in replicate ...	0	
NOAMP	No amplification	0	
NOISE	Noise higher than others in plate	0	
SPIKE	Noise spikes	0	
NOSIGNAL	No signal in well	0	
OUTLIER...	Outlier in replicate group	1	B11
EXPFAIL	Exponential algorithm failed	0	
BLFAIL	Baseline algorithm failed	0	
THOLDFAIL	Thresholding algorithm failed	0	
CTFAIL	Ct algorithm failed	0	
MTP	Multiple Tm peaks	0	

Figure 5.17: A QC summary of the parameters used to exclude reactions from the analyses, as shown in the HID Real-Time PCR Analysis Software program.

NTC and ‘no-RT’ controls (figures 5.18 and 5.19 respectively) resulted in an undetectable  $C_q$  reading that the software denotes “undeterminable” or primer dimers that were identified by a melt curve with a temperature lower than 80°C.

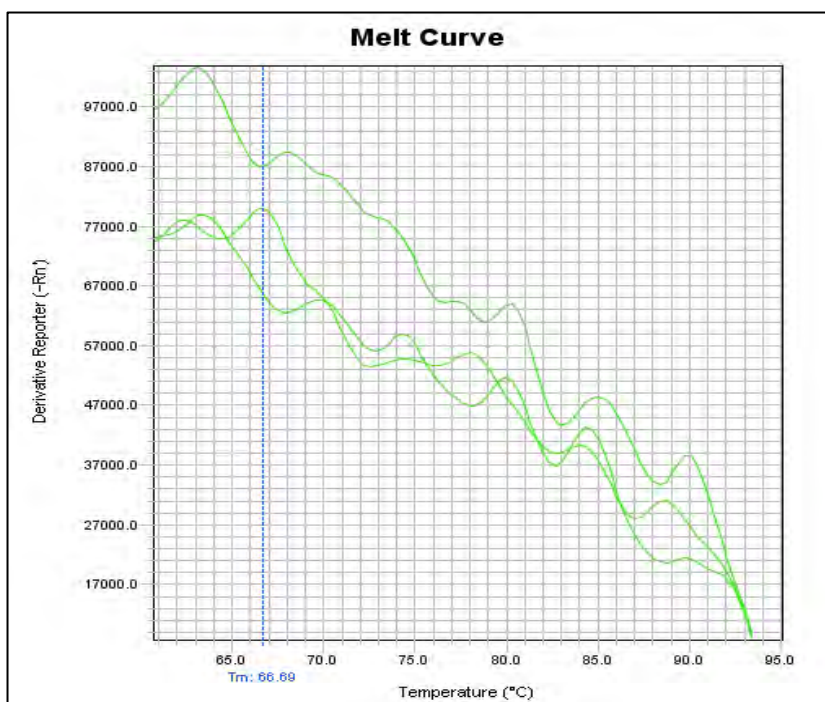


Figure 5.18: Melt curve analysis for an *Aqp1* NTC control with a melting temperature at 66.69°C.

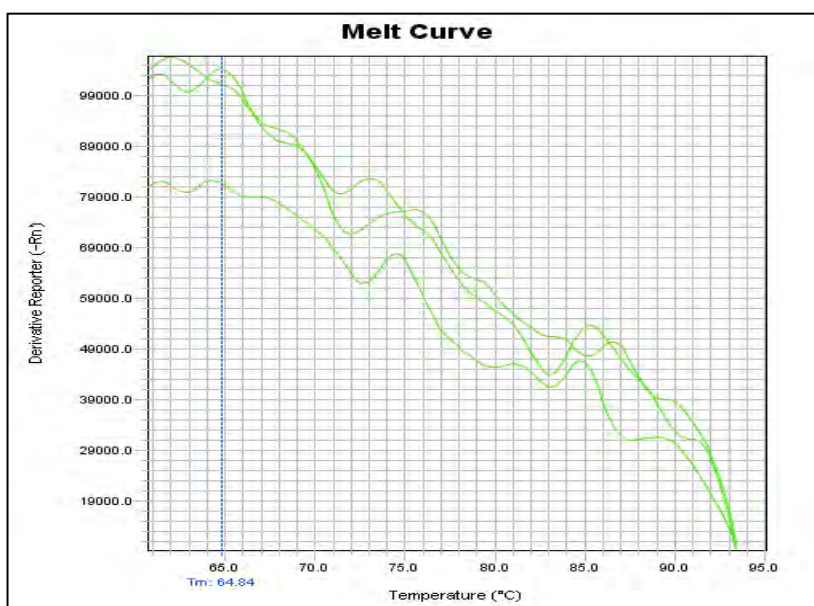


Figure 5.19: Melt curve analysis for an *Aqp1* 'no-RT' control with a melting temperature at 64.84°C.

### 1.12 Reference Genes

Gene expression data must be normalised against reference genes (also referred to as internal control genes or housekeeping genes) in order to perform accurate and reliable gene expression analyses (De Jonge *et al.*, 2007). A recent study conducted by Shei *et al.*, 2013 used both  *$\beta$ -actin* and *HPRT* as reference genes for qPCR analyses in murine corneal endothelium and cell culture (Shei *et al.*, 2013). In this study, the expression levels of the target genes were normalised against that of the reference genes  *$\beta$ -actin* and *Hprt*, which rank first and eighth in the list of the 12 most reliable commonly used reference genes (De Jonge *et al.*, 2007).

### 1.13 $^{-\Delta\Delta Ct}$ Method

The  $C_q$  values generated by the HID Real-Time PCR Analysis Software version 1.2 (Applied Biosystems) were analysed using the  $2^{-\Delta\Delta Ct}$  method (Livak and Schmittgen, 2001). This method identifies the fold-change expression of the target gene relative to the reference genes which accounts for basal gene expression levels. Reactions for each target gene in each cell line were performed in triplicate and the average  $C_q$  for each target gene was then normalised against the geometric mean of the two reference genes. The fold-change in expression was then calculated as follows:

$$\Delta Ct = C_q \text{ target gene} - C_q \text{ reference gene}$$

$$\Delta\Delta Ct = \Delta C_q (\text{target gene}) - \Delta C_q (\text{reference gene})$$

$$\text{Thus, } \Delta\Delta Ct (\text{reference gene}) = \Delta Ct (\text{reference gene}) - \Delta Ct (\text{reference gene}) = 0$$

$$\text{Therefore, } 2^{-\Delta\Delta Ct} \text{ of the reference gene} = 2^0 = 1$$

$$\text{For each target gene, the fold change value} = 2^{-(\Delta Ct \text{ target gene}) - (\Delta Ct \text{ reference gene})}$$

### 1.14 Statistics

qPCR data were analysed using (IBM) SPSS Statistics Version 21. A one-way ANOVA was used to determine the statistical significance of the relative fold change of the target genes relative to the reference genes. The assumption that the residuals from the analysis are normally distributed was tested using a one-sample Kolmogorov-Smirnov test. A Levene's test was used to test the assumption that the residuals must be homoscedastic. These assumptions must be satisfied for the ANOVA to yield valid statistical results. A Tukey HSD post-hoc test was used to determine if there was statistical significance in gene expression of target genes between different developmental stages. All tests for normality were satisfied and significance was determined at  $p < 0.05$ . Results are presented as bar graphs with error bars that represent the standard deviation of the normalised expression calculated from an average of the triplicate values given for each target gene and the two reference genes.

### 2. Ponceau S staining used to detect total protein for western blot analysis.

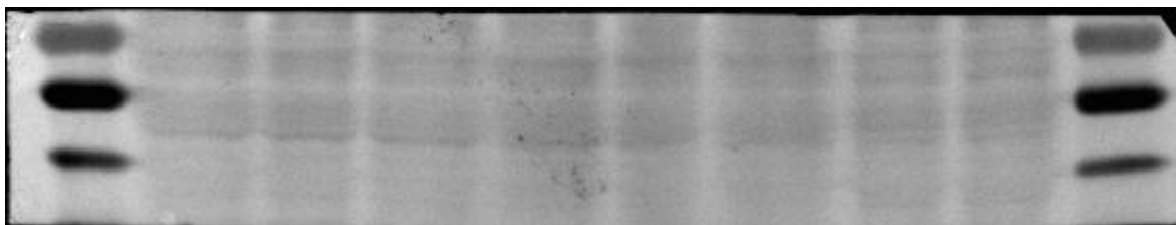


Figure 5.20: Ponceau S image of Aqp1 protein expression at different stages of corneal endothelial development. This is a single representative image.

Total protein was detected by imaging the membrane using the Molecular Marker protocol as done for the protein ladder. A single representative Ponceau S image was analysed by densitometry.

### 3. Immunocytochemistry

#### a) Controls

For the negative controls, primary and secondary antibodies were substituted by 1x PBS in no-primary controls and no-secondary controls respectively, to identify non-specific binding of each antibody. P13 monolayer and hanging drop negative controls are shown for both Zo1 and Aqp1 as representative images for all the cell lines.

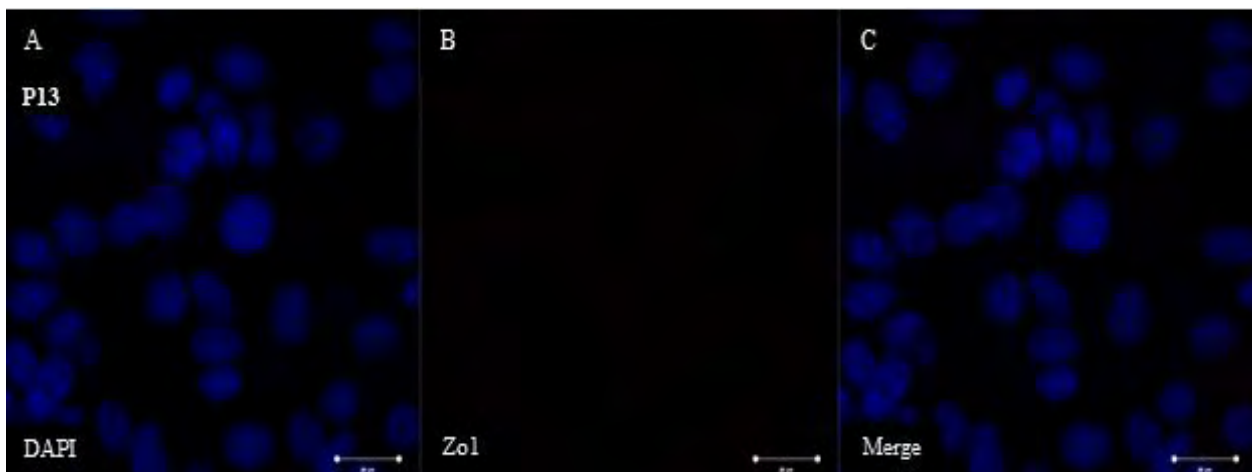


Figure 5.21: 63x confocal microscopy image showing no-primary antibody control for Zo1 monolayer cultures. A) DAPI stained cells B) no-primary control C) Merged image. Scale bar is 20  $\mu\text{m}$ .

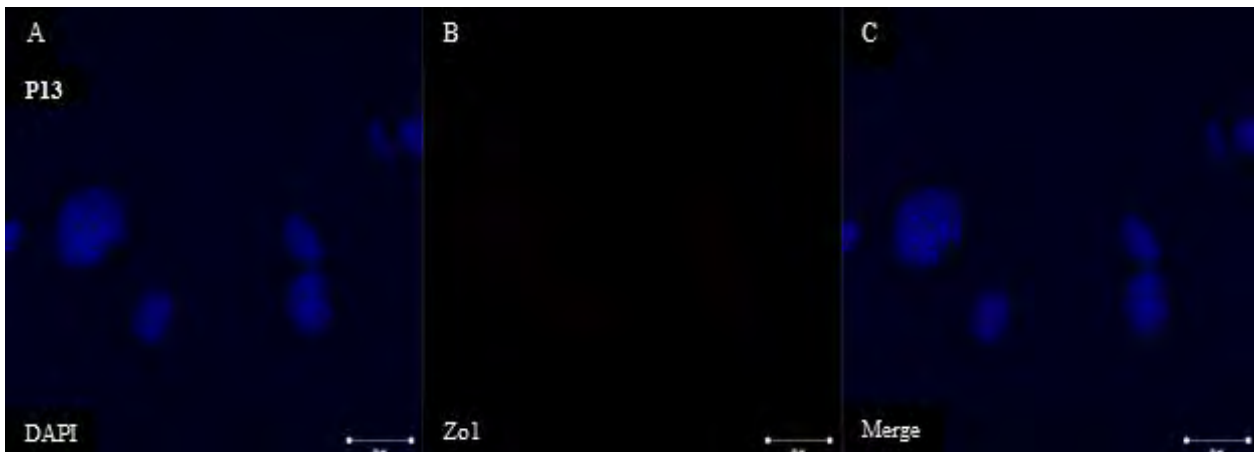


Figure 5.22: 63x confocal microscopy image showing no-secondary antibody control for Zo1 monolayer cultures. A) DAPI stained cells B) no-secondary control C) Merged image. Scale bar is 20  $\mu\text{m}$ .

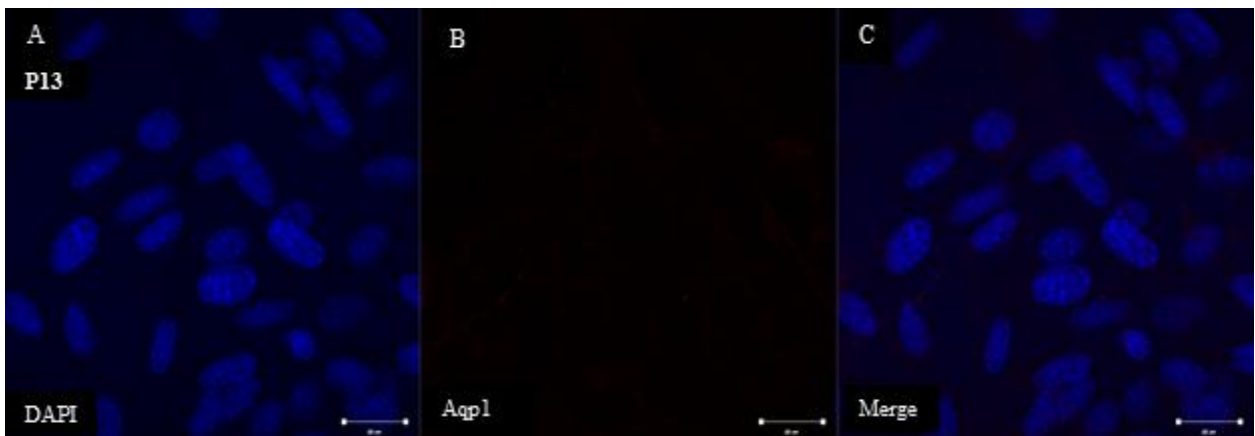


Figure 5.23: 63x confocal microscopy image showing no-primary antibody control for Aqp1 monolayer cultures. A) DAPI stained cells B) no-primary control C) Merged image. Scale bar is 20  $\mu\text{m}$ .

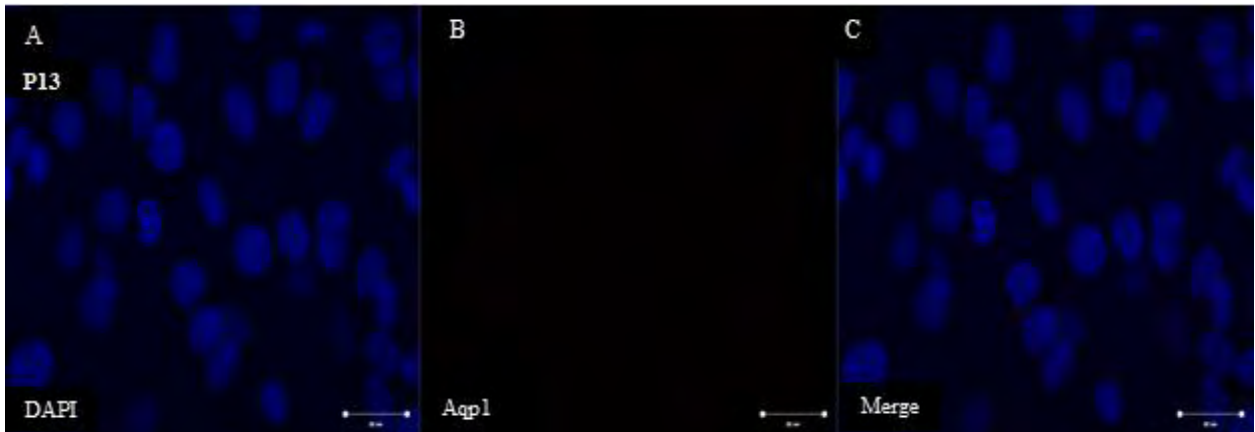


Figure 5.24: 63x confocal microscopy image showing no-secondary antibody control for Aqp1 monolayer cultures. A) DAPI stained cells B) no-secondary control C) Merged image. Scale bar is 20  $\mu\text{m}$ .

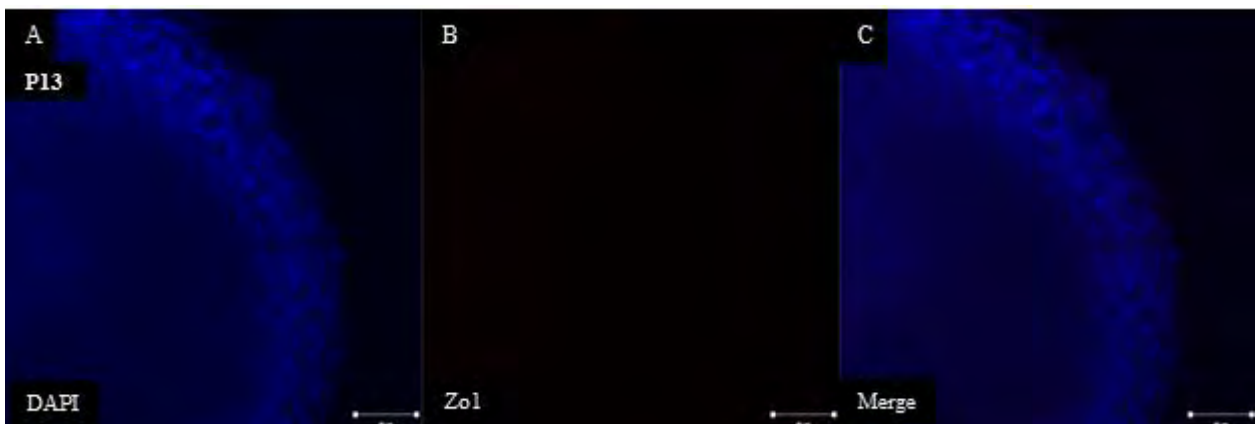


Figure 5.25: 25x confocal microscopy image showing no-primary antibody control for Zo1 hanging drop cultures. A) DAPI stained cells B) no-primary control C) Merged image. Scale bar is 50  $\mu\text{m}$ .

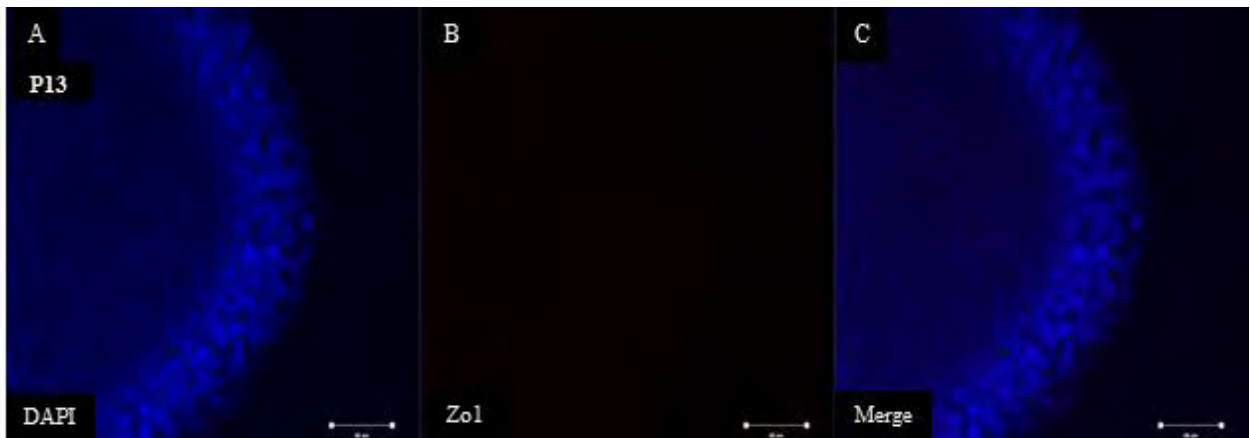


Figure 5.26: 25x confocal microscopy image showing no-secondary antibody control for Zo1 hanging drop cultures. A) DAPI stained cells B) no-secondary control C) Merged image. Scale bar is 50  $\mu\text{m}$ .

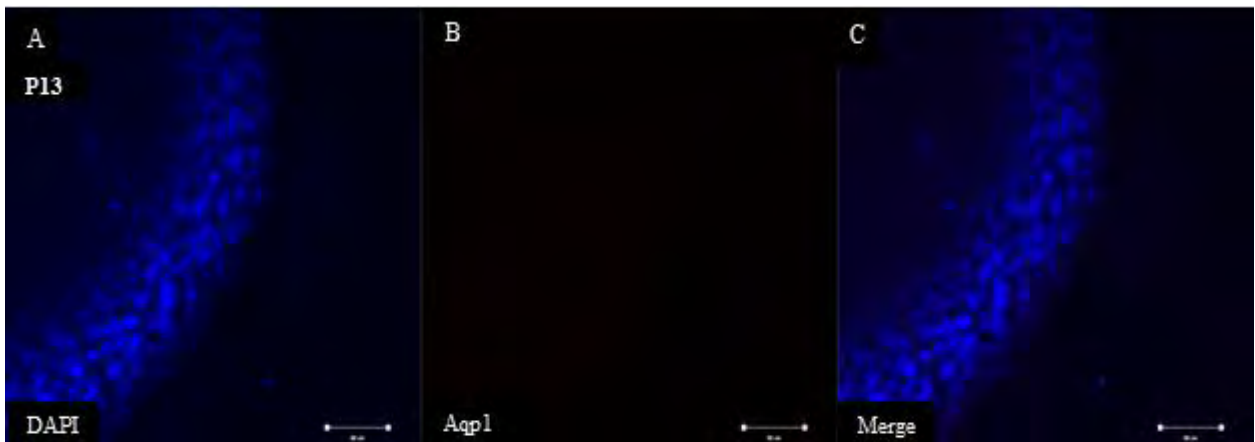


Figure 5.27: 25x confocal microscopy image showing no-primary antibody control for Aqp1 hanging drop cultures. A) DAPI stained cells B) no-primary control C) Merged image. Scale bar is 50  $\mu\text{m}$ .

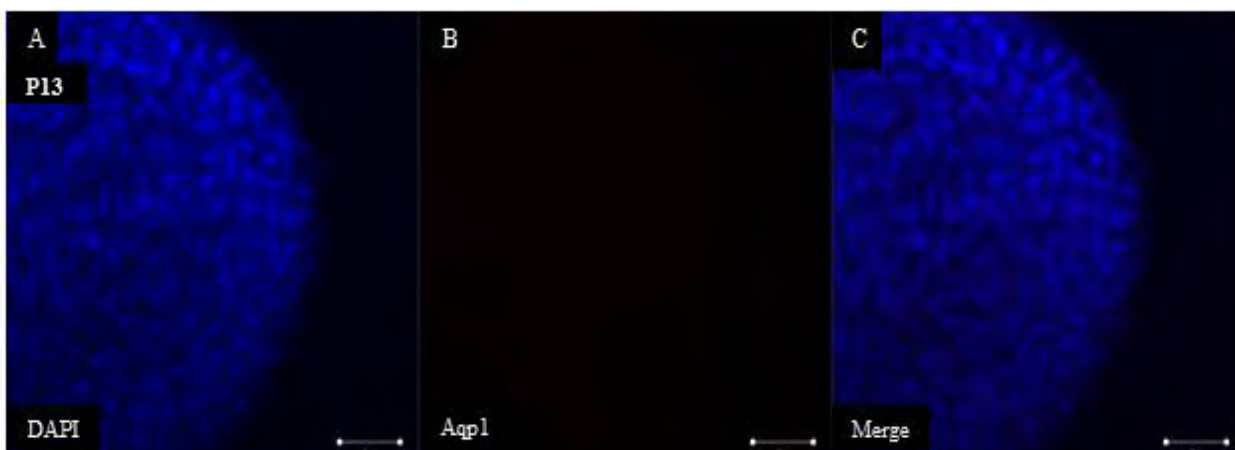


Figure 5.28: 25x confocal microscopy image showing no-secondary antibody control for Aqp1 hanging drop cultures. A) DAPI stained cells B) no-secondary control C) Merged image. Scale bar is 50  $\mu\text{m}$ .

### b) Troubleshooting

To optimise Zo1 staining for confocal microscopy, Zo1 antibody concentrations ranging from 1:50 to 1:1000 as well as various Cy3 incubation times (2, 4, 6 and 24 hours) were attempted. Monolayer cultures were also grown in serum free media to assess whether protein factors in the serum affected Zo1 expression (Appendix 3b). However, despite this, very little Zo1 staining was seen in monolayer culture.

## 4. Recipes

### 4.1 General Recipes

#### a) 1M Potassium hydroxide (KOH)

Reagents	Volume (200 mL)
KOH	11.22 g
Ultra-pure Water	200 mL

KOH was dissolved in ultra-pure water and stored at room temperature. Tungsten needles used for micro-dissections were sharpened on a wetstone, followed by electrochemical sharpening using 1M KOH and 150V power supply.

**b) 70% Ethanol**

Reagents	Volume (1 L)
100% Ethanol	700 mL
Ultra-pure Water	300 mL

700 mL 100% ethanol was diluted with 300 mL ultra-pure water.

**c) 1x PBS Buffer**

Reagents	Volume (1 L)
KH <sub>2</sub> PO <sub>4</sub> (Merck)	0.24 g
Na <sub>2</sub> HPO <sub>4</sub> (Merck)	1.44 g
NaCl (Merck)	8 g
KCL (Merck)	0.2 g
Ultra-pure water	450 mL

The components were dissolved in 800 mL ultra-pure water. The pH was then adjusted to pH 7.4. Thereafter, the volume was made up to 1 L with ultra-pure water, autoclaved and allowed to cool before it was diluted for use.

**d) 1x Trypsin-EDTA Solution**

Reagents	Volume (10 mL)
10x Trypsin	1 mL
Sodium EDTA	9 mL

1 part 10x Trypsin was diluted with 9 parts sodium EDTA.

**e) Hoechst nuclear stain stock solution**

Reagents	Volume (15 mL)
Hoechst (bis benzimide) (Sigma-Aldrich®)	0.00075 g

1x PBS (See Appendix 3.1c)	15 mL
----------------------------	-------

0.00075 g Hoechst was diluted in 15 mL 1x PBS to yield a final concentration of 0.05 mg/mL.

Hoechst working solution

<b>Reagents</b>	<b>Volume (100 mL)</b>
Hoechst stock solution	1 mL
1x PBS (See Appendix 3.1c)	99 mL

1 mL Hoechst stock solution was diluted in 99 mL 1x PBS to yield a final concentration of 0.5  $\mu$ /mL.

**f) Bleach agarose gel**

Ethidium bromide working solution

Reagents	Volume (100 mL)
Ethidium bromide	500 $\mu$ l
1x TBE buffer	100 mL

The ethidium bromide stock solution was diluted in 1x TBE buffer (1:200) to yield a 0.5  $\mu$ g/mL ethidium bromide working solution.

Bleach agarose gel

Reagents	Volume (40 mL)
Agarose	0.6 g
Commercial bleach (3.5% m/v)	680 $\mu$ l
10x TAE buffer	40 mL
0.5 $\mu$ g/mL ethidium bromide	2.5 $\mu$ l

The agarose was weighed using a triple beam balance. The agarose and bleach were added to a conical flask and incubated at room temperature for 5 minutes with occasional swirling. The solution was melted in 10x TAE buffer in a conical flask using a microwave until the agarose was completely dissolved. The solution was allowed to cool briefly before ethidium bromide was added in a fume hood.

**g) 50x TAE Buffer**

Reagents	Volume (100 mL)
Tris Base	24.2 g
Glacial acetic acid	5.71 mL
0.5M EDTA (Merck)	10 mL
Ultra-pure water	85 mL

Tris-base; glacial acetic acid; 0.5 M EDTA and ultra-pure water were combined, autoclaved and allowed to cool before it was diluted for use.

20 mL 10x TAE buffer was diluted with 980 mL autoclaved ultra-pure water to obtain x mL 1x TAE buffer.

#### h) 1.5% Agarose Gel

Reagents	Volume (40 mL)
Agarose	0.6 g
1x TBE buffer	40 mL
0.5 $\mu$ g/mL ethidium bromide	2.5 $\mu$ l

The agarose was weighed using a triple beam balance. It was melted in 1x TBE buffer in a conical flask using a microwave until the agarose was completely dissolved. The solution was allowed to cool briefly before ethidium bromide was added in a fume hood.

#### i) 10x TBE Buffer

Reagents	Volume (400 mL)
Tris Base	43.2 g
Boric Acid	22 g
EDTA (Merck)	3.72 g
Ultra-pure water	320 mL

Tris base, boric acid and EDTA were dissolved in 320 mL ultra-pure water to make a 10x TBE buffer.

100 mL 10x TBE buffer was diluted in 900 mL ultra-pure water to make a 1x TBE buffer.

## 4.2 Immunoblot recipes

#### a) 10% SDS stock solution

Reagents	Volume (50 mL)
SDS	5 g
Ultra-pure water	50 mL

SDS was dissolved in ultra-pure water to create a 10% m/v solution. 5 mL of the 10% SDS stock solution was diluted with 45 mL ultra-pure water to create a 1% m/v solution when needed.

**b) Reducing sample treatment buffer/protein loading dye**

Reagents	Volume (10 mL)
10% SDS stock solution (see appendix 3.2a)	4 mL
4x Stacking gel buffer (see appendix 3.2c)	2.5 mL
Glycerol	2 mL
2-Mercaptoethanol (Sigma-Aldrich <sup>®</sup> )	1 mL
Bromothymol Blue (Sigma-Aldrich <sup>®</sup> )	0.1 g
Ultra-pure water	0.5 mL

The 4x stacking gel buffer; SDS solution; glycerol and 2-Mercaptoethanol were combined. The bromothymol blue was added to the solution which was then mixed until it turned blue/purple. The solution was then made up to 10 mL with ultra-pure water.

**c) 12.5% SDS PAGE gel**

Solutions	12.5 % Resolving Gel	4% Stacking gel
30% Bis-acrylamide solution (Bio-rad)	3.375 mL	0.47 mL
4x Running gel buffer	1.875 mL	-
4x Stacking gel buffer	-	0.875 mL
Ultra-pure water	2.099 mL	2.15 mL
10% SDS	75 µl	35 µl
15% APS initiator	37.5 µl	17.5 µl
TEMED (Sigma-Aldrich <sup>®</sup> )	3.75 µl	7.5 µl

## 4x Running gel buffer

Reagents	Volume (50 mL)
Tris-HCL (Calbiochem)	9.09 g
Ultra-pure water	50 mL

Tris-HCL was dissolved in ultra-pure water and the pH was adjusted to pH 8.8

## 4x Stacking gel buffer

Reagents	Volume (50 mL)
Tris-HCL (Calbiochem)	3 g
Ultra-pure water	50 mL

Tris-HCL was dissolved in ultra-pure water and the pH was adjusted to pH 6.8

## 15% ammonium persulfate (APS) initiator solution

Reagents	Volume (500 $\mu$ L)
Ammonium persulfate	0.033 g
Ultra-pure water	500 $\mu$ L

Ammonium persulfate was dissolved in ultra-pure water to create a 15% m/v solution.

## 1x Electrode buffer

Reagents	Volume (1 L)
Tris-HCL	3 g
Glycine (Sigma-Aldrich <sup>®</sup> )	14.4 g
SDS	10 mL
Ultra-pure water	990 mL

The components were combined in 800 mL ultra-pure water. The pH was adjusted to pH 8.3, after which the volume was adjusted to 1 L with ultra-pure water.

**d) Protein transfer buffer**

Reagents	Volume (1 L)
Tris-HC	3.03 g
Glycine (Sigma-Aldrich®)	14.4 g
Methanol (Merck)	200 mL
SDS	1 g
Ultra-pure water	600 mL

Tris-HCL, glycine and SDS were combined in 600 mL ultra-pure water. Methanol was then added to the solution. The pH was adjusted to pH 8.3, after which the volume was adjusted to 1 L with ultra-pure water.

**e) Tris-Buffered Saline-Tween (TBS-T)**

Reagents	Volume (1 L)
NaCl	8 g
KCL	0.2 g
Tris-base	3 g
Tween-20	1 mL
Ultra-pure water	800 mL

NaCl, KCL and Tris-base were combined in 800 mL ultra-pure water. The pH was adjusted to pH 7.5, after which the volume was adjusted to 1 L with ultra-pure water. Tween-20 was then added to the solution.

**f) 6% Skim milk blocking solution**

Reagents	Volume (50 mL)
Skim milk powder	3 g
TBS-T (see appendix 3.2f)	50 mL

The skim milk powder was dissolved in TBST.

**g) 1x Ponceau S Stain**

Reagents	Volume (500 mL)
0.1% Ponceau S (Sigma-Aldrich <sup>®</sup> )	0.5 g
Glacial acetic acid	5 mL
Ultra-pure water	495 mL

The components were dissolved in ultra-pure water and stored in a dedicated container at room temperature.

**h) 1x Ponceau destain**

Reagents	Volume (500 mL)
1% Glacial acetic acid	5 mL
Ultra-pure water	495 mL

1% glacial acetic acid was dissolved in ultra-pure water and stored in a dedicated container at room temperature.

**4.3 Immunocytochemistry recipes****a) 4% Paraformaldehyde (PFA)**

Reagents	Volume (100 mL)
PFA	4 g
0.1x PBS	96 mL

PFA was added to 96 mL 0.1x PBS solution. The solution was heated and stirred on a magnetic stirrer at 65°C to dissolve the PFA. Drops of 1N NaOH were used to make the solution clear whilst stirring the solution. The solution was filter sterilised through a 0.2 µm filter. PFA aliquots were stored at -20°C. Aliquots were only thawed once and discarded after use.

**b) 0.5% Bovine serum albumin (BSA)**

Reagents	Volume (100 mL)
BSA	0.25 g
1x PBS	50 mL

BSA was dissolved in 1x PBS. The solution was mixed by vortexing. Fresh BSA was prepared for each use.

**c) 0.2M TRIS buffer pH 8.5**

Reagents	Volume (500 mL)
TRIS base	12.12 g
Ultra-pure water	400 mL

The TRIS base was dissolved in 400 mL ultra-pure water and the pH was adjusted to 8.5. Thereafter the volume was made up to 500 mL with ultra-pure water.

**d) Mowial with DABCO mountant**

Reagents	Volume (100 mL)
Mowial 40-88 (Sigma-Aldrich <sup>®</sup> )	8 g
0.2M TRIS buffer pH 8.5	40 mL
Glycerol	25 mL
Ultra-pure water	25 mL
DABCO D-2522 (Sigma-Aldrich <sup>®</sup> )	1 g

The Tris buffer and ultra-pure water were added into a beaker that was heated to 60°C on a magnetic stirrer. The mowial was added to the solution, after which the beaker was covered in foil. The mowial was left to dissolve for several hours to form a viscous solution. Glycerol and DABCO were added to the viscous solution and heated at 60°C until the reagents dissolved. The solution was left to stir on the magnetic stirrer for several hours until a homogenous solution was formed. The resultant mountant was then aliquoted in 1.5

mL micro-centrifuge tubes and stored in the dark at  $-20^{\circ}\text{C}$ . The mowial was brought to room temperature for 5-10 minutes before use and slides were stored at  $4^{\circ}\text{C}$ .

## 5. Cloning recipes

### a) Agar plates

Reagents	Volume (100 mL $\pm$ 10 plates)
Luria agar	2 g
100 mg/mL Ampicillin	100 $\mu\text{l}$
Ultra-pure water	100 mL

The agar was dissolved in ultra-pure water and autoclaved. The solution was left to cool slightly before ampicillin was added. The solution was then swirled gently and poured into petri dishes. Agar plates were then stored upside down to prevent condensate forming on the agar surface at  $4^{\circ}\text{C}$ .

### b) Luria-Bertani (LB) broth

Reagents	Volume (1 L)
LB broth	40 g
100 mg/mL Ampicillin	1 mL
Ultra-pure water	1 L

The LB broth powder was dissolved in ultra-pure water and autoclaved. The solution was left to cool slightly before ampicillin was added. The solution was then swirled gently and stored at  $4^{\circ}\text{C}$ .

### c) Glycerol stocks

150  $\mu\text{l}$  aliquots of 100% glycerol were autoclaved in 1.5 mL sterile micro-centrifuge tubes. Following overnight growth in LB broth, 850  $\mu\text{l}$  of the cell suspension containing the plasmid colonies was transferred into the sterilised glycerol. The solution was mixed gently by pipetting and the glycerol stocks were stored at  $-20^{\circ}\text{C}$ .

**d) TE buffer**

1M Tris-base

<b>Reagents</b>	<b>Volume (100 mL)</b>
TRIS base	12.1 g
Ultra-pure water	100 mL

Tris-base was dissolved in 60 mL ultra-pure water. The pH was adjusted to pH 8.0 and the total volume was made up to 100 mL with ultra-pure water.

0.5M EDTA

<b>Reagents</b>	<b>Volume (100 mL)</b>
EDTA	18.6 g
Ultra-pure water	100 mL

EDTA was dissolved in 60 mL ultra-pure water. The pH was adjusted to pH 8.0 and the total volume was made up to 100 mL with ultra-pure water.

TE buffer

<b>Reagents</b>	<b>Volume (1 L)</b>
1M Tris-base	10 mL
0.5M EDTA	2 mL
Ultra-pure water	990 mL

Tris-base and EDTA were diluted with ultra-pure water.

## e) T7 Sequencing Primers

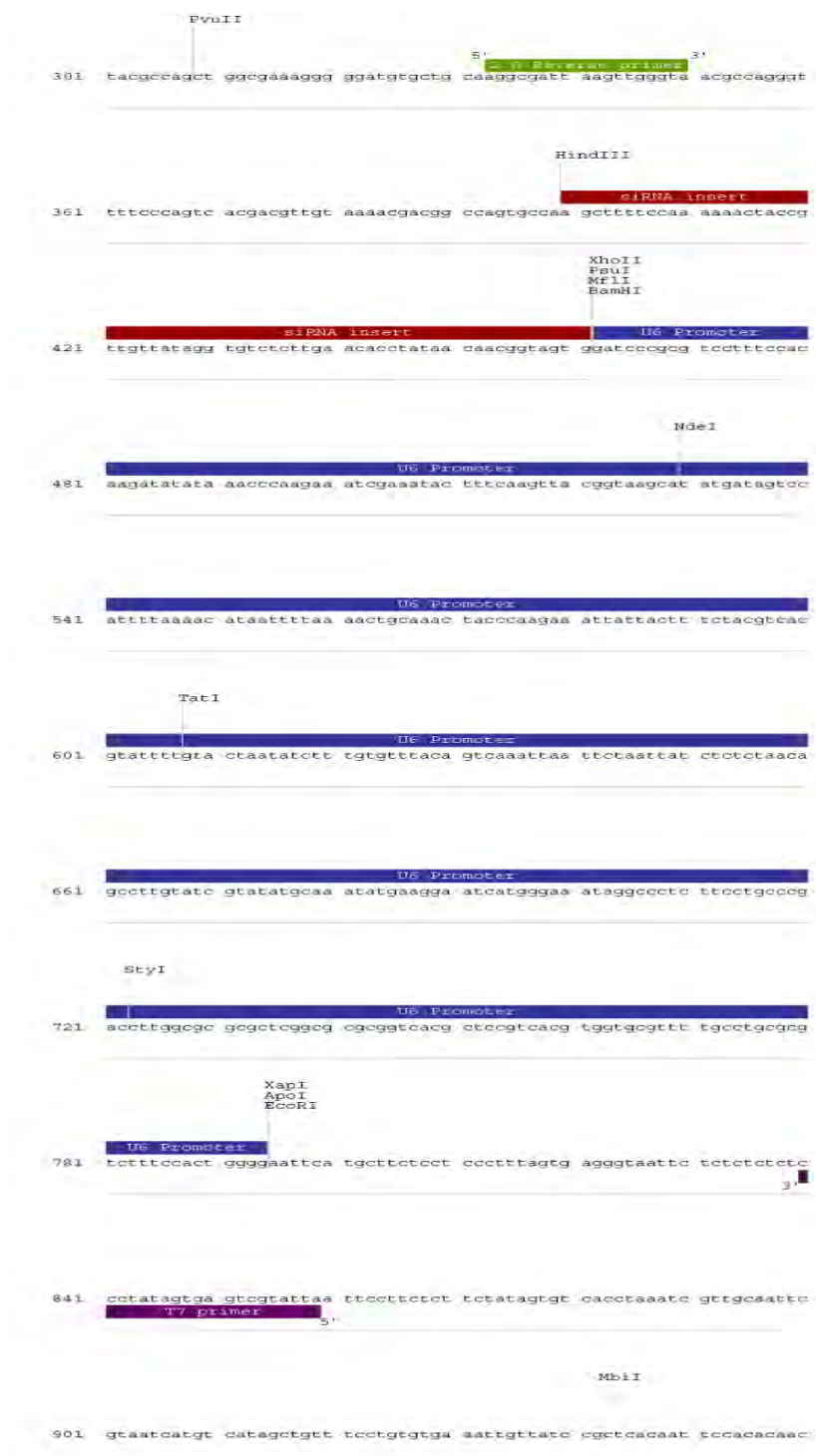


Figure 5.29: T7 sequencing primers used for conventional PCR to verify that the clones contained the siRNA insert.

**f) 8% Native PAGE gel**

<b>Solutions</b>	<b>8 % Resolving Gel</b>
30% Bis-acrylamide solution (Bio-rad)	3.375 mL
4x Running gel buffer	1.875 mL
4x Stacking gel buffer	-
Ultra-pure water	2.099 mL
Nuclease free water	75 µl
15% APS initiator	37.5 µl
TEMED (Sigma-Aldrich®)	3.75 µl

**g) Super Optimal Broth (SOB) with catabolite repression (SOC)**

SOB medium

<b>Reagents</b>	<b>Volume (1 L)</b>
Tryptone	20 g
Yeast extract	5 g
NaCL	0.5 g
Ultra-pure water	1 L

The components were dissolved in ultra-pure water and autoclaved.

SOC medium

<b>Reagents</b>	<b>Volume (10 mL)</b>
SOB medium	10 mL
1M MgCl <sub>2</sub>	0.1 mL/0.02 g
1M MgSO <sub>4</sub>	0.1 mL/0.012 g
Glucose (20% w/v)	0.2 mL

The SOB medium, MgCl<sub>2</sub> and MgSO<sub>4</sub> were combined and filter sterilised using filter paper. Thereafter the glucose was filter sterilised through a 0.2 µm filter and added to the other components.

## 6. Cloning results

We followed the manufacturer's instructions

([http://www.youbio.cn/sites/default/files/product/documents/vector/pSilencer3.0-H1\\_manual.pdf](http://www.youbio.cn/sites/default/files/product/documents/vector/pSilencer3.0-H1_manual.pdf)), annealed the oligonucleotides (Figure 5.29), performed the ligation and transformed the plasmid into competent cells.

We then performed a mini-prep of the plasmid and performed PCR using T7 primers (Figure 5.31). Because the product leaflet assured that the vector could not re-ligate, we assumed any PCR product of the correct size would contain the insert. Sanger sequencing revealed this not to be the case as all clones sequenced did not contain any insert and thus represented re-ligated clones.

We then repeated the procedure, but this time separated the PCR products and restriction digest products on an 8% native PAGE gel (Appendix 3.4e) with greater resolving capacity to distinguish the presence of the small oligonucleotide insert in the hope that we had previously had bad luck with selection. We also designed a restriction digest to discriminate between vector and insert and ran these out on a native PAGE gel. PAGE analysis did not reveal any clones containing the insert (Figure 5.32).

Because the oligonucleotide insert is so small (65bp), we were worried that we were missing the band because of low yield from mini-prep. We then grew the cells in SOC medium and performed a midi-prep. Re-analysis did not reveal the presence of the insert. We then re-performed the entire procedure and sent potential clones for sequencing. Although there was the presence of an insert in some of the clones, the insert was not 100% similar to the designed oligonucleotides (Figure 5.33).

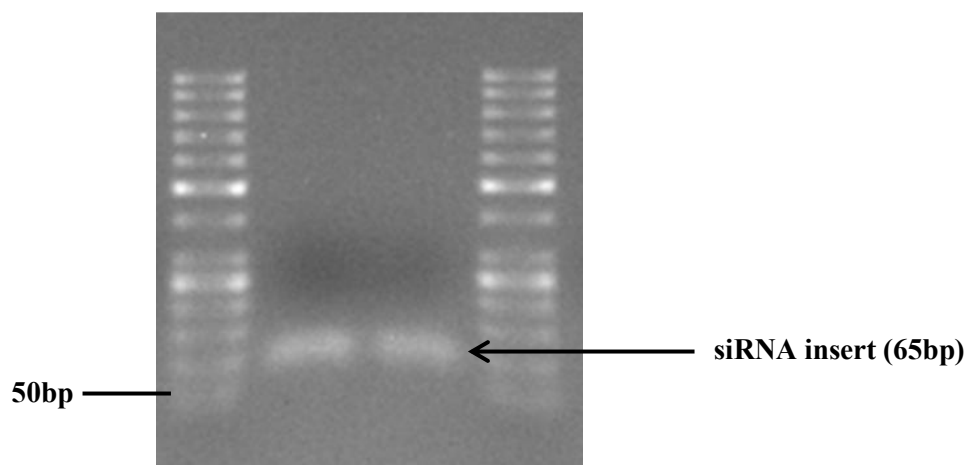


Figure 5.30: siRNA insert. The annealed oligonucleotides were separated on a 1.5% agarose gel to confirm the insert size of 65bp.

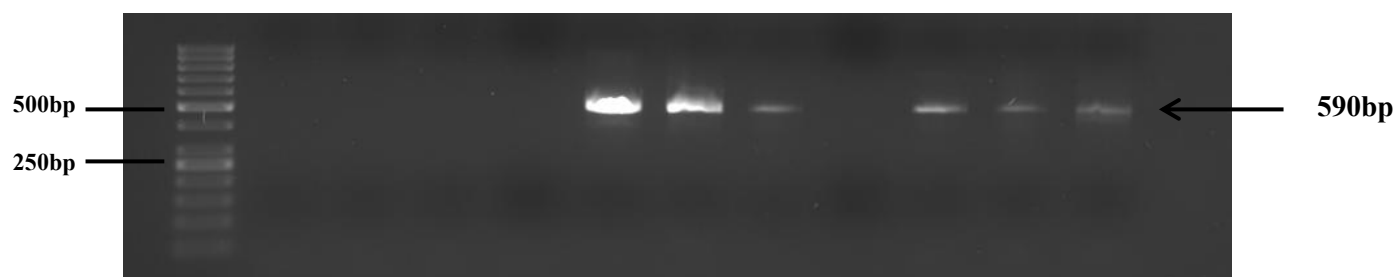


Figure 5.31: PCR products using T7 primers. The expected product size was 590bp.

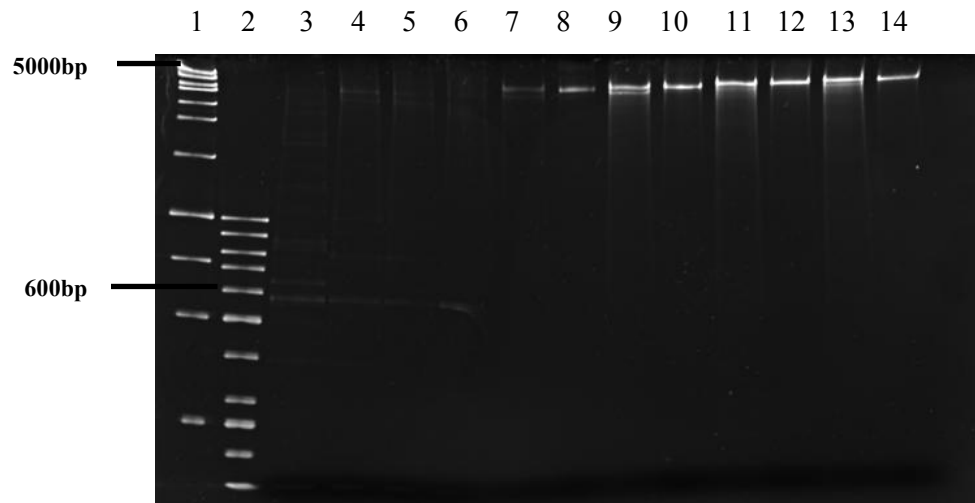


Figure 5.32: PCR and restriction digest products separated on an 8% native PAGE gel. 1) MW (1Kb); 2) MW (50bp); 3-6) PCR products (590bp); 7-14) restriction digest products. Vector size is 4900bp. The siRNA insert (65bp) was not detected.

```
[BiQ Analyzer Documentation (automatically generated)]
Date of quality check: 23 June 2015
Conversion type: C -> T
Genomic Sequence (original): GTGGGAATAGTACTGTGCAGATCTGACCCCAATCTGCACAGCTACTATTCCCATTTTT
Genomic Sequence (fully converted): GTGGGAATAGTACTGTGTGTAGATTTTGAITTAATTTGATAGTATATTATTTTTTTTT

[BiQ Analyzer Quality Data (automatically generated)]
No sequences were excluded during the analysis.

List of sequence identities relative to the genomic sequence in the final pileup (gaps ignored):
Sequence [2]: 80%
Sequence [3]: 73%
Sequence [4]: 61%
Sequence [5]: 75%
Sequence [6]: 69%
Sequence [7]: 67%
Sequence [8]: 72%
Sequence [9]: 80%
Sequence [10]: 72%
Sequence [11]: 73%

List of the sequences' conversion rates in the final pileup:
Sequence [2]: 93% (13 out of 14)
Sequence [3]: 92% (11 out of 12)
Sequence [4]: 50% (4 out of 8)
Sequence [5]: 100% (13 out of 13)
Sequence [6]: 92% (12 out of 13)
Sequence [7]: 100% (9 out of 9)
Sequence [8]: 100% (11 out of 11)
Sequence [9]: 93% (13 out of 14)
Sequence [10]: 100% (11 out of 11)
Sequence [11]: 100% (11 out of 11)
```

## Sequence Pileup

Needleman-Wunsch pairwise alignment

```
Genomic Sequence -----
[2]seq_A.fasta -----
[3]seq_B.fasta -----
[4]seq_C.fasta -----
[5]seq_D.fasta -----
[6]seq_E.fasta -----
[7]seq_F.fasta -----
[8]seq_G.fasta -----
[9]seq_H.fasta -----
[10]seq_I.fasta -----
[11]seq_J.fasta -----

Genomic Sequence -----G-I-GG-GAA--IAG-IAGT-IGI
[2]seq_A.fasta -----ITCGGGATTGTTTTTITAGTAGGTGAAGTTTTGTTATGGATTTTTTITGGGGTTTTG
[3]seq_B.fasta -----ITGTTGTTTTGTTTTITAGTGTGTGGTGAAGTTG-T-GG-TIG--T-G-TAG--TG-
[4]seq_C.fasta -----CATCCAAAACCTC-I-TC-GAACCTA--UACTCCCT
[5]seq_D.fasta -----TCCGGGATCGTTTTTITAG-TAGGTG-A--AG-T-II-IGI
[6]seq_E.fasta -----ITTGGGATTGTTTTTITAGCAGGTGAAGTTTTGTTA-I--G-G-A--III-ITII-IGI
[7]seq_F.fasta -----II-C-GG-G-A--ICG-T-II-III
[8]seq_G.fasta -----TGTGTTTTGTTTTITAGTGTGTGGTGAAGTTG-T-GG-TIG--T-G-TAGG-TG-
[9]seq_H.fasta -----ITCGGGATTGTTTTTITAG-TAGGTG-A--AG-T-II-IGI
[10]seq_I.fasta -----TGTGTTTTGTTTTITAGTGTGTGGTGAAGTTG-T-GG-TIG--T-G-TAGG-TG-
[11]seq_J.fasta -----ITTGGGATTGTTTTTITAGTGTGGTGAAGTTG-T-GG-TIG--T-G-TAGG-TG-

Genomic Sequence -----
[2]seq_A.fasta -----T-A--G-A-III-TGAT-TT--AAT-TT-GATA-G--TT-AT-TAT-T-T-TTATTTT
[3]seq_B.fasta -----T-AIGG-ATTTT-TTTTGTGGGGT-ITCG-T--G--TT-GT-T-T-TGT-TGTTTTT
[4]seq_C.fasta -----T-A--G--TGT-TG-T-GT----T-IT-G-TC-G--II-GT-ITGT-I-TTGTITGT
[5]seq_D.fasta -----CC-AC-SAA-TTC-CIA--AA--AAA-AA-AATACGCATT-R--TAGGC-G--AACACCT
[6]seq_E.fasta -----T-AIGG-A-III-T-CI-TI----G-TT-G-GG-G--II--T-IGGT-IGTI-TGTI
[7]seq_F.fasta -----TGS--G-G-III-TGATTT--GTT-TC-GTTT-G--TT-TC--TAG-T-T-TI-TGTT
[8]seq_G.fasta -----T-A--GTA--GG-TGA-----AST-TT--T--G--TT-AIGGAT-T-T-TT-ITCGT
[9]seq_H.fasta -----T-A--G--TGT-TG-T-GT----T-IT-G-TC-G--II-GT-ITGT-I-TTGTITGT
[10]seq_I.fasta -----T-AIGG-ATTTT-TTTTGTGGGGT-ITCG-T--G--TT-GT-T-T-TGT-TGTTTTT
[11]seq_J.fasta -----T-A--G--TGT-TG-T-GT----T-IT-G-TT-G--II-GT-ITGT-I-TTGTITGT
T----T-T-ITATGSI-TAAAAATGTT-G-GG-G--TAAATGTT-T-G-TT-TTGT

Genomic Sequence -----T-----
[2]seq_A.fasta -----TGTGTTGGTTAAGGAAAAAAAAAATAGTGTGCGGTTTCGTGCGTITTAGTTTTGTTC
[3]seq_B.fasta -----TGTGTTGGATGTTGTTGTGTACAGTGTGTATTTTTTTTTCAGGAATTTTGGAGGGGA
[4]seq_C.fasta -----TCCACAAACACGACAAACAAACGAAACGACGAGGGAACGACACTACGCCTACGCGACCGC
[5]seq_D.fasta -----TTCCTTAGTGTGTTAAGGTTGTGTTGTGTAGGTTGTGTTGTGTTGTGTTGTGTTGTG
[6]seq_E.fasta -----TAAGGTGCGGTTGTGTAGGCGTGTGCGGTTTGTGTTGTGTTGTGTTGTGTTGTGTTGTG
[7]seq_F.fasta -----TGGGTTTTGTTGTCCTGTTGTTTTTASTGTTGTTAAGGCTCCGTTCCGTTAGCC
[8]seq_G.fasta -----TGTGTTGGAAGTGTGTTGTTGTAGCAATGTGTATTTTTTTTTCAGGAATTTTGGAGGGGA
[9]seq_H.fasta -----TGTGTTGTTGTIANGGTGCGGTTGCGGTTAGGCGTATGTGCGGTTTTCGTGTTGTTTTGT
[10]seq_I.fasta -----TGTGTTGGAAGTGTGTTGTTGTAGTAATGTGTATTTTTTTTTCAGGAATTTTGGAGGG
[11]seq_J.fasta -----TSTAATAGTTTGGGGCCITTTTGTGTTGGGGGTTAGTGTGTTGGGGGTTGGGGTTG
```

Figure 5.33: *In silico* screen of the sequencing results obtained from BiQ Analyzer Software version 2.00. The insert was not 100% similar to the designed oligonucleotides.

## 6. REFERENCES

- Acharya, M., Huang, L., Fleisch, V. C., Allison, W. T. and Walter, M. A. (2011). A complex regulatory network of transcription factors critical for ocular development and disease. *Human Molecular Genetics* 20:1610-1624
- Agre, P. (2004). Aquaporin water channels. *Bioscience reports* 24:127-163
- Agre, P., Preston, G. M., Smith, B. L., Jung, J., Raina, S., Moon, C., Guggino, W. B. and Nielsen, S. (1993). Aquaporin CHIP: the archetypal molecular water channel. *American Journal of Physiology-Renal Physiology* 265:F463-F476
- Alward, W. L. M. (2000). Axenfeld-Rieger syndrome in the age of molecular genetics. *American Journal of Ophthalmology* 130:107-115
- Aranda, P. S., LaJoie, D. M. and Jorcyk, C. L. (2012). Bleach gel: a simple agarose gel for analyzing RNA quality. *Electrophoresis* 33:366-369
- Araujo Silva, G., Filipa Silva, N. and Moderno Fortunato, T. (2011). Stem Cell and Tissue Engineering Therapies for Ocular Regeneration. *Current Stem Cell Research & Therapy* 6:255-272
- Ban, Y., Dota, A., Cooper, L. J., Fullwood, N. J., Nakamura, T., Tsuzuki, M., Mochida, C. and Kinoshita, S. (2003). Tight junction-related protein expression and distribution in human corneal epithelium. *Experimental Eye Research* 76:663-669
- Bauer, H., Zweimueller-Mayer, J., Steinbacher, P., Lametschwandtner, A. and Bauer, H. (2010). The dual role of zonula occludens (ZO) proteins. *BioMed Research International* 2010
- Baum, B., Settleman, J. and Quinlan, M. P. (2008). Transitions between epithelial and mesenchymal states in development and disease. *Seminars in Cell & Developmental Biology*, Elsevier. **19**: 294-308.
- Beebe, D. C. and Coats, J. M. (2000). The Lens Organizes the Anterior Segment: Specification of Neural Crest Cell Differentiation in the Avian Eye. *Developmental Biology* 220:424-431
- Berry, F. B., Lines, M. A., Oas, J. M., Footz, T., Underhill, D. A., Gage, P. J. and Walter, M. A. (2006). Functional interactions between FOXC1 and PITX2 underlie the sensitivity to FOXC1 gene dose in Axenfeld-Rieger syndrome and anterior segment dysgenesis. *Human Molecular Genetics* 15:905-919

- Besharse, J., Dana, R. and Dartt, D. A. (2010). Encyclopedia of the Eye, Four-Volume Set, Elsevier Science
- Bock, C., Reither, S., Mikeska, T., Paulsen, M., Walter, J. and Lengauer, T. (2005). BiQ Analyzer: visualization and quality control for DNA methylation data from bisulfite sequencing. *Bioinformatics* 21:214067-4068
- Bonanno, J. A. (2012). Molecular mechanisms underlying the corneal endothelial pump. *Experimental Eye Research* 95:12-7
- Bustin, S. A., Benes, V., Garson, J. A., Hellems, J., Huggett, J., Kubista, M., Mueller, R., Nolan, T., Pfaffl, M. W. and Shipley, G. L. (2009). The MIQE guidelines: minimum information for publication of quantitative real-time PCR experiments. *Clinical Chemistry* 55:4611-622
- Cao, Z., Wu, H. K., Bruce, A., Wollenberg, K. and Panjwani, N. (2002). Detection of differentially expressed genes in healing mouse corneas, using cDNA microarrays. *Investigative Ophthalmology and Visual Science* 43:2897-2904
- Carlsson, P. and Mahlapuu, M. (2002). Forkhead Transcription Factors: Key Players in Development and Metabolism. *Developmental Biology* 250:11-23
- Chen, Y., Huang, K., Nakatsu, M. N., Xue, Z., Deng, S. X. and Fan, G. (2013). Identification of novel molecular markers through transcriptomic analysis in human fetal and adult corneal endothelial cells. *Human Molecular Genetics* 22:1271-1279
- Chow, R. L. and Lang, R. A. (2001). Early eye development in vertebrates. *Annual review of cell and developmental biology* 17:255-296
- Cvekl, A. and Tamm, E. R. (2004). Anterior eye development and ocular mesenchyme: new insights from mouse models and human diseases. *Bioessays* 26:4374-386
- De Jonge, H., Fehrmann, R., De Bont, E., Hofstra, R., Gerbens, F., Kamps, W. A., De Vries, E., Van Der Zee, A., te Meerman, G. J. and ter Elst, A. (2007). Evidence based selection of housekeeping genes. *PLoS ONE* 2:e898
- Du, Y., Carlson, E. C., Funderburgh, M. L., Birk, D. E., Pearlman, E., Guo, N., Kao, W. W. Y. and Funderburgh, J. L. (2009). Stem Cell Therapy Restores Transparency to Defective Murine Corneas. *Stem Cells* 27:1635-1642
- Dua, H. S., Faraj, L. A., Said, D. G., Gray, T. and Lowe, J. (2013). Human corneal anatomy redefined: a novel pre-Descemet's layer (Dua's layer). *Ophthalmology* 120:1778-1785
- Fan, T., Zhao, J., Ma, X., Xu, X., Zhao, W. and Xu, B. (2011). Establishment of a continuous untransfected human corneal endothelial cell line and its biocompatibility to denuded amniotic membrane. *Molecular Vision* 17:469-480

Fischbarg, J. (1997). Mechanism of fluid transport across corneal endothelium and other epithelial layers: a possible explanation based on cyclic cell volume regulatory changes. *British Journal of Ophthalmology* 81:185-89

Flügel-Koch, C., Ohlmann, A., Piatigorsky, J. and Tamm, E. R. (2002). Disruption of anterior segment development by TGF- $\beta$ 1 overexpression in the eyes of transgenic mice. *Developmental Dynamics* 225:111-125

Fujita, M., Mehra, R., Lee, S. E., Roh, D. S., Long, C., Funderburgh, J. L., Ayares, D. L., Cooper, D. K. and Hara, H. (2013). Comparison of proliferative capacity of genetically-engineered pig and human corneal endothelial cells. *Ophthalmic research* 49:3127

Gage, P. J., Rhoades, W., Prucka, S. K. and Hjalt, T. (2005). Fate Maps of Neural Crest and Mesoderm in the Mammalian Eye. *Investigative Ophthalmology and Visual Science* 46:114200-4208

Gage, P. J., Suh, H. and Camper, S. A. (1999). Dosage requirement of Pitx2 for development of multiple organs. *Development* 126:204643-4651

Gage, P. J. and Zacharias, A. L. (2009). Signaling “cross-talk” is integrated by transcription factors in the development of the anterior segment in the eye. *Developmental Dynamics* 238:92149-2162

Hemmavanh, C., Koch, M., Birk, D. E. and Espana, E. M. (2013). Abnormal corneal endothelial maturation in collagen XII and XIV null mice. *Investigative Ophthalmology and Visual Science* 54:53297

Hendriks, G., Koudijs, M., van Balkom, B. W., Oorschot, V., Klumperman, J., Deen, P. M. and van der Sluijs, P. (2004). Glycosylation is important for cell surface expression of the water channel aquaporin-2 but is not essential for tetramerization in the endoplasmic reticulum. *Journal of Biological Chemistry* 279:42975-2983

Hjalt, T. A., Amendt, B. A. and Murray, J. C. (2001). Pitx2 Regulates Procollagen Lysyl Hydroxylase (Plod) Gene Expression: Implications for the Pathology of Rieger Syndrome. *The Journal of Cell Biology* 152:3545-552

Hjalt, T. A., Semina, E. V., Amendt, B. A. and Murray, J. C. (2000). The Pitx2 protein in mouse development. *Developmental Dynamics* 218:1195-200

Ito, Y. A. and Walter, M. A. (2014). Genomics and anterior segment dysgenesis: a review. *Clinical & Experimental Ophthalmology* 42:113-24

Ittner, L. M., Wurdak, H., Schwerdtfeger, K., Kunz, T., Ille, F., Leveen, P., Hjalt, T. A., Suter, U., Karlsson, S., Hafezi, F., Born, W. and Sommer, L. (2005). Compound

developmental eye disorders following inactivation of TGFbeta signaling in neural-crest stem cells. *Journal of Biology*4311

Ju, C., Gao, L., Wu, X. and Pang, K. (2012). A human corneal endothelium equivalent constructed with acellular porcine corneal matrix. *The Indian journal of medical research*1356887

Ju, C., Zhang, K. and Wu, X. (2012). Derivation of corneal endothelial cell-like cells from rat neural crest cells in vitro. *PLoS ONE*77e42378

Kao, W. W.-Y., Xia, Y. and Liu, C.-Y. (2008). Signaling pathways in morphogenesis of cornea and eyelid. *The ocular surface*619-23

Kidson, S. H., Kume, T., Deng, K., Winfrey, V. and Hogan, B. L. M. (1999). The Forkhead/Winged-Helix Gene, Mf1, Is Necessary for the Normal Development of the Cornea and Formation of the Anterior Chamber in the Mouse Eye. *Developmental Biology*2112306-322

Kim, E. Y., Song, J. E., Park, C. H., Joo, C.-K. and Khang, G. (2014). Recent advances in tissue-engineered corneal regeneration. *Inflammation and Regeneration*341004-014

Kojima, T., Murata, M., Yamamoto, T., Lan, M., Imamura, M., Son, S., Takano, K.-i., Yamaguchi, H., Ito, T. and Tanaka, S. (2009). Tight junction proteins and signal transduction pathways in hepatocytes

Kume, T., Deng, K. and Hogan, B. L. (2000). Murine forkhead/winged helix genes Foxc1 (Mf1) and Foxc2 (Mfh1) are required for the early organogenesis of the kidney and urinary tract. *Development*12771387-1395

Kume, T., Jiang, H., Topczewska, J. M. and Hogan, B. L. (2001). The murine winged helix transcription factors, Foxc1 and Foxc2, are both required for cardiovascular development and somitogenesis. *Genes & Development*15182470-2482

Langenberg, T., Kahana, A., Wszalek, J. A. and Halloran, M. C. (2008). The eye organizes neural crest cell migration. *Developmental Dynamics*23761645-1652

Levin, M. H. and Verkman, A. (2004). Aquaporin-dependent water permeation at the mouse ocular surface: in vivo microfluorimetric measurements in cornea and conjunctiva. *Investigative Ophthalmology & Visual Science*45124423-4432

Liu, H., Zhang, J., Liu, C.-Y., Wang, I. J., Sieber, M., Chang, J., Jester, J. V. and Kao, W. W. Y. (2010). Cell Therapy of Congenital Corneal Diseases with Umbilical Mesenchymal Stem Cells: Lumican Null Mice. *PLoS ONE*55e10707

Livak, K. J. and Schmittgen, T. D. (2001). Analysis of Relative Gene Expression Data Using Real-Time Quantitative PCR and the  $2^{-\Delta\Delta CT}$  Method. *Methods* 254402-408

Lu, H., Lu, Q., Zheng, Y. and Li, Q. (2012). Notch signaling promotes the corneal epithelium wound healing. *Molecular Vision* 18403

Macnamara, E., Sams, G. W., Smith, K., Ambati, J., Singh, N. and Ambati, B. K. (2004). Aquaporin-1 expression is decreased in human and mouse corneal endothelial dysfunction. *Molecular Vision* 1051-56

Makgotloe, A. M. and Carmichael, T. R. (2009). Plummeting corneal donations at the Gauteng Cornea and Eye Bank

Maurice, D. (1981). *The Cornea and Sclera*. Academic Press New York

Meyer, D. (2007). The new challenge of corneal transplantation in South Africa

Montiel, V., Gomez, E. L., Bouzin, C., Esfahani, H., Perez, M. R., Lobysheva, I., Devuyt, O., Dessy, C. and Balligand, J.-L. (2014). Genetic deletion of aquaporin-1 results in microcardia and low blood pressure in mouse with intact nitric oxide-dependent relaxation, but enhanced prostanoids-dependent relaxation. *Pflügers Archiv-European Journal of Physiology* 4662237-251

Niessen, C. M. (2007). Tight junctions/adherens junctions: basic structure and function. *Journal of Investigative Dermatology* 127112525-2532

Nishimura, D. Y., Searby, C. C., Alward, W. L., Walton, D., Craig, J. E., Mackey, D. A., Kawase, K., Kanis, A. B., Patil, S. R. and Stone, E. M. (2001). A spectrum of FOXC1 mutations suggests gene dosage as a mechanism for developmental defects of the anterior chamber of the eye. *The American Journal of Human Genetics* 682364-372

Nishimura, D. Y., Searby, C. C., Alward, W. L., Walton, D., Craig, J. E., Mackey, D. A., Kawase, K., Kanis, A. B., Patil, S. R., Stone, E. M. and Sheffield, V. C. (2001). A spectrum of FOXC1 mutations suggests gene dosage as a mechanism for developmental defects of the anterior chamber of the eye. *Am J Hum Genet* 682364-372

Norman, B., Davis, J. and Piatigorsky, J. (2004). Postnatal Gene Expression in the Normal Mouse Cornea by SAGE. *Investigative Ophthalmology & Visual Science* 452429-440

Pajooresh-Ganji, A. and Stepp, M. A. (2005). In search of markers for the stem cells of the corneal epithelium. *Biology of the Cell* 974265-276

Parekh, M., Graceffa, V., Bertolin, M., Elbadawy, H. and Salvalaiov, G. (2013). Reconstruction and regeneration of the corneal endothelium: a review on the current methods and future aspects. *Journal of Cell Science & Therapy* 43

Peh, G. S. L., Beuerman, R. W., Colman, A., Tan, D. T. and Mehta, J. S. (2011). Human Corneal Endothelial Cell Expansion for Corneal Endothelium Transplantation: An Overview. *Transplantation* 91:8811-819 10.1097/TP.0b013e3182111f01

Peh, G. S. L., Toh, K.-P., Wu, F.-Y., Tan, D. T. and Mehta, J. S. (2011). Cultivation of Human Corneal Endothelial Cells Isolated from Paired Donor Corneas. *PLoS ONE* 6:12e28310

Ramachandran, C. and Srinivas, S. P. (2010). Formation and disassembly of adherens and tight junctions in the corneal endothelium: regulation by actomyosin contraction. *Investigative Ophthalmology and Visual Science* 51:42139

Reneker, L. W., Silversides, D. W., Xu, L. and Overbeek, P. A. (2000). Formation of corneal endothelium is essential for anterior segment development - a transgenic mouse model of anterior segment dysgenesis. *Development (Cambridge, England)* 127:533-542

Ruiz-Ederra, J. and Verkman, A. (2006). Accelerated cataract formation and reduced lens epithelial water permeability in aquaporin-1-deficient mice. *Investigative Ophthalmology & Visual Science* 47:3960-3967

Ryeom, S. W., Paul, D. and Goodenough, D. A. (2000). Truncation mutants of the tight junction protein ZO-1 disrupt corneal epithelial cell morphology. *Molecular Biology of the Cell* 11:1687-1696

Saika, S., Saika, S., Liu, C.-Y., Azhar, M., Sanford, L. P., Doetschman, T., Gendron, R. L., Kao, C. W. C. and Kao, W. W. Y. (2001). TGF $\beta$ 2 in Corneal Morphogenesis during Mouse Embryonic Development. *Developmental Biology* 240:419-432

Sanford, L. P., Ormsby, I., Gittenberger-de Groot, A. C., Sariola, H., Friedman, R., Boivin, G. P., Cardell, E. L. and Doetschman, T. (1997). TGF $\beta$ 2 knockout mice have multiple developmental defects that are non-overlapping with other TGF $\beta$  knockout phenotypes. *Development* 124:132659-2670

Schwartzkopff, J., Schlereth, S. L., Berger, M., Bredow, L., Birnbaum, F., Böhringer, D. and Reinhard, T. (2010). NK cell depletion delays corneal allograft rejection in baby rats. *Molecular Vision* 16:1928-1935

Shei, W., Liu, J., Htoon, H. M., Aung, T. and Vithana, E. N. (2013). Differential expression of the Slc4 bicarbonate transporter family in murine corneal endothelium and cell culture. *Molecular Vision* 19:1096-1106

Silla, Z. T., Naidoo, J., Kidson, S. H. and Sommer, P. (2014). Signals from the lens and Foxc1 regulate the expression of key genes during the onset of corneal endothelial development. *Experimental Cell Research* 322:2381-388

Smith, B. L., Preston, G. M., Spring, F. A., Anstee, D. J. and Agre, P. (1994). Human red cell aquaporin CHIP. I. Molecular characterization of ABH and Colton blood group antigens. *Journal of Clinical Investigation* 94:31043-1049

Sommer, P., Napier, H. R., Hogan, B. L. and Kidson, S. H. (2006). Identification of Tgf beta1i4 as a downstream target of Foxc1. *Development, growth & differentiation* 48:5297-308

Sowden, J. (2007). Molecular and developmental mechanisms of anterior segment dysgenesis. *Eye* 21:101310-1318

Stepp, M. A., Gibson, H. E., Gala, P. H., Iglesia, D. D. S., Pajooohesh-Ganji, A., Pal-Ghosh, S., Brown, M., Aquino, C., Schwartz, A. M. and Goldberger, O. (2002). Defects in keratinocyte activation during wound healing in the syndecan-1-deficient mouse. *Journal of Cell Science* 115:234517-4531

Stevenson, B. R., Siliciano, J. D., Mooseker, M. S. and Goodenough, D. A. (1986). Identification of ZO-1: a high molecular weight polypeptide associated with the tight junction (zonula occludens) in a variety of epithelia. *The Journal of Cell Biology* 103:3755-766

Strungaru, M. H., Dinu, I. and Walter, M. A. (2007). Genotype-Phenotype Correlations in Axenfeld-Rieger Malformation and Glaucoma Patients with FOXC1 and PITX2 Mutations. *Investigative Ophthalmology and Visual Science* 48:1228-237

Sugrue, S. P. and Zieske, J. D. (1997). ZO1 in corneal epithelium: association to the zonula occludens and adherens junctions. *Experimental Eye Research* 64:111-20

Suzuki, M., Seki, G., Yamada, H., Horita, S. and Fujita, T. (2012). Functional roles of electrogenic sodium bicarbonate cotransporter NBCe1 in ocular tissues. *The open ophthalmology journal* 6:36

Takahashi, K. and Yamanaka, S. (2006). Induction of Pluripotent Stem Cells from Mouse Embryonic and Adult Fibroblast Cultures by Defined Factors. *Cell* 126:4663-676

Thiagarajah, J. R. and Verkman, A. (2002). Aquaporin deletion in mice reduces corneal water permeability and delays restoration of transparency after swelling. *Journal of Biological Chemistry* 277:2119139-19144

Thiery, J. P. (2003). Epithelial–mesenchymal transitions in development and pathologies. *Current Opinion in Cell Biology* 15:6740-746

Thut, C. J., Rountree, R. B., Hwa, M. and Kingsley, D. M. (2001). A Large-Scale in Situ Screen Provides Molecular Evidence for the Induction of Eye Anterior Segment Structures by the Developing Lens. *Developmental Biology* 231:163-76

Verkman, A. S. (2009). Knock-out models reveal new aquaporin functions. *Aquaporins*, Springer: 359-381.

Wang, H., Ding, T., Brown, N., Yamamoto, Y., Prince, L. S., Reese, J. and Paria, B. (2008). Zonula occludens-1 (ZO-1) is involved in morula to blastocyst transformation in the mouse. *Developmental Biology* 318:1112-125

Ying-Ting, Z., Hayashida, Y., Kheirkhah, A., He, H., Sue-Yue, C. and Tseng, S. C. (2008). Characterization and comparison of intercellular adherent junctions expressed by human corneal endothelial cells in vivo and in vitro. *Investigative Ophthalmology and Visual Science* 49:3879

Zhang, D., Vetrivel, L. and Verkman, A. (2002). Aquaporin deletion in mice reduces intraocular pressure and aqueous fluid production. *The Journal of general physiology* 119:561-569

Zhang, Y., Overbeek, P. A. and Govindarajan, V. (2007). Perinatal ablation of the mouse lens causes multiple anterior chamber defects

Zhu, Y.-T., Hayashida, Y., Kheirkhah, A., He, H., Chen, S.-Y. and Tseng, S. C. (2008). Characterization and comparison of intercellular adherent junctions expressed by human corneal endothelial cells in vivo and in vitro. *Investigative Ophthalmology & Visual Science* 49:3879-3886

Zieske, J. D. (2004). Corneal development associated with eyelid opening. *International Journal of Developmental Biology* 48:9903-911